



Octubre - Diciembre
Volumen 62
Número 4

October - December
Volume 62
Number 4

Geofísica Internacional

Revista Trimestral Publicada por el Instituto de Geofísica de la Universidad Nacional Autónoma de México
Quarterly Journal Published by the Institute of Geophysics of the National Autonomous University of Mexico

<http://revistagi.geofisica.unam.mx/>

ISSN 2954-436X



MÉXICO MEXICO

— Geofísica Internacional —

Dr. José Luis Macías Vázquez
Director of Instituto de Geofísica

Dr. Arturo Iglesias Mendoza
President of Unión Geofísica Mexicana

Editor Chief

Dr. Servando De la Cruz-Reyna
Instituto de Geofísica, UNAM
sdelacr@geofisica.unam.mx

Technical Editor

Mtro. Saúl Armendáriz Sánchez
Instituto de Geofísica, UNAM
asaul@igeofisica.unam.mx

Editorial Board

Donald Bruce Dingwell
Earth and Environment
Ludwig Maximilian University of Munich,
Germany

Eric Desmond Barton
Departamento de Oceanografía
Instituto de Investigaciones Marinas, Spain

Jorge Clavero
Amawta Consultores, Chile

Gerhardt Jentzsch
Institut für Geowissenschaften
Friedrich-Schiller-Universität Jena, Germany

Peter Malischewsky
Institut für Geowissenschaften
Friedrich-Schiller-Universität Jena, Germany

François Michaud
Géosciences Azur
Université Pierre et Marie Curie, France

Olga Borisovna Popovicheva
Scobeltzine Institute of Nuclear Physics
Moscow State University, Rusia

Jaime Pous
Facultad de Geología
Universidad de Barcelona, Spain

Joaquín Rui
UA Science
University of Arizona, United States

Angelos Vourlidas
Solar Physics Branch
NASA Goddard Space Flight Center, United States

Théophile Ndougsa Mbarng
Department of Physics
University of Yaounde I, Cameroon

Associate Editors
José Agustín García Reynoso
Atmospheric Science Centro de Ciencias de la
Atmósfera UNAM, Mexico

Tereza Cavazos
Atmospheric Science
Departamento de Oceanografía Física CICESE,
Mexico

Dante Jaime Morán-Zenteno
Geochemistry
Instituto de Geología, UNAM, Mexico

Margarita López
Geochemistry
Instituto de Geología UNAM, Mexico

Avto Gogichaisvili
Geomagnetism And Paleomagnetism
Instituto de Geofísica UNAM, Mexico

Jaime Urrutia-Fucugauchi
Geomagnetism And Paleomagnetism
Instituto de Geofísica, UNAM, Mexico

Felipe I. Arreguín Cortés
Hydrology
Instituto Mexicano de Tecnología del Agua IMTA,
Mexico

William Lee Bandy
Marine Geology And Geophysics
Instituto de Geofísica UNAM, Mexico

Fabian García-Nocetti
Mathematical And Computational
Modeling
Instituto de Investigaciones en Matemáticas
Aplicadas y en Sistemas UNAM, Mexico

Graciela Herrera-Zamarrón
Mathematical Modeling
Instituto de Geofísica, UNAM, Mexico

Ismael Herrera Revilla
Mathematical And Computational
Modeling
Instituto de Geofísica UNAM, Mexico

Rene Chávez Segura
Near-Surface Geophysics
Instituto de Geofísica UNAM, Mexico

Juan García-Abdeslem
Near-Surface Geophysics
División de Ciencias de la Tierra CICESE, Mexico

Alec Torres-Freyermuth
Oceanography
Instituto de Ingeniería, UNAM, Mexico

Jorge Zavala Hidalgo
Oceanography
Centro de Ciencias de la Atmósfera UNAM,
Mexico

Shri Krishna Singh
Seismology
Instituto de Geofísica, UNAM, Mexico

Xyoli Pérez-Campos
Seismology
Servicio Sismológico Nacional, UNAM, Mexico

Blanca Mendoza Ortega
Space Physics
Centro de Ciencias de la Atmósfera, UNAM,
Mexico

Inez Staciari Batista
Space Physics
Pesquisador Senior Instituto Nacional de Pesquisas
Espaciais, Brazil

Roberto Carniel
Volcanology
Laboratorio di misure e trattamento dei segnali
DPIA - Università di Udine, Italy

Miguel Moctezuma-Flores
Satellite Geophysics
Facultad de Ingeniería, UNAM, Mexico

Assistance

Elizabeth Morales Hernández,
Management
eliedit@igeofisica.unam.mx



GEOFÍSICA INTERNACIONAL, Año 62, Vol. 62, Núm. 4, octubre - diciembre de 2023 es una publicación trimestral, editada por la Universidad Nacional Autónoma de México, Ciudad Universitaria, Alcaldía Coyoacán, C.P. 04510, Ciudad de México, a través del Instituto de Geofísica, Circuito de la Investigación Científica s/n, Ciudad Universitaria, Alcaldía Coyoacán, C.P. 04510, Ciudad de México, Tel. (55)56 22 40 36. URL: <http://revistagi.geofisica.unam.mx>, correo electrónico: revistagi@igeofisica.unam.mx. Editor responsable: Saúl Armendáriz Sánchez. Certificado de Reserva de Derechos al uso Exclusivo del Título: 04-2022-081610251200-102, eISSN: 2954-436X, otorgados por el Instituto Nacional del Derecho de Autor (INDAUTOR). Responsable de la última actualización, Minerva Castro Escamilla Editora Técnica. Fecha de la última modificación: 1 de octubre de 2023, Circuito de la Investigación Científica s/n, Ciudad Universitaria, Alcaldía Coyoacán, C.P. 04510, Ciudad de México.

El contenido de los artículos es responsabilidad de los autores y no refleja el punto de vista de los árbitros, del Editor o de la UNAM. Se autoriza la reproducción total o parcial de los textos siempre y cuando se cite la fuente completa y la dirección electrónica de la publicación.

<https://doi.org/10.22201/igeof.2954436xe.2023.62.4>



Esta obra está bajo una Licencia Creative Commons Atribución-NoComercial-SinDerivadas 4.0 Internacional.

Contents

Gold ore identification in Santa Catarina Gabbro using electrical resistivity tomography (ERT) and visualization of mineralization in three dimensions, São Sepé, Rio Grande do Sul, Brazil

Bruno Daniel Lenhare, César Augusto Moreira, Lenon Melo Ilha

591

Analysis and Interpretation of Regional Gravity Data in the Swayze greenstone belt of the Superior Province, Canada

Satizabal, D. , Nitescu, B

607

Structural Traits of Cuitzeo Lake, Central Mexico, and Areas of Geothermal Potential

Elizabeth Rivera-Calderón and Román Alvarez

617

Gold ore identification in Santa Catarina Gabbro using electrical resistivity tomography (ERT) and visualization of mineralization in three dimensions, São Sepé, Rio Grande do Sul, Brazil

Bruno Daniel Lenhare¹, César Augusto Moreira¹, Lenon Melo Ilha²

Abstract

This work presents the geological-geophysical characterization of a probable occurrence of gold in Santa Catarina Gabbro, in São Sepé region, Rio Grande do Sul state, southern Brazil. Previous works have indicated the presence of gold in the region in current sediments geochemical prospecting campaigns and suggests that the source area would be the Santa Catarina Gabbro. To investigate over this probable occurrence of gold, geological and structural surveys were conducted, followed by the acquisition of geophysical information using the DC-resistivity and IP methods, with the dipole-dipole array. The geophysical data were processed in 2D inversion and then interpolated to allow the three-dimensional visualization of possible mineralization. Interpretations based on the compilation of geological and geophysical data, in association with the regional structural context, suggest that the probable mineralization were originated from the intrusion of the São Sepé Granite, whose hydrothermal fluids were hosted in fractures during the tectonic events that occurred in the region. The results obtained in this work allow to outline a feasible deposit architecture with the geological context of the region and to assist a future drilling strategy aimed at the identified probable targets.

Key words: Mineral research, Resistivity Chargeability, Electrical tomography, Gold.

Resumen

Este trabajo presenta la caracterización geológica-geofísica de una probable ocurrencia de oro en el Gabro Santa Catarina, en la región de São Sepé, estado de Rio Grande do Sul, sur de Brasil. Trabajos anteriores han indicado la presencia de oro en la región en las actuales campañas de prospección geoquímica de sedimentos y sugieren que el área de origen sería el Gabro Santa Catarina. Para investigar sobre esta probable ocurrencia de oro, se realizaron estudios geológicos y estructurales, seguidos de la adquisición de información geofísica utilizando los métodos de resistividad DC e IP, con el arreglo dipolo-dipolo. De estos datos se obtuvieron inversiones 2D las cuales luego fueron interpolados para permitir la visualización tridimensional de la posible mineralización. Interpretaciones basadas en la recopilación de datos geológicos y geofísicos, en asociación con el contexto estructural regional, sugieren que la probable mineralización se originó a partir de la intrusión del Granito São Sepé, cuyos fluidos hidrotermales se alojaron en fracturas durante los eventos tectónicos ocurridos en la región. Los resultados obtenidos en este trabajo permiten delinear una arquitectura de yacimiento factible con el contexto geológico de la región y ayudar a una futura estrategia de perforación dirigida a los objetivos probables identificados.

Palabras clave: Investigación mineral, Resistividad, Cargabilidad, Tomografía eléctrica, Oro.

Received: December 19, 2022; Accepted: July 26, 2023; Published on-line: October, 2023.

Editorial responsibility: Dr. Ambrosio Aquino López

* Corresponding author: Bruno Daniel Lenhare brunolenhare@gmail.com

¹ São Paulo State University (Universidade Estadual Paulista), Department of Geology, Av. 24A, 1515, CEP: 13506-900, Rio Claro (SP), Brazil.

² Universidade Federal do Pampa, Centro de Ciências Exatas e da Terra. Av. Pedro Anunciação, 111 Vila Batista 96570000 - Caçapava do Sul, RS - Brasil.

Bruno Daniel Lenhare, César Augusto Moreira, Lenon Melo Ilha

<https://doi.org/10.22201/igeof.2954436xe.2023.62.4.1454>

1. Introduction

The world demand for mineral resources has increased significantly in recent years and, on the other hand, the number of discoveries of new economically viable mineral deposits has decreased. The discovery of new mineral deposits means ensuring the provider of metallic and non-metallic goods to supply the current demand (Marjoribanks, 2010; Mostafaei & Ramazi, 2018). Giant mineral deposits have already been discovered over the course of the 20th century and new probable deposits are far from economic consumer centers, in places whose complex climatic and geological conditions require technology and large financial investments to detect or even exploit them.

The geophysical methods applied in prospecting and mineral research use the contrast of physical properties between the host rock and a potentially mineralized target and assist in the determination of new mineral deposits. DC resistivity (DC) and induced polarization (IP) are important survey techniques for mineral prospecting and enable fast and low cost surveys in mineral deposit studies (Chapman & Mortensen, 2016; Deng & Wang, 2016; Dentith & Mudge, 2014; Marjoribanks, 2010; Moon *et al.*, 2006; Zonge *et al.*, 2005). The use of automated geoelectric data acquisition systems, due to its versatility, has been widely disseminated to solve environmental, hydrological, geotechnical, and especially mineral research, in which a greater detail of the subsoil is sought. The low cost, high speed and wide area of data acquisition and good response in complex and heterogeneous geological environments has driven the use of this technique by several authors in the last decades and has been successful in determining targets (Amidu & Olayinka, 2006; Côrtes *et al.*, 2016; Dahlin & Loke, 1997; Gouet *et al.*, 2016; Griffiths & Barker, 1993).

Gold has high mobility in soils, especially in tropical regions, as is the case in the study area. The formation of some deposits depends on the mobility, transport, and precipitation

of gold in regions of strong weathering. The acquisition of geochemical data is also very important, since the high mobility of gold can lead to the concentration and generation of rich deposits (Biondi, 2015; Mann, 1984; Vasconcelos & Kyle, 1991). The association of geochemical and structural methods can direct the geoelectrical studies in the detection or detailing of targets and achieve the success in the investigation.

The southern center of Rio Grande do Sul state was an important mining province in the early 20th century. The mineralization of the São Sepé region, where the present study area is located, is associated with milky quartz lodes intruded in basic and metabasic rocks. The main deposits of gold were recognized in the mines of Bossoroca, Cerrito do Ouro, Passo da Juliana, Guardinha, Lavrinha, Viúva Guerra Durval and Estuque (Bettencourt, 1972; CPRM, 1995, 2014).

The presence of gold in the Santa Catarina Gabbro was indicated geochemical exploration in current sediments in recent fluvial sedimentary deposits conducted in previous geological and metalogenetic surveys (CPRM, 1995). Similar DC ($> 5,000 \Omega \cdot m$) and IP ($> 10mV/V$) values for this type of mineralization have been described in geophysical surveys carried out in the region by some authors and served as a basis for correlation in this work, and this shows that, in fact, the use of electrical methods are reliable for metals prospecting (Côrtes *et al.*, 2016; Moreira *et al.*, 2012, 2016; Moreira & Ilha, 2011).

2. Materials and Methods

Investigations in the study area started with detailed geological mapping and collection of structural data. Then, the acquisition of geophysical information was carried out. The equipment used in the geophysical survey was the Terrameter LS resistivity meter, manufactured by ABEM Instruments (Sweden), with a resolution of $1\mu V$ (ABEM, 2012). This equipment is calibrated for resistivity measurements by periodic

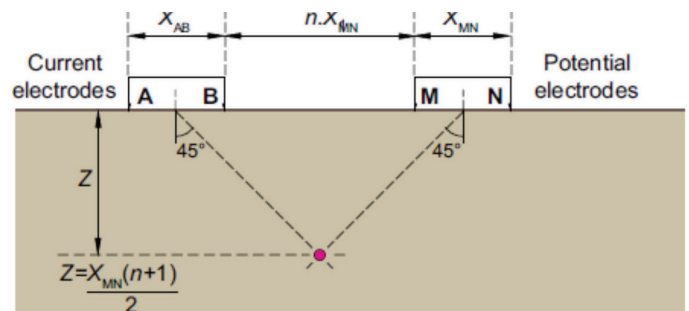
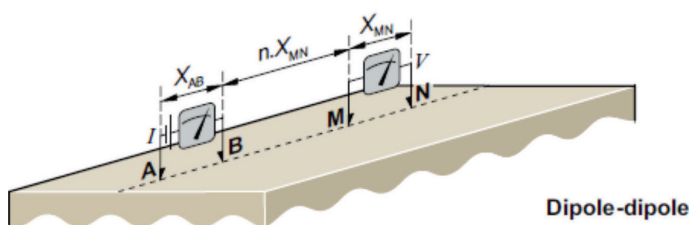


Figure 1. Sketch of the dipole-dipole array used in this study that was adapted from dipole-dipole array. Adapted from Keary (2009).

cycles of alternating and low frequency electrical current. This procedure allows the noise filtering of the acquired signal. Data was obtained by using the dipole-dipole arrangement and the methods of Electroresistivity and Induced Polarization (Dentith & Mudge, 2014). The dipole-dipole array presents good lateral resolution and good results in the identification of vertical structures, as it is the geological context of the study area (Moreira *et al.*, 2016; 2018; 2020; Cortês *et al.*, 2019). For the studied targets the dipole-dipole arrangement, associated with the geological and structural surveys carried out in the field, returned promising results with the geological reality of the mineralized bodies.

The dipole-dipole array is the most widespread among the several existing for the realization of electrical imaging. It consists of an arrangement widely used in mining, underground water prospecting, environmental studies and engineering geology (Telford *et al.*, 1990). In the dipole-dipole array the electrodes are arranged in lines and the spacing between the pairs of current and potential electrodes remains fixed during data acquisition. The data acquisition consists in obtaining several measurements, with fixed and equal spacing of the emission dipole (AB) and of the reception dipole (MN) (Figure 1).

During the acquisition of geophysical data, both resistivity and chargeability the arrangement is displaced “n” times the distance equal to the dipoles spacing. The measured value is then represented at a point on the surface located at the intersection of the lines that depart 45° from the center of the dipoles, positioned at the midpoint between them. Higher depths of investigation are achieved as the distance between the dipoles increases but limited by an acceptable value where that corresponds to the potential readings higher than the noise level present at the investigated site. By repeating this procedure, a pseudosection of apparent electrical resistivity is generated along the survey line (Coggon, 1973).

The geophysical data collected were processed using the software Res2Dinv (Geotomo, 2003). This software is able to analyze large data sets and to determine, based on inversion method, a two-dimensional model of resistivity and chargeability for the subsurface (Griffiths & Barker, 1993).

In the inversion process the pseudo section generated by the acquired data is represented by a mesh of rectangular equal area, each with its own resistivity (Milsom & Eriksen, 2011). The smoothing inversion method, used in this work, is based on the mathematical method of least squares, which aims to minimize the sum of the squares of errors between the model response and the observations. The RMS values are high, possibly due to the large contrast of values in each section. During the data acquisition period, which took place towards

the end of the rainy season, the contact resistance values were low consequently. Information regarding the topography and azimuth along each line were obtained by compass and a digital elevation model. The distance between the lines were determined using a measuring tape. In this way, the data processing considered the topographic adjustment and the inversion model.

The difference between the apparent resistivity values, measured in the field and calculated by the resistivity adjustment of the block model is expressed by the RMS error. The final data are presented in the form of sections of resistivity and chargeability in terms of distance versus depth, with a logarithmic graph scale and interpolation intervals of color values (Loke & Barker, 1996).

After the 2D inversion at each line, the generated data were collected in a single file, later used as a database for the generation of quasi 3D models and depth maps, using Oasis Montaj software (Geosoft, 2010).

The interpolation of the data for 3D visualization was performed using the kriging method, followed by the application of the statistical method of minimum curvature for smoothing the central values in relation to the extremities. The least curvature statistical method was used to solve the kriging border effect.

The ERT lines were set perpendicular to the main structures of the selected targets, allowing a greater contrast between the hosting rock and the structures like fractures and quartz veins, with emphasis on the mineralized zones. The main foliation of the rock is millimetric, penetrative and occurs in several directions, but there is a predominance for NW and NE, which are the main trends for the region, according to the literature (Biondi, 2015; CPRM, 1995; Jackson *et al.*, 1973).

3. Results and Discussion

3.1. Geologic and metallogenetic context

The Santa Catarina Gabbro is located at Sul-rio-grandense Shield (SRGS), which is a geotectonic unit located in the southern portion of the Mantiqueira Province, with predominance of metamorphic and sedimentary igneous rocks, in the south center of the state of Rio Grande do Sul, southernmost Brazil (Almeida *et al.*, 1981; Hasui *et al.*, 1975).

During the Neoproterozoic (~ 900-550 Ma) the SRGS was an important area of crustal accretion and reworking. The geochronological information indicates three main orogenic events: (i) crustal accretion phase with juvenile magmatism

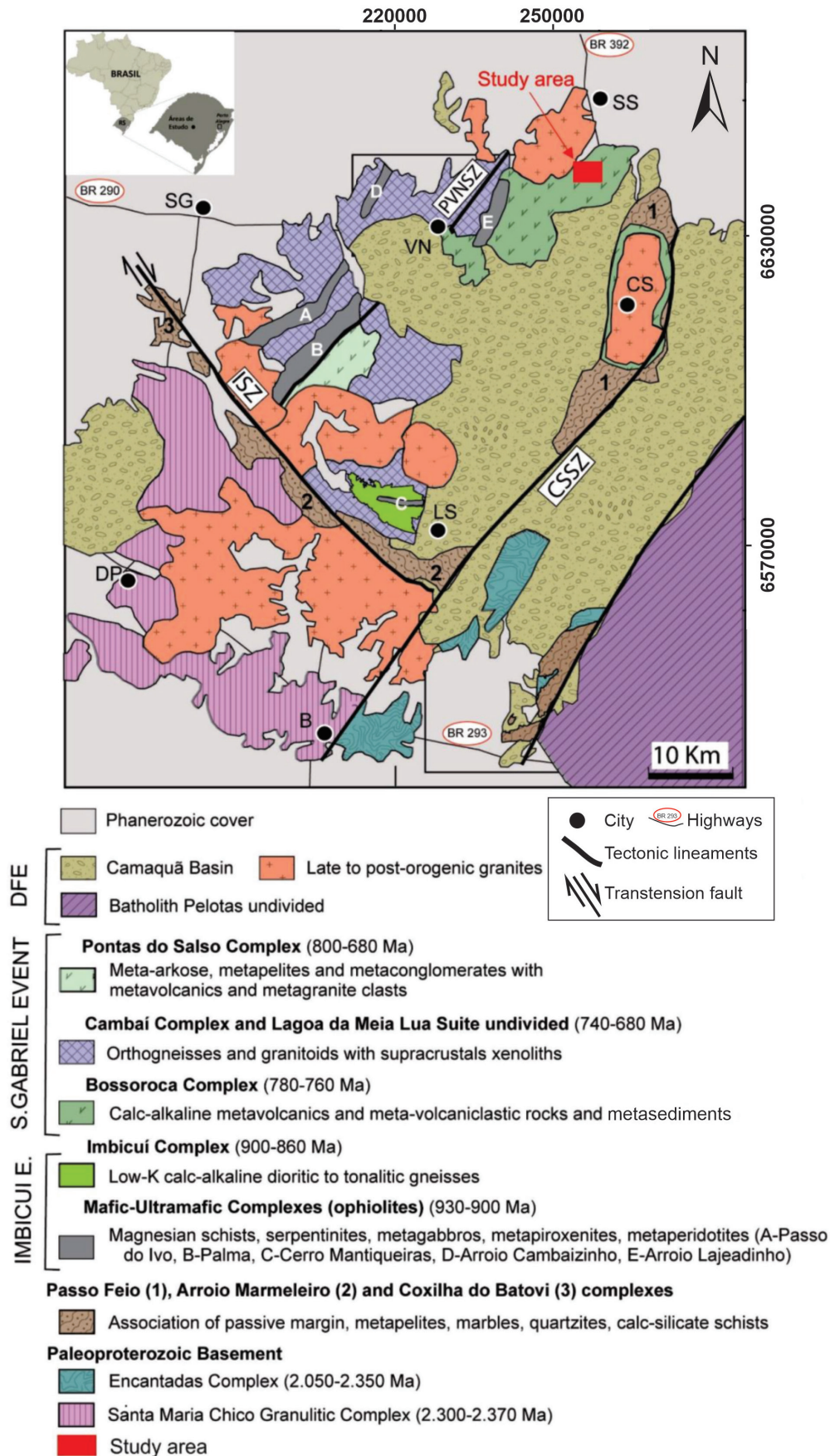


Figure 2. Regional geologic map. B: Bagé, CS: Caçapava do Sul, DP: Dom Pedrito, LS: Lavras do Sul, SG: São Gabriel, SS: São Sepé. Shear zones: SZPVN-Shear Zone Passinho/Vila Nova; SZI-Shear Zone Ibaré; SZCS-Shear Zone Caçapava do Sul (Philipp *et al.*, 2016).

between ca. 890 and 860 Ma; (ii) continental arc magmatism and accretion between ca. 770 and 680 Ma; (iii) collisional metamorphism between 650 and 620 and main magmatic phase between ca 650-550 Ma with a strong crustal anatexis caused by injection of magmas (Fragoso Cesar, 1991; Philipp *et al.*, 2016). The SRGS is limited by regional NE-SW lineaments and is divided in the terrains Taquarembó, São Gabriel (where the study area is located), Tijucas, Santana da Boa Vista and Pelotas (Andriotti, 1999; Fragoso Cesar, 1980; Fragoso Cesar *et al.*, 1982; Goñi *et al.*, 1962; Hartmann *et al.*, 2000; Pertille *et al.*, 2015; Philipp *et al.*, 2016).

The tectonic evolution in the SRGS indicates the closure of ancient oceans and the metamorphism of a sedimentary sequence (Bossoroca Metamorphic Complex) and marine bottom magmatism (Basic Metamorphic Ultrabasic Complex). The rocks of the Ultrabasic-Basic Metamorphic Complex show evidence of a genesis related to the sea bottom magmatism, possibly related to ophiolite sequences and reaction between basaltic magmas and peridotite rocks (Biondi, 2015; Philipp *et al.*, 2016).

Mineralized zones are not random geological accidents and devoid of connection with geological processes forming the earth's crust. The gold occurrences of Santa Catarina Gabbro probably were hosted in different portions and depths of that body by a specific post-magmatic event that produced heat in

sufficient quantity to cause the mineralized solutions to flow to the host rock, the gabbro (Hartmann *et al.*, 2000; Koppe, 1990; Skinner, 1997).

The Basic-Ultrabasic Stratigraphic Complex is composed of ultrabasic portions of serpentinized peridotites, pyroxenites, in variable proportions; and another basic portion that includes gabbros, leucogabbros and anortosites, related to intrusive and tectonic events dating from the Lower Proterozoic (Rêgo, 1981).

This unit is divided into two plutonic bodies: the Pedras Pretas Massif and the Santa Catarina Gabbro. Pedras Pretas Massif has its geological, petrological and geochemical details characterized in previous works (CPRM, 1995; Rêgo, 1981). Santa Catarina Gabbro was originally described by early authors and will be detailed below (Rodrigues *et al.*, 1982).

The contact relation between the Vacacaí Complex and the rocks of the Basic-Ultrabasic Stratigraphic Complex is controversial, since authors discuss whether the bodies are related to the evolution of the basic-ultrabasic metamorphites (Issler *et al.*, 1973; Koppe *et al.*, 1985) or if they are considered as belonging to the transamazonian base exposed in nuclei of dipole structures (Soliani Jr., 1986). For the Santa Catarina Gabbro, which has a considerable extension in depth according to the magnetometric profiles of the Camaquã Aerogeophysical Project (Jackson *et al.*, 1973), there is no evidence

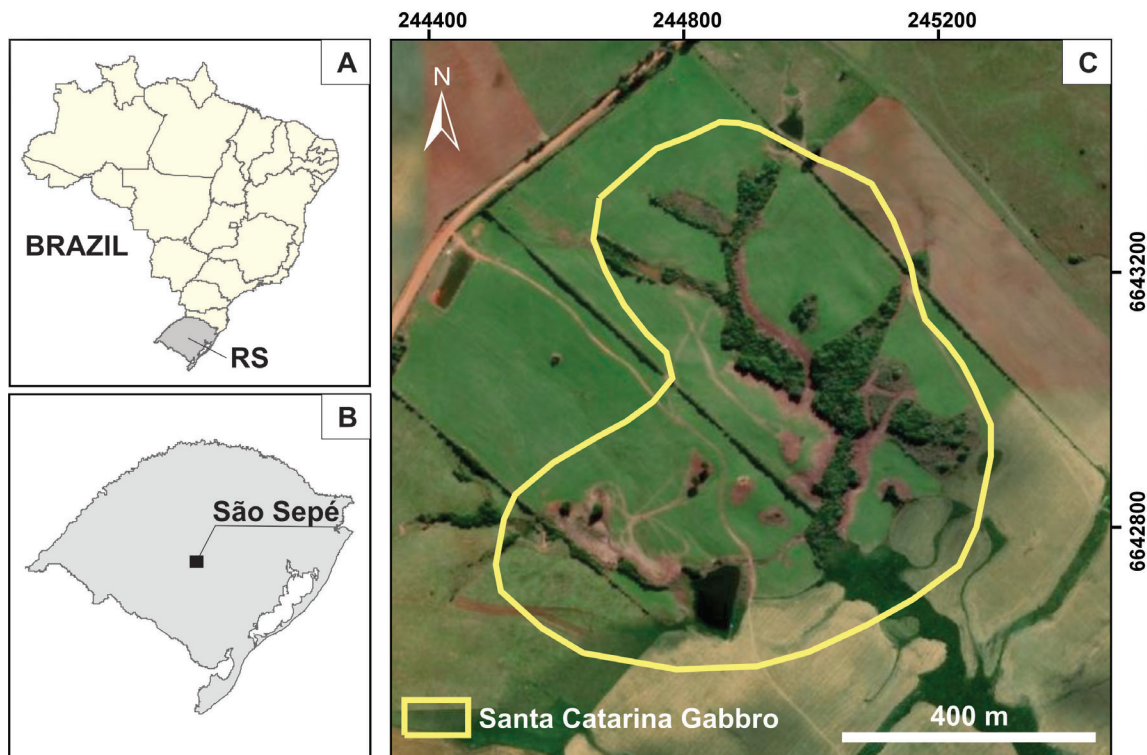


Figure 3. Localization of the study area.

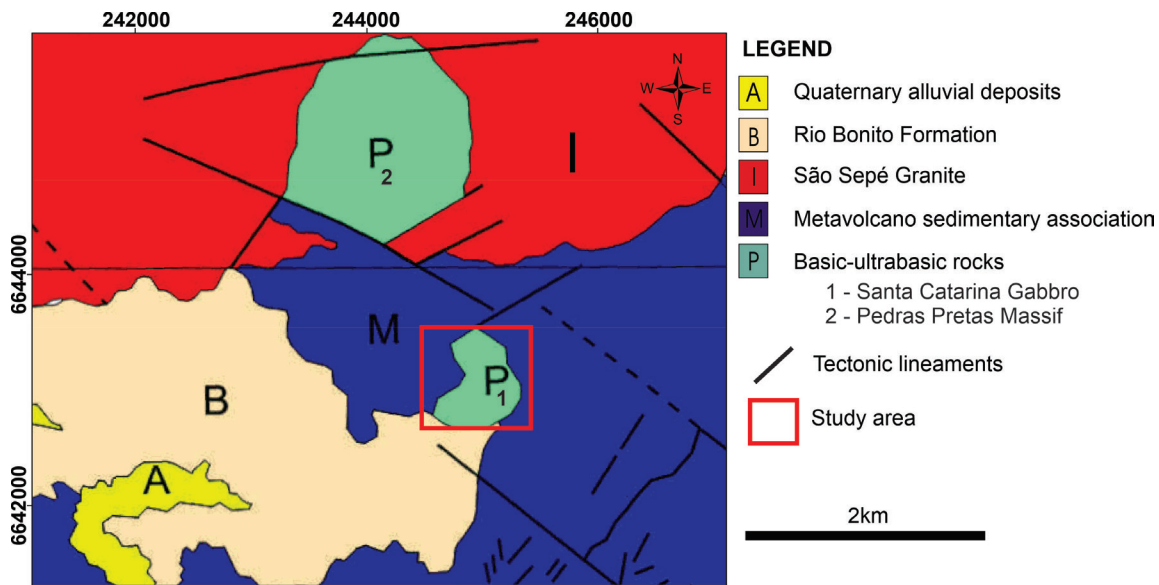


Figure 4. Local geologic map. Adapted from Andriotti (1999).

that it has been affected by the tangential deformation phases imposed on the rocks of the Vacacaí Complex.

Previous works correlate the Santa Catarina Gabbro with the Mata Grande Gabbro, whose adopted age is 2.2 Ga (CPRM, 1995; Rodrigues *et al.*, 1982). The relation of contact with the Pedras Pretas Massif is not clear, mainly due to the fact that these rocks are exposed in the form of blocks. However, in the ultrabasic nucleus in the southeastern portion of the Pedras Pretas Massif an intense fracturing is observed, which is the tectonic contact with Santa Catarina Gabbro. The Santa Catarina Gabbro exposed area covers 0.8 km² with outcrops of rounded boulders scattered across the field, whose dimensions reach up to one meter in diameter, and in slabs in drainage beds (Figure 4).

Due to the outcrop characteristics of this unit, it is difficult to visualize primary magmatic structures, although a fine irregular and discontinuous banding is observed, represented by the concentration of mafic minerals in levels of millimeter thickness. In the outcrops surveyed it was observed that the gabbro is quite fractured, whose directions predominate in the NNW direction.

Santa Catarina Gabbro mineralogy consists of plagioclase (45 to 80%), pyroxene (5%), opaque minerals (5%), apatite (2%), quartz (7%) and traces of alkali feldspar and zircon. The secondary mineralogy is composed of amphibole (30 to 50%), epidote (5%), chlorite (10%), sericite, carbonates, and secondary opaque (Rêgo, 1981; Rodrigues *et al.*, 1982).

The most common texture is the cumulate, with differentiated terms and unequigranular texture optic to subophic.

The structure of the rock is massive, equigranular of fine granulation to medium and dark coloration. Therefore, the above authors classify this unit as gabbros, diorites and quartz diorites (subordinates).

Although the Santa Catarina Gabbro is inserted in a context of a metamorphic belt, the mineralogical composition does not indicate that the rock has been affected by regional metamorphism and can be classified as a gabbro. The absence of deformations suggests that Santa Catarina Gabbro is an autochthonous body, of Transamazonian age (Sartori, 1978). By means of these data Santa Catarina Gabbro is nowadays understood as a tectonic window of an older basement, on which were lodged rocks of the Metavolcanic Sedimentary Belt.

The gold mineralizations of the São Sepé region are associated with milky quartz veins deposits and are intruded in basic and metabasic rocks that may correspond to tectonic imbrications of the Basic-Ultrabasic Metamorphic Complex. These deposits are recognized in the mines of Bossoroca, Cerrito do Ouro, Passo da Juliana, Guardinha, Lavrinha, Viúva Guerra Durval and Estuque (CPRM, 1995). It is suggested that the metalogenesis of the Bossoroca, Cerrito do Ouro and Passo da Juliana mines are classified as depth source orogenic hydrothermal deposits (Groves *et al.*, 1998; Remus, 1999).

The orogenic model was originally applied strictly to the syntectonic deposits formed in compressional or transpressional systems, that is, syn-orogenic deposits. However, the term has been progressively expanded to include deposits that are post-orogenic in relation to processes at their crustal depth of formation. The orogenic hydrothermal deposits occur in

all grades of metamorphic rocks, associated with accretion and collisional orogenic ages ranging from the Archaean to the Cenozoic. The hydrothermal source is derived from the juvenile crust at about 700 Ma during the dynamothermal regional metamorphism and TTG magmatism of the volcanic arc region, associated with extensional veins, from E-W to NW-SE directions, connected to the shear zone (Groves *et al.*, 1998).

The petrographic analysis of the Santa Catarina Gabbro shows that gold (Au) is not present in its mineralogical composition, however the geological and geochemical data show a potential area for Au \pm sulfides (Rêgo, 1981; Rodrigues *et al.*, 1982). Therefore, the gold may have been leached from the Vacacaí Metamorphic Complex, during the regional metamorphism phase, with reconcentration along the low angle shear zones, in the form of fractions and hydrothermal lodes.

There are no specific studies on the origin of the hydrothermal fluid and source of metals that originated the auriferous mineralizations in the gabbro, however, evidence of metamorphism in green shale facies above amphibolite as contact metamorphism (hornblende facies) generated by the intrusion of the São Sepé Granite, evidences that this was the source of heat responsible for the concentration of ore in the gabbro fractures (D'Ávila *et al.*, 1985).

Previous work on geochemical prospecting in current sediments identified the occurrence of 48 gold pints in a drainage that flows from Santa Catarina Gabbro (CPRM, 1995). After the publication of the results of that work, there was no further mineral research to delimit the probable occurrence of gold in the study site. The work of geological mapping and acquisition of geophysical survey was carried out to test the hypothesis that Santa Catarina Gabbro is the source rock and that there is a probable mineral deposit there (Figure 5).

3.2. Geological mapping and structural survey

Geological mapping and structural survey data indicated that Santa Catarina Gabbro has a massive structure with the presence of fractures (Figure 6). To evaluate the local structural pattern, 130 fracture measurements were taken. The fractures are arranged in different directions, but with families of fractures arranged according to the NNW direction. Then, it was possible to obtain a reliable statistic of the structural measures and to plot this information in the stereogram, using OpenStereo software (Grohmann & Campanha, 2010) (Figure 7). These fractures may be related to a crustal relaxation phase

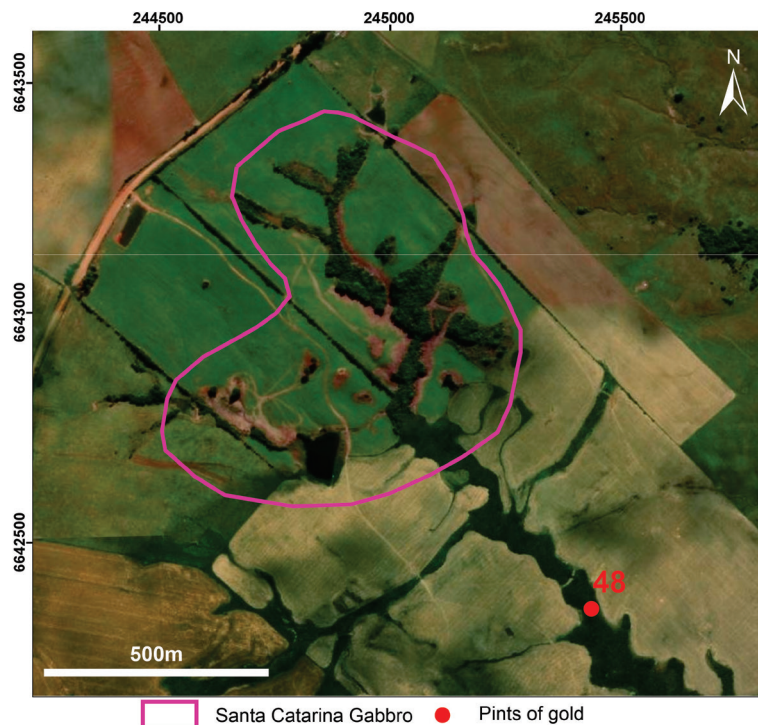


Figure 5. The numbered points are the places where gold pints were found in geochemistry of current sediments and pan concentrate. The number indicates the amount of gold pints found in each location (CPRM, 1995).

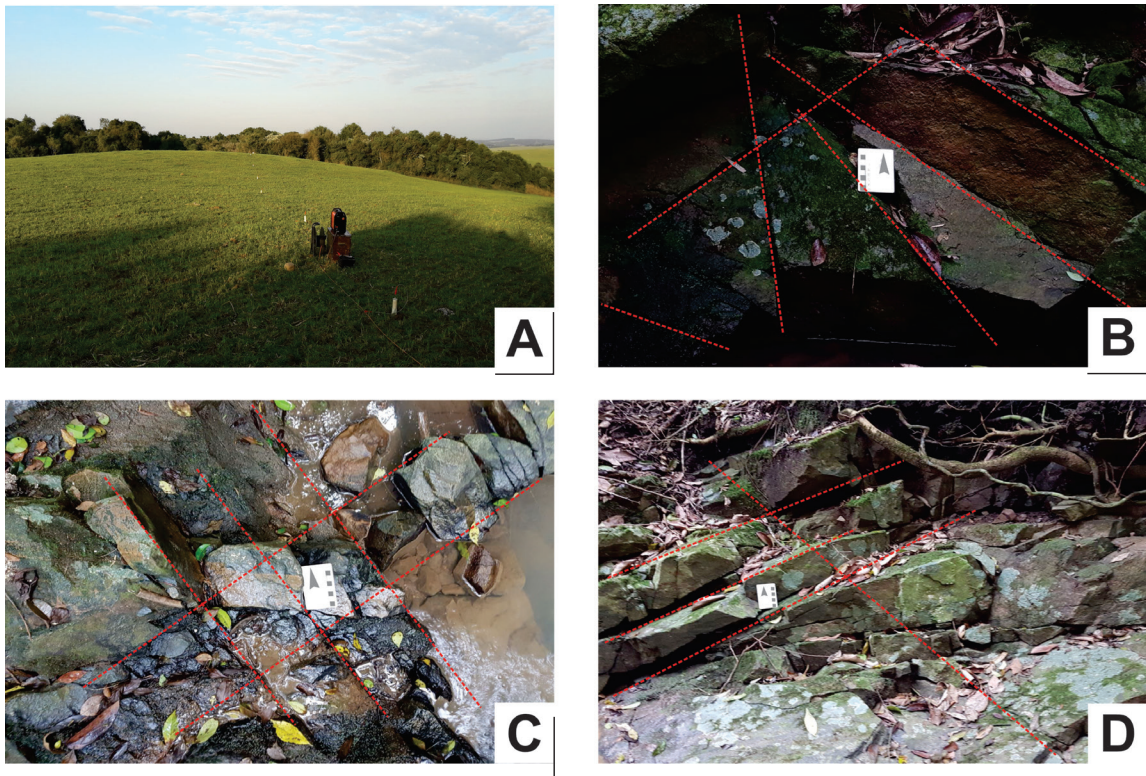


Figure 6. A: predominant land cover in the study area (pastures); b, c and d: Santa Catarina Gabbro outcrops with presence of fractures, with predominance of the NE-SW and NW-SE directions (the arrow direction of the card in the photo is to the north).

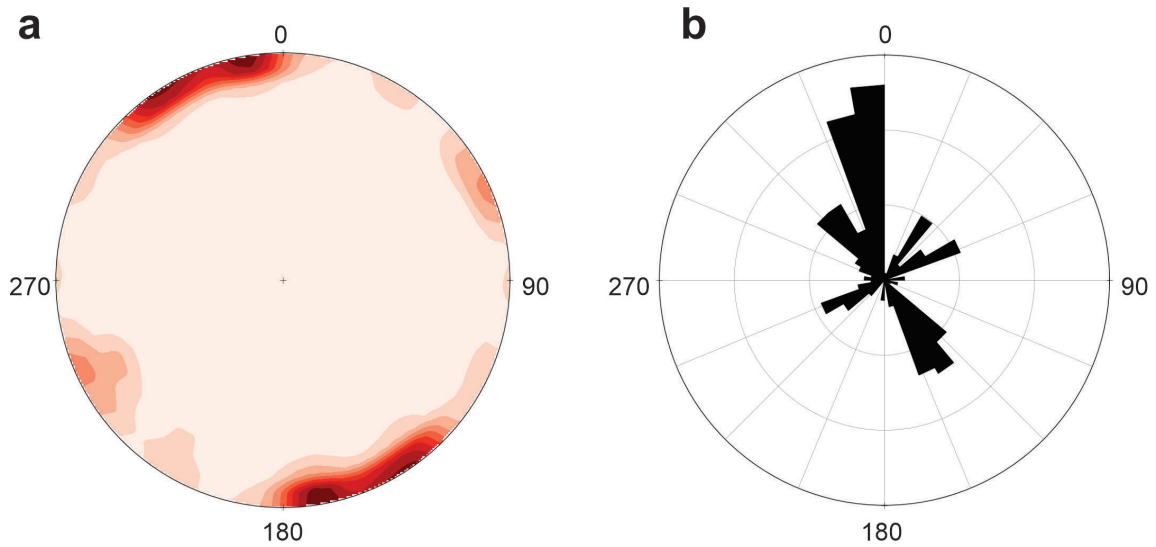


Figure 7. Stereogram of the main directions of the Santa Catarina Gabbro fractures.

after the intrusion of the Caçapava and São Sepé granites and probably acted as preferred paths for metasomatic liquids of the probable mineralization. The study of the structural arrangement for ore prospecting is fundamental for planning the distribution of electrical tomography lines, since previous works show that the gold mineralizations in the region are associated with fractures (Moreira *et al.*, 2012). From this information, the electrical tomography lines were distributed in a E-W direction.

3.3. Geophysical survey

The geophysical survey consisted of 5 parallel lines of electrical tomography each with 400 meters of length spaced 100 meters and with 10 meters electrode spacing heading N90, and 10 levels readings of electrical resistivity and chargeability (Figure 8).

Petrography works did not detect primary gold in the original chemical composition of the Santa Catarina Gabbro, therefore, the anomalies can be attributed to the strong polarization of structures and can be interpreted as high concentrations of metallic minerals probably distributed in

fractures (D'Ávila *et al.*, 1985; Rodrigues *et al.*, 1982).

The analysis of the resistivity models allows to discriminate areas of low resistivity ($<35 \Omega.m$) in the central domain of the sections, possibly associated with percolation of water in preferred flow paths. The resistivity is inversely proportional to the salinity of water, as the dissolved salts act as a pathway for electric current flow. In the field was recognized a high angle foliation in the central band of electrical tomography lines, besides fracturing in several points. Such structures can serve as preferential percolation zones of meteoric waters, whose interaction with amphiboles and pyroxenes results in hydration and generation of clay minerals. This process results in water saturated alteration zones which justifies the characteristic of low resistivity observed in practically all sections (Delgado-Rodríguez *et al.*, 2014).

The 2D inversion models show that the spatial distribution of the contrast values for the explored levels is not uniform, with zones of low resistivity and high chargeability in the form of rounded or elliptical pockets throughout the sections and at various levels of depth. Specific ranges of resistivity values (between $0.5 \Omega.m$ and $10,000 \Omega.m$) and chargeability (between 0.01 mV/V and 20.0 mV/V) were selected for

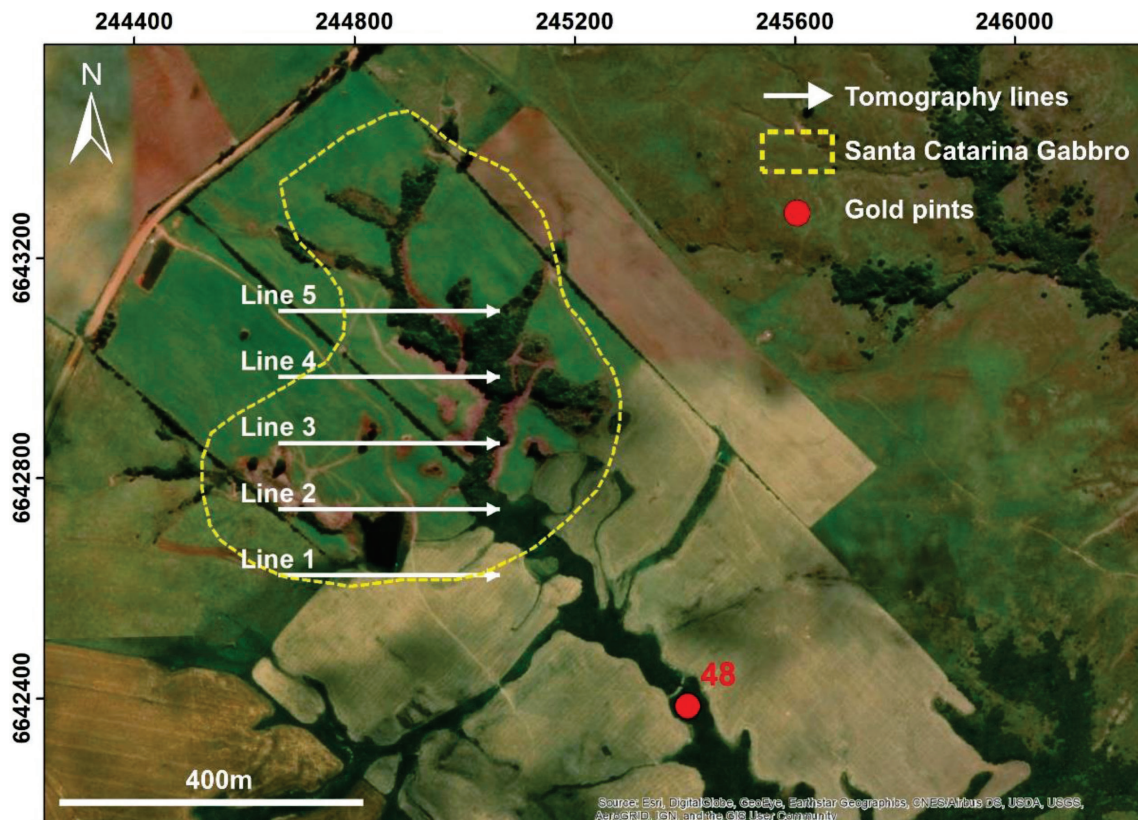


Figure 8. Location of the electric tomography with the direction N90°E.

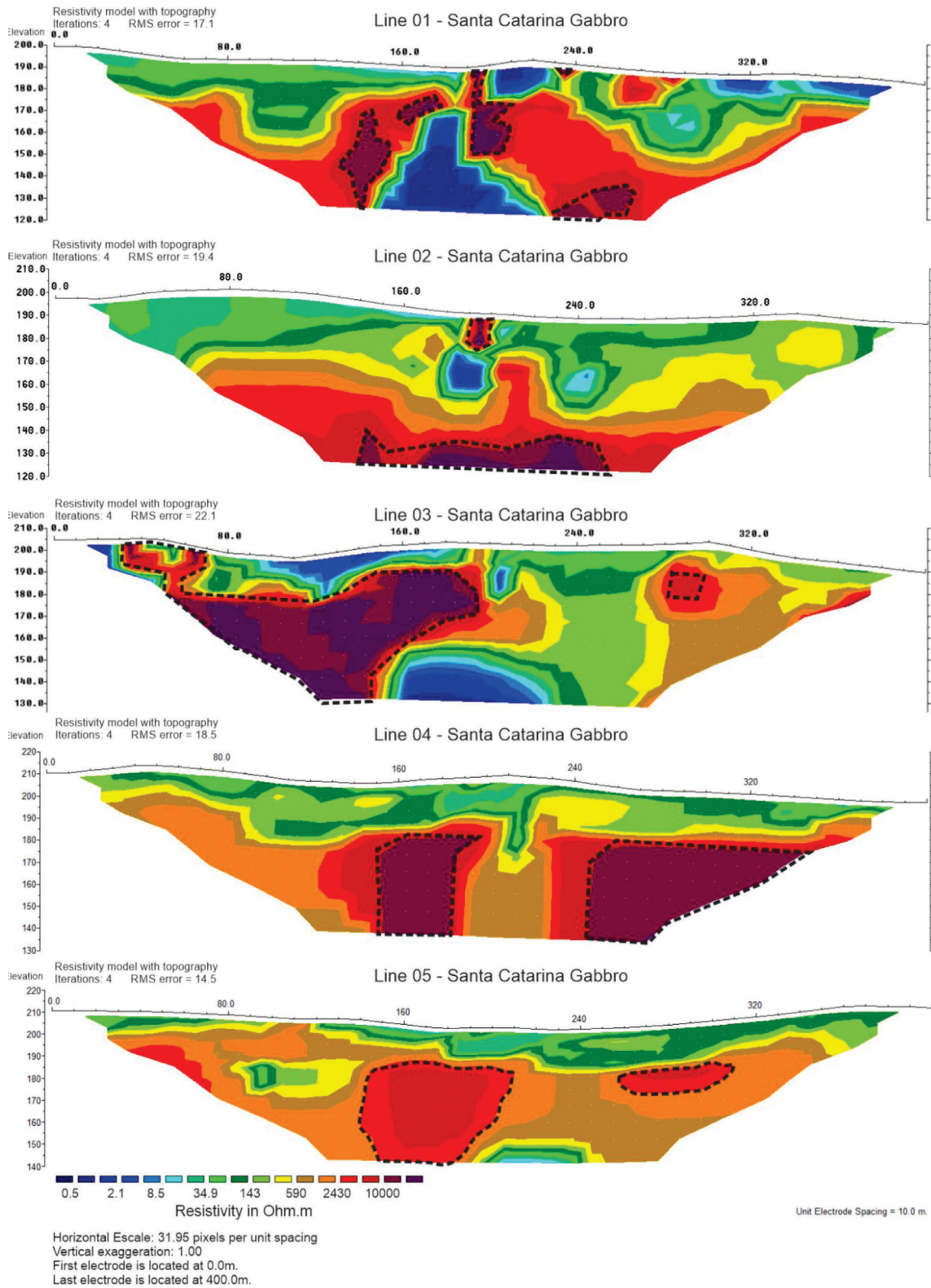


Figure 9. Inversion models for resistivity (ER).

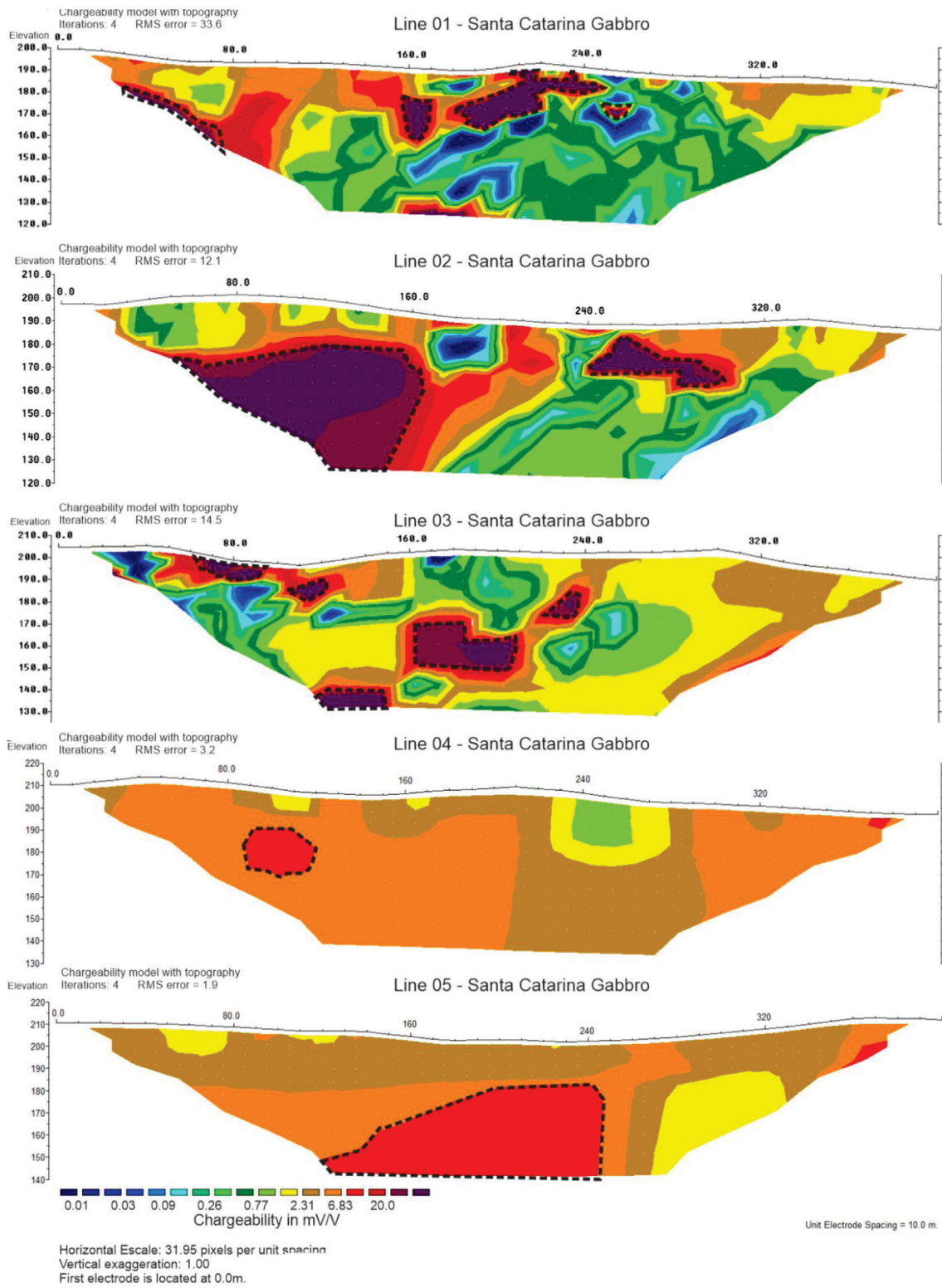


Figure 10. Inversion models for chargeability (ER) High chargeability values are marked.

modeling in the form of 3D visualization model surfaces, to evaluate the forms of zones of resistivity and chargeability anomalies (Figures 9 and 10).

The analysis of the 2D inversion models also indicate zones of high resistivity ($> 10.000 \Omega.m$), both in deep and outcrop positions. In the field, gabbro boulders were observed, which justifies the high resistivity and, therefore, the regions of high resistivity located in depth should then be analogous and represent the rocky massif (probably with some degree of silicification and some late quartz veins). Likewise, the inversion models for chargeability show gradients that represent a possible mineralized structure, with areas of high chargeability disposed in most extension of the sections, with gradients higher than 20 mV/V, not necessarily coincident with areas of low resistivity.

The mineralization was hosted in the gabbro through several tectonic events, and the difference of chargeability between these and the host rock were detected in the inversion models. Similar values were acquired for this scenario and served as a basis for correlation in this work (Moreira *et al.*, 2012).

Several evidence support the concept that Au is mobile as dissolved or colloidal complexes in surficial environments. Several studies have found elevated dissolved Au concentrations in the vicinity of Au mineralization (Hamilton *et al.*, 1983; Xie *et al.*, 1987). Therefore, according to the authors above mentioned, near-surface chargeability anomalies may refer to gold mineralization, which, although deep-hosted associated with quartz veins, migrated to shallower levels given the mobility properties of the metal.

However, these anomalies correlates with earlier works where the authors describe the occurrence of gold pints (between 7 and 48 pints), magnetite (80% by volume of concentrate) and pyrite (CPRM, 1995). Similar IP values for this type of mineralization were described in another geophysical survey carried out in the region by some authors and served as a basis for correlation in this work (Moreira & Ilha, 2011).

The distorted form of field propagation of the dipole-dipole array is effective in the detection in verticalized structures. The size and shape analysis of the potentially mineralized zones and the 2D inversion models were combined in 3D visualization models, in association with the structural data collected in the field. From the blocks with interpolated resistivity surfaces, isovalues surfaces were modeled for each block, representative of the acquisition array, which may reveal structures and the possible mineralization architecture (Figures 11 and 12).

After the discrimination of regions of high chargeability and low resistivity, obtained from the interpolation of

those acquired in the pseudo-sections, the information was correlated to stablish locations with overlapping of these values, which may indicate the occurrence of a mineralized zone (Figure 12).

The humid tropical climate of Brazil favors the chemical weathering of rocks and the consequent formation of residual soil. This weathering can reach depths of a few tens of meters and act on the mineralized zone, as is the case of the study area. The natural evolution of the relief, associated with the humid climate, the formation of soil by the breakdown of rock and mineralized zone can favor the incorporation of gold nuggets in the soil. Erosion and surface water runoff acting in this location can condition the transport of gold particles to the following region's drainages.

The information on the localization of possible gold mineralization from the three-dimensional visualization model, allows to indicate on map probable occurrences on a map that could be useful in the stage of establishing strategies for a future drilling campaign. The following mineralization localization map integrate geoelectric, geological and structural information for Santa Catarina Gabbro, described along this work and it can lead to the localization of the main occurrences of gold in the region. (Figure 13).

Conclusions

Previous work on geochemical prospecting in stream sediments found an attractive amount of gold pints, which lead to suggest that Santa Catarina Gabbro could be the source rock for gold mineralization (Rodrigues *et al.*, 1982). This work gathered geological, structural, and geophysical information that aimed to test this hypothesis.

Geological reconnaissance in the Santa Catarina Gabbro area allowed the description of a basic rock whose structure is relatively simple, composed of fractures in some preferred directions. The gabbro petrography analyses indicated the absence of gold in its composition; therefore, the ore possibly is hosted in fractures, or possible quartz veins that are further introduced in the rock.

The geophysical information associated to the data collected in the geological reconnaissance, allowed the imaging of structures contrasting with the physical parameters, closely related to the tectonic elements of a deposit. It also allowed the delimitation of a possible sulphide mineralization in depth and marginal silicification zones, characterized by low resistivity and high chargeability anomalies. These results are consistent with those described in works reported in the academic journals.

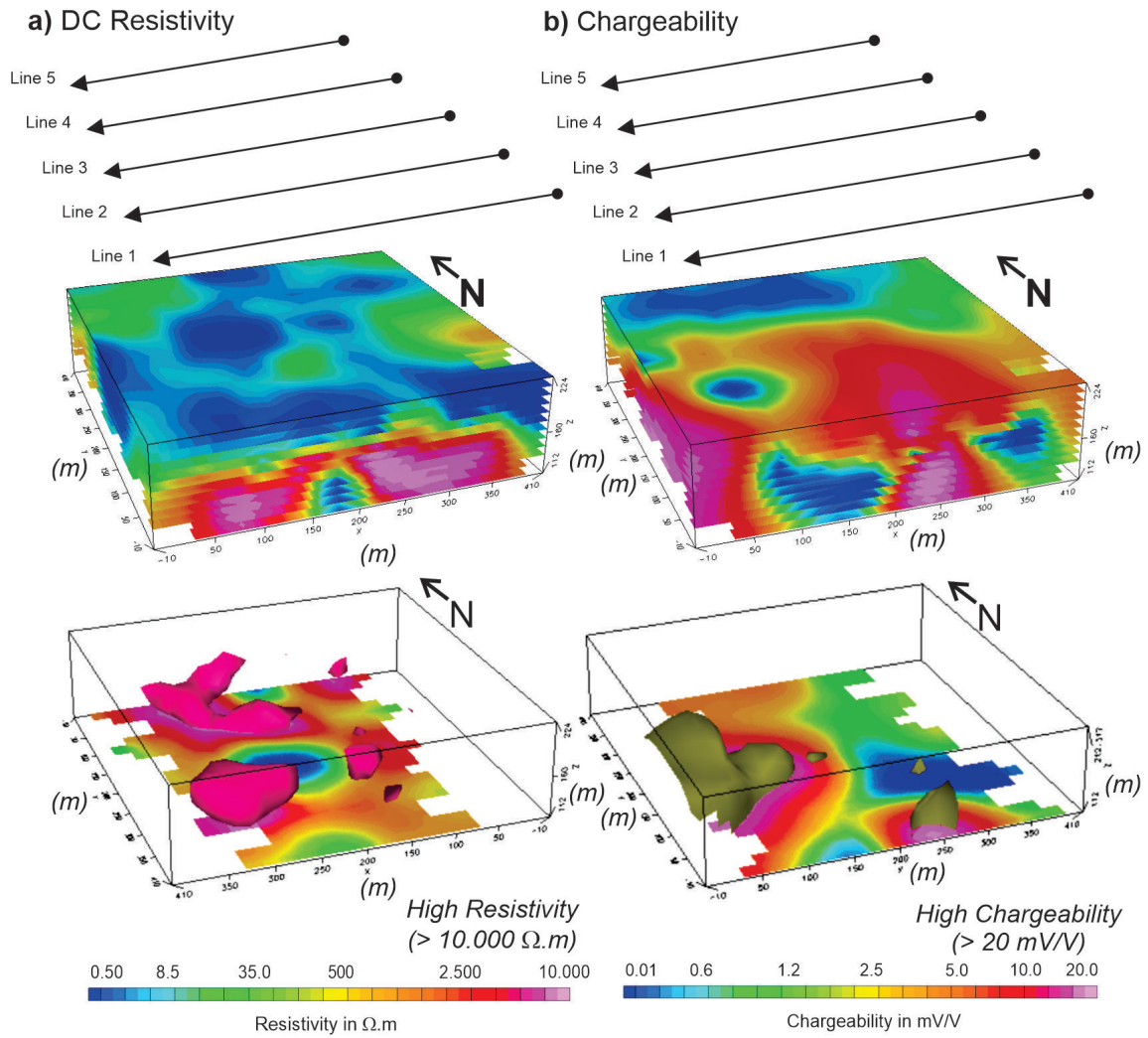


Figure 11. a) 3D visualization (upper panel of resistivity distribution), and bodies with resistivities > 10,000 Ohm.m. b) Chargeability distribution (upper panel), and isosurface with a chargeability of 29 mV/V (lower panel).

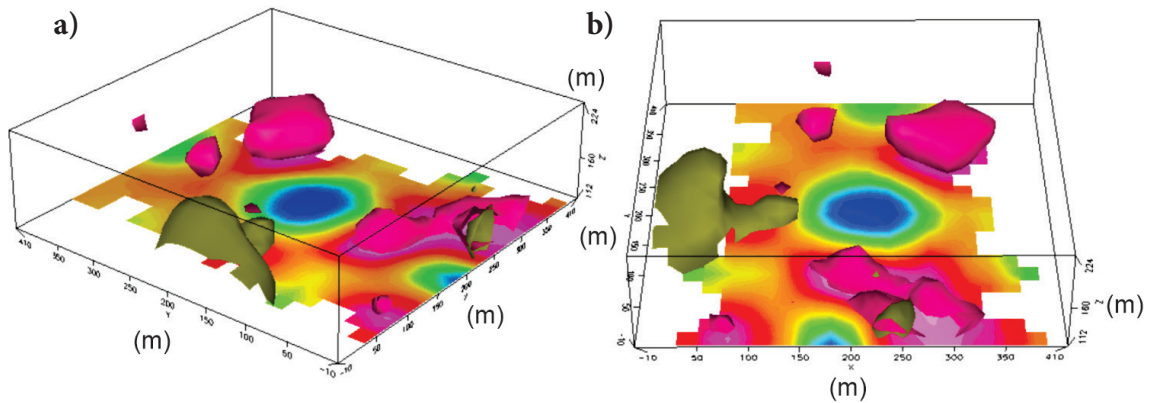


Figure 12. a) 3D view where high resistivity (> 10,000 Ohm.m) and high chargeability (> 20 mV/V), b) Rotated 3D view shown in a).

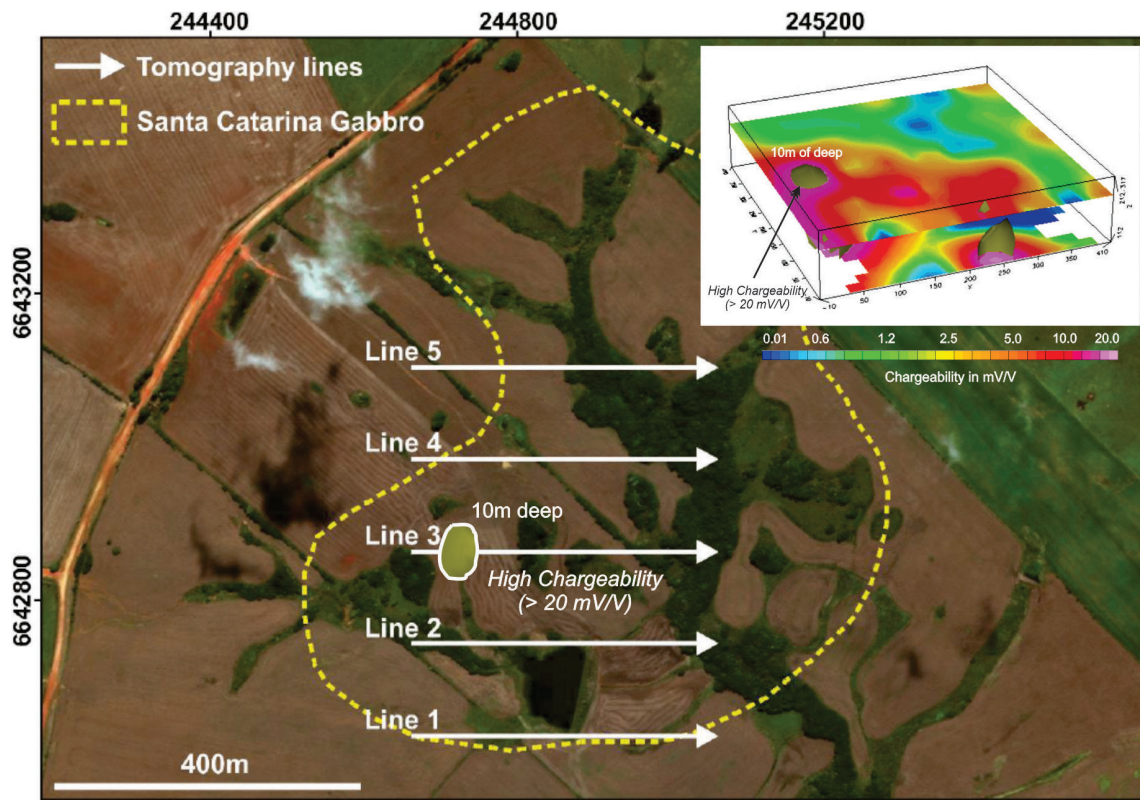


Figure 13. Position of the shallow high chargeability area (10m deep) in the study area.

The humid tropical climate of Brazil favors the chemical weathering of rocks and the consequent formation of residual soil. This weathering can reach depths of a few tens of meters and act on the mineralized zone, as is the case of the study area. The natural evolution of the relief, associated with the humid climate, the formation of soil by the breakdown of rock and mineralized zone can favor the incorporation of gold nuggets in the soil. Erosion and surface water runoff acting in this location can condition the carriage of gold particles to the region's drainages.

The analysis and interpretation of the results were based on the regional geological evolution, structural context and metallogenesis of the deposits, which resemble the occurrences of Bossoroca and Cerrito do Ouro, which are deactivated mines, but which explored deposits of hydrothermal origin. The occurrence of sulfide mineralization with associated gold comes from hydrothermal fluids from the intrusion of the São Sepé Granite. This regional metallogenetic context gave rise to small volume bodies, but with great potential for high levels of gold.

From the analysis and interpretation of 2D inversion models and 3D visualization acquired in the geophysical survey, it is understood that the dipole-dipole arrangement is

suitable for this study, as it presents good resolution of rock structures, such as fractures.

The results allowed the three-dimensional determination of the morphology of the possible sulphide mineralizations, through the integration of geoelectric and structural data. However, the confirmation of the targets requires research work with the use of direct investigation methods, such as, for example, drilling campaigns and collection of samples and further geochemical analysis. The information obtained in this work reveals that the probable mineralizations present a structural control, whose disposition in depth is conditioned by fractures attitudes.

These results make possible to outline a strategy for a drilling campaign directed at the targets identified, with reduction of uncertainties, which is decisive in terms of an adequate quantification of reserves and economic feasibility of mineral occurrences and are incentives for the use of geoelectrical methods.

Acknowledgments

The authors are thankful to Geology Department at São

Paulo State University, Rio Claro—SP, for the technical support.

Conflicts of Interest

“The authors declare no conflict of interest.”

References

- ABEM. (2012). *Terrameter LS - Instruction Manual*. Sundyberg: ABEM Instruments.
- Almeida, F. F. M. de, Hasui, Y., Brito Neves, B. B. de, & Fuck, R. A. (1981). Brazilian structural provinces: An introduction. *Earth-Science Reviews*, 17, 1–21. [https://doi.org/10.1016/0012-8252\(81\)90003-9](https://doi.org/10.1016/0012-8252(81)90003-9)
- Amidu, S. A., & Olayinka, A. I. (2006). Environmental assessment of sewage disposal systems using 2D electrical-resistivity imaging and geochemical analysis: A case study from Ibadan, 2 Southwestern Nigeria. *Environmental and Engineering Geoscience*, 12(3), 261–272. <https://doi.org/10.2113/gseegeosci.12.3.261>
- Andriotti, J. L. S. (1999). *Interpretação e modelamento de dados geoquímicos e de sensoriamento remoto por meio da análise de componentes principais: implicações na exploração de depósitos de metais no escudo sul-rio-grandense*. Universidade Federal do Rio Grande do Sul.
- Bettencourt, J. S. (1972). *A mina de cobre de Camaquã, Rio Grande do Sul*. Universidade de São Paulo.
- Biondi, J. C. (2015). *Processos metalogenéticos e os depósitos minerais brasileiros* (Atual (ed.); 2nd ed.). Oficina de Textos.
- Chapman, R. J., & Mortensen, J. K. (2016). Characterization of gold mineralization in the northern Cariboo gold district, British Columbia, Canada, through integration of compositional studies of lode and detrital gold with historical placer production: A template for evaluation of orogenic gold. *Economic Geology*, 111(6), 1321. <https://doi.org/10.2113/econgeo.111.6.1321>
- Coggon, J. H. (1973). A comparison of IP electrode arrays. *Geophysics*, 38(4), 737. <https://doi.org/10.1190/1.1440372>
- Côrtes, A. R. P., Moreira, C. A., Veloso, D. I. K., Vieira, L. B., & Bergonzoni, F. A. (2016). Geoelectrical prospecting for a copper-sulfide mineralization in the Camaquã sedimentary basin, Southern Brazil. *Geofísica Internacional*, 55(3), 55–58. <https://doi.org/10.19155/rgi20165531608>
- CPRM. (1995). *Programa Levantamentos Geológicos Básicos do Brasil. Folha Passo do Salsinho SH.22-Y-A-I-4. Escala 1:250.000*.
- CPRM. (2014). *Metalogênese das províncias tectônicas brasileiras* (M. da G. da Silva, M. B. da R. Neto, H. Jost, & R. M. Kuyumjian (eds.)).
- D'Ávila, R. S. F., Strieder, A. J., Loss, E. L., & Hartmann, L. A. (1985). Reavaliação de alguns aspectos petrológicos e geoquímicos do Complexo Básico-Ultrabásico de Pedras Pretas (RS). *SBG - Atas*, 2, 277–286.
- Dahlin, T., & Loke, M. H. (1997). Quasi-3D resistivity imaging - mapping of three dimensional structures using two dimensional DC resistivity techniques. *3rd EEGS Meeting*. <https://doi.org/10.3997/2214-4609.201407298>
- Delgado-Rodríguez, O., Flores-Hernández, D., Amezcua-Allieri, M. A., Shevnin, V., Rosas-Molina, A., & Marin-Córdova, S. (2014). Joint interpretation of geoelectrical and volatile organic compounds data: A case study in a hydrocarbons contaminated urban site. *Geofísica Internacional*, 53(2), 183–198.
- Deng, J., & Wang, Q. (2016). Gold mineralization in China: Metallogenic provinces, deposit types and tectonic framework. *Gondwana Research*, 36(219–274). <https://doi.org/10.1016/j.gr.2015.10.003>
- Dentith, M., & Mudge, S. (2014). Geophysics for the mineral exploration geoscientist. In *AusIMM Bulletin*. Cambridge University Press.
- Fragoso Cesar, A. R. S. (1980). *O Cráton do Rio de La Plata e o Cinturão Dom Feliciano no Escudo Sul-Riograndense*. (5).
- Fragoso Cesar, A. R. S. (1991). *Tectônica de Placas no Ciclo Brasileiro: As orogenias dos Cinturões Dom Feliciano e Ribeira no Rio Grande do Sul*. Universidade de São Paulo, São Paulo.
- Fragoso Cesar, A. R. S., Wernick, E., & Soliani Jr., E. (1982). *Evolução geotectônica do Cinturão Dom Feliciano, uma contribuição através da aplicação do modelo de tectônica de placas*. (No. 1).
- Geológico, S., & Brasil, D. O. (2014). *Geologia E Recursos Minerais Da Folha Viçosa **. In *Programa Geologia do Brasil (PGB). Levantamentos Geológicos Básicos, escala 1:100.000*. CPRM.
- Geosoft, I. (2010). *Oasis montaj™ Research Advanced Version 7.2* (Version 7.2).
- Geotomo, S. (2003). *Rapid 2D resistivity and IP inversion using the least-square method - Geoelectrical Imaging 2-D and 3D* (p. 129).
- Goñi, J. C., Goso, H., & Issler, R. S. (1962). Estratigrafia e geologia econômica do pré-cambriano e eopaleozóico uruguaio e sul-riograndense. *Revista Da Escola de Geologia*, 3, 1–105.
- Gouet, D. H., Assemble, S. P., Meying, A., Bialou, M. B., Haskandi, J. K., & Ndougsa-Mbarga, T. (2016). Combined Geoelectrical Approach DC and IP Methods in the Identification of the Mineralized Bodies Parallel to the NE-SW Tectonic Line of Kadei River: Case of Quartz or Pegmatite Gold Bearing Veins of Ngoura Subdivision (East Cameroon). *International Journal of Geosciences*, 6(6), 891–903. <https://doi.org/10.4236/ijg.2016.77066>
- Griffiths, D. H., & Barker, R. D. (1993). Two-dimensional resistivity imaging and modelling in areas of complex geology. *Journal of Applied Geophysics*, 29(3–4), 211–226. [https://doi.org/10.1016/0926-9851\(93\)90005-J](https://doi.org/10.1016/0926-9851(93)90005-J)
- Grohmann, C. H., & Campanha, G. A. (2010). OpenStereo: Open Source, Cross-Platform Software for Structural Geology Analysis. *2010 Fall Meeting, AGU, San Francisco, Calif., 13-17 Dec*.
- Groves, D. I., Goldfarb, R. J., Gebre-Mariam, M., Hagemann, S. G., & Robert, F. (1998). Orogenic gold deposits: a proposed classification

- in the context of their crustal distribution and relationship to other gold deposit types. *Ore Geology Reviews*, 13(1–5), 7–27. [https://doi.org/10.1016/S0169-1368\(97\)00012-7](https://doi.org/10.1016/S0169-1368(97)00012-7)
- Hamilton, T., Ellis, J., Florence, T., & Fardy, J. (1983). Analysis of gold in surface waters of Australian goldfields: An investigation into direct hydrogeochemical prospecting for gold. *Economic Geology*, 78, 1335–1341.
- Hartmann, L. A., Porcher, C. C., & Remus, M. V. D. (2000). Evolução das Rochas Metamórficas do Rio Grande do Sul. In M. HOLZ & L. F. DE ROS (Eds.), *Geologia do Rio Grande do Sul* (pp. 79–118). Universidade Federal do Rio Grande do Sul.
- Hasui, Y., Carneiro, C. dal R., & Coimbra, A. M. (1975). The Ribeira Folded Belt. *Revista Brasileira de Geociências*, 5, 257–266. <https://doi.org/10.25249/0375-7536.1975257266>
- Issler, R. S., Dresch, R. A. C., & Roisenberg, A. (1973). Geocronologia do Gabro de Mata Grande Município de São Sepé Estado do Rio Grande do Sul. *Revista Brasileira de Geociências*, 3, 124–127.
- Jackson, V. N., Ramos, V. A., Terry, S. A., & Zuzek, A. B. (1973). *Projeto aerogeofísico Camaquã Estado do Rio Grande do Sul*. <http://rigeo.cprm.gov.br/jspui/handle/doc/7075>
- Kearey, P., Brooks, M., & Hill, I. (2009). *Geofísica de Exploração*. Oficina de Textos.
- Koppe, J. C. (1990). *Metalogênese do ouro na mina da Bossoroca São Sepé – RS*. Universidade Federal do Rio Grande do Sul.
- Koppe, J. C., Hartmann, L. A., Lisboa, P., & Monteiro, R. N. (1985). *Aspectos geológicos e estratigráficos do Complexo Bossoroca São Sepé RS*.
- Loke, M. H., & Barker, R. D. (1996). Practical techniques for 3D resistivity surveys and data inversion 1. *Geophysical Prospecting*, 44, 131–152. <https://doi.org/10.1111/j.1365-2478.1996.tb00162.x>
- Mann, A. W. (1984). Mobility of gold and silver in lateritic weathering profiles: some observations from Western Australia. *Economic Geology*, 79(1), 38–49. <https://doi.org/10.2113/gsecongeo.79.1.38>
- Marjoribanks, R. (2010). Geological methods in mineral exploration and mining. In *Geological Methods in Mineral Exploration and Mining*. <https://doi.org/10.1007/978-3-540-74375-0>
- Milsom, J., & Eriksen, A. (2011). Field Geophysics, 4th ed. In *The geological field guide series*. A John Wiley and Sons, Ltd., Publication. <https://doi.org/10.1002/9780470972311>
- Moon, C. J., Whateley, M. E. G., & Evans, A. M. (2006). *Introduction to Mineral Exploration*. Blackwell.
- Moreira, C. A., & Ilha, L. M. (2011). Prospecção geofísica em ocorrência de cobre localizada na bacia sedimentar do Camaquã (RS). *Rem: Revista Escola de Minas*, 64(3), 305–311. <https://doi.org/10.1590/s0370-44672011000300008>
- Moreira, C. A., Lapola, M. M., & Carrara, A. (2016). Comparative analyzes among electrical resistivity tomography arrays in the characterization of flow structure in free aquifer. *Geofísica Internacional*, 55(2), 55–57.
- Moreira, C. A., Lopes, S. M., Schweig, C., & Seixas, A. da R. (2012). Geoelectrical prospection of disseminated sulfide mineral occurrences in Camaquã Sedimentary Basin, Rio Grande do Sul State, Brazil. *Revista Brasileira de Geofísica*, 30(2), 169–179. <https://doi.org/10.22564/rbgf.v30i2.90>
- Mostafaei, K., & Ramazi, H. (2018). Compiling and verifying 3D models of 2D induced polarization and resistivity data by geostatistical methods. *Acta Geophysica*, 66, 959–971. <https://doi.org/10.1007/s11600-018-0175-5>
- Pertille, J., Hartmann, L. A., Philipp, R. P., Petry, T. S., & de Carvalho Lana, C. (2015). Origin of the Ediacaran Porongos Group, Dom Feliciano Belt, southern Brazilian Shield, with emphasis on whole rock and detrital zircon geochemistry and U-Pb, Lu-Hf isotopes. *Journal of South American Earth Sciences*. <https://doi.org/10.1016/j.jsames.2015.09.001>
- Philipp, R. P., Pimentel, M. M., & Chemale Jr, F. (2016). Tectonic evolution of the Dom Feliciano Belt in Southern Brazil: Geological relationships and U-Pb geochronology. *Brazilian Journal of Geology*. <https://doi.org/10.1590/2317-4889201620150016>
- Rêgo, I. T. S. F. (1981). Aspectos petrológicos e geoquímicos do Complexo Básico-Ultrabásico de Pedras Pretas, Rio Grande do Sul. *Acta Geológica Leopoldensia*, 5, 197–278.
- Remus, M. V. D. (1999). *Metalogênese dos Depósitos Hidrotermais de Metais Base e Au do Ciclo Brasileiro do Bloco São Gabriel, RS*. Universidade Federal do Rio Grande do Sul.
- Rodrigues, C. R. O., Bennedetti, O. J., & Strohschoen, J. R. O. (1982). *Geologia da Faixa II da Folha Passo do Salsinho, RS*.
- Sartori, P. L. P. (1978). *Petrografia do Complexo Granítico de São Sepé, RS: modelo evolucionar de granitos do sul do Brasil*. Universidade de São Paulo.
- Skinner, B. J. (1997). Hydrothermal mineral deposits: What we do and what we don't know. In *Geochemistry of hydrothermal ore deposits* (3th ed., pp. 1–29). John Wiley & Sons.
- Soliani Jr., E. (1986). *Os dados geocronológicos do Escudo Sul-Rio-grandense e suas implicações de ordem geotectônica*. Universidade de São Paulo.
- Telford, W. M. W., Geldart, L. P., & Sheriff, R. E. (1990). *Applied Geophysics* (2nd ed.). Cambridge University Press.
- Vasconcelos, P., & Kyle, R. J. (1991). Supergene geochemistry and crystal morphology of gold in a semiarid weathering environment: application to gold exploration. *Journal of Geochemical Exploration*, 40(1–3), 115–132. [https://doi.org/10.1016/0375-6742\(91\)90034-R](https://doi.org/10.1016/0375-6742(91)90034-R)
- Xie, X., Hou, Z., & Liu, S. (1987). The genesis of placer gold in Tuanjieyou (TJG), Northwest China. *Geologic Prospecting*, 23(10), 46–55.
- Zonge, K., Wynn, J., & Urquhart, S. (2005). Resistivity, Induced Polarization, and Complex Resistivity. In D. K. Butler (Ed.), *Near Surface Geophysics* (pp. 265–300). *Society of Exploration Geophysicists*. <https://doi.org/10.1190/1.9781560801719.ch9>

Analysis and Interpretation of Regional Gravity Data in the Swayze greenstone belt of the Superior Province, Canada

Satizabal, D.^{1*}, Nitescu, B.¹

Abstract

The Swayze greenstone belt (SGB) is an Archean granitoid-greenstone terrain located in the central part of the Superior Province in Canada. The main objective of this project consisted in doing an analysis and modelling of public regional gravity data of the Swayze greenstone belt with the aim of examining the geometry and depth extent of the geological bodies that occur in the area of this greenstone belt. Gravity data from the Geophysical Data Repository of Natural Resources Canada was used to obtain forward 2.75D gravity models along three profiles, two transversal and one longitudinal to the geological structures of the Swayze greenstone belt. Gravity forward modelling along these profiles was performed using different constraints such as mapped geological contacts at the surface and petrophysical data of different type of rocks of the Abitibi greenstone belt. The models provide an attempt to characterize the geometry and depth extent of the geological units composing the SGB, using regional gravity data.

Key words: Gravity Data, Bouguer anomaly, Gravity modelling, Swayze greenstone belt, Superior Province

Resumen

El cinturón de rocas verdes Swayze (Swayze greenstone belt - SGB) es un terreno compuesto de granitoides y rocas verdes del Arcaico ubicado en la parte central de la Provincia Superior de Canadá. El objetivo principal de este proyecto consistió en realizar un análisis y modelado de datos gravitacionales regionales públicos del cinturón de rocas verdes Swayze con el objetivo de examinar la geometría y extensión en profundidad de los cuerpos geológicos que ocurren en el área estudiada. Se utilizaron datos de gravedad del Repositorio de Datos Geofísicos de Recursos Naturales de Canadá para obtener modelos de gravedad 2,75D a lo largo de tres perfiles, dos transversales y uno longitudinal a las estructuras geológicas del cinturón de rocas verdes Swayze. El modelado de gravedad a lo largo de estos perfiles se llevó a cabo utilizando diferentes restricciones, como los contactos geológicos cartografiados en la superficie y los datos petrofísicos de diferentes tipos de rocas del cinturón de rocas Abitibi. Los modelos proporcionan una aproximación de caracterizar la geometría y la extensión en profundidad de las unidades geológicas que componen el SGB, utilizando datos gravimétricos regionales.

Palabras claves: Datos de gravedad, Anomalía de Bouguer, Modelado de gravedad, Cinturón de rocas verdes Swayze, Provincia Superior

Received: October 7, 2022; Accepted: September 5, 2023; Published on-line: October 1, 2023.

Editorial responsibility: Dr. Joel Rosales Rodríguez

* Corresponding author: Daniel Satizabal (dm.satizabal10@uniandes.edu.co)

¹ Departamento de Geociencias, Universidad de los Andes, Carrera 1 # 18A – 12 Edificio M1 - Tercer Piso, Bogotá – Colombia

Daniel Mauricio Satizabal Pazos, Bogdan Nitescu

<https://doi.org/10.22201/igeof.2954436xe.2023.62.4.1438>

Introduction

The Swayze greenstone belt (SGB) is located in the western Abitibi subprovince of the Superior Province in Ontario, Canada (Figure 1). It is an Archean-age greenstone belt composed of metavolcanic, metasedimentary and metaplutonic rock types (Heather *et al.*, 1995). The SGB was a focus area of the Metal Earth project of the MERC (Mineral Exploration Research Centre, Laurentian University, Sudbury), which involved crustal-scale geophysical investigations of the Swayze greenstone belt area with reflection seismic, magnetotelluric and gravity surveys. Geological mapping was also done along the geophysical transects, to provide an up-to-date base for the interpretation of the geophysical data (Haugaard *et al.*, 2017).

The current project is focused on the analysis and modelling of public regional gravity data of the SGB that is openly available for the area of study with the purpose of contributing to the geological comprehension of the main characteristics of the upper crust in this area. Thus, the depth and geometry of the different bodies that form the subsurface structure of the SGB were investigated using gravity modelling.

Bouguer Anomaly data was downloaded from the Geoscience Data Repository for Geophysical Data of Natural Resources Canada (<http://gdr.aggr.nrcan.gc.ca/gdrdap/dap/search-eng.php>). Three 2.75D forward gravity models are presented for selected profiles, which were obtained with the GM-SYS extension of the Geosoft Oasis montaj software.

Forward gravity modelling was done by taking into account certain constraints, such as the density contrast of the different type of rocks that crop out in the Swayze area and the mapped geological contacts at the surface. The gravity models obtained in this study are compared with other known gravity models of Archean greenstone belts from Canada, with the purpose of correlating the resulting geometry and depth extents as well as identifying if the presented models resemble the general characteristics of other Archean greenstone belts.

Regional Geology

The Swayze greenstone belt (SGB) is located in the Western part of the Abitibi subprovince of the Superior Province

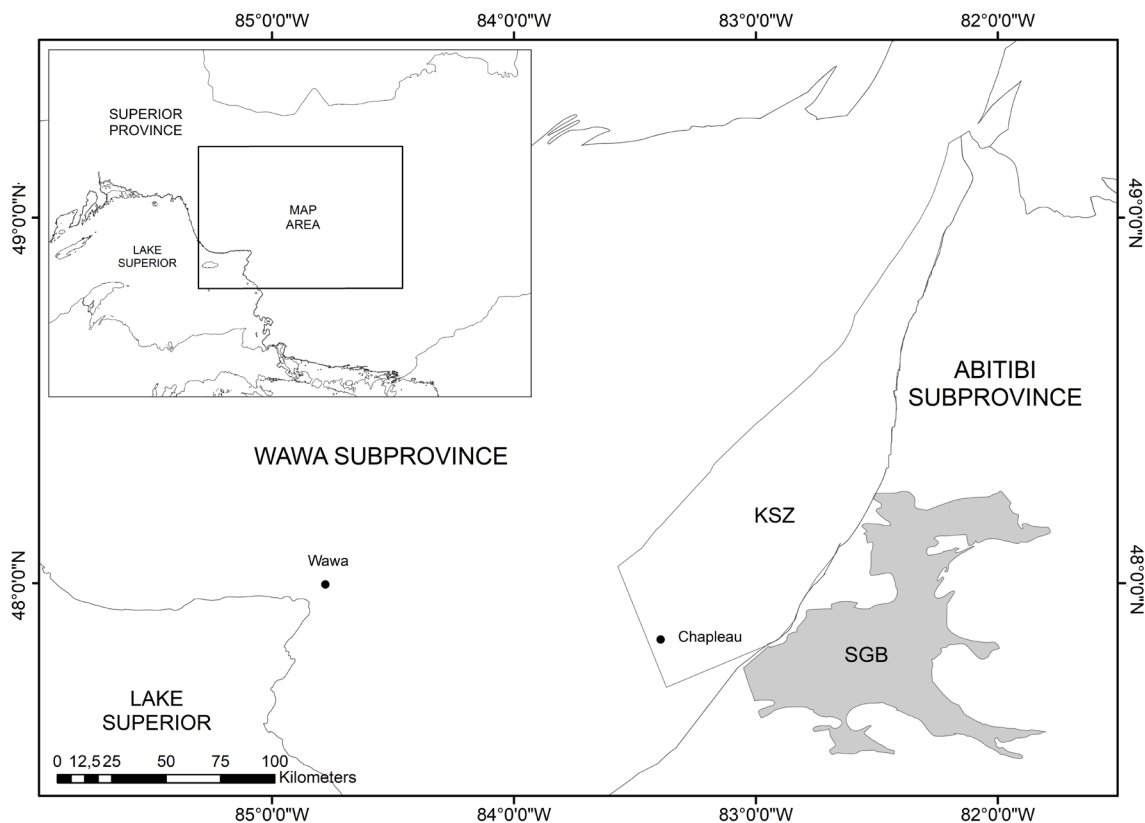


Figure 1. Sketch map of the central Superior Province showing the location of the Swayze greenstone belt (SGB). KSZ - Kapuskasing Structural Zone. The map is based on data downloaded from the ArcGIS website (<https://www.arcgis.com/home/item.html?id=d87347457bc84e5c985db9e904b66b10>) and from the Mineral Exploration Research Centre (MERC) website (<https://merc.laurentian.ca/research/metal-earth/superior-compilation>).

in Ontario, Canada. It is described as a Neo-Archean granitoid-greenstone terrain developed between 2.8 and 2.6 Ga (Jackson & Fyon, 1991). It is bounded by the (a) Kapuskasing structural zone to the west, the (b) Kenogamissi batholith complex to the east, the (c) Nat River granitoid complex to the north and the (d) Ramsey-Algoma granitoid complex to the south (Heather, 2001). The SGB consists of intrusive and extrusive rocks of ultramafic to felsic composition (Figure 2), as well as both chemical and clastic metasedimentary rocks, most of which underwent metamorphism of greenschist to sub-greenschist facies, and amphibolite facies along the boundaries of the belt with large granitoid complexes (Hastie *et al.*, 2020). Despite the SGB having similar geology and greenstone stratigraphy as others greenstone belts of the Abitibi subprovince, the SGB has been considered an area with less (significant) mineral potential (Cheraghi *et al.*, 2019).

The SGB is connected with the southern Abitibi belt by thin slivers of volcanic-sedimentary rocks associated with the Porcupine-Destor deformation zone (PDDZ) and the Ridout deformation zone (RDZ) in the northern and in the southern margins, respectively, of the Kenogamissi granitoid complex (van Breemen *et al.*, 2006). The Kenogamissi batholith complex and the Ramsey-Algoma granitoid complex mainly comprise felsic to intermediate intrusive rocks.

There are two main folds in the SGB: the Brett Lake Syncline and the Woman River Anticline which are labeled in Figure 2 and in Figure 3 with the letters BL and WR, respectively. The SGB is divided in six supracrustal groups from the oldest to the youngest: Chester, Marion, Biscotasing, Trailbreaker, Swayze and Ridout groups (Heather, 2001). For the purpose of gravity modelling in this project, this package of supracrustal groups was considered as a mafic metavolcanic body, given the fact that this rock type is dominant.

It is important to highlight that there is a lack of previous academic or exploration studies of the SGB in comparison with the Abitibi greenstone belt (Maepa & Smith, 2020). Geological work done on the SGB comprises: (1) detailed mapping of the SGB performed by Heather (2001), (2) mapping and data compilation by Ayer *et al.* (2002) and (3) remapping by Haugaard *et al.* (2017). Geophysical work, such as magnetotelluric resistivity sections, seismic surveys, including high-resolution seismic imaging and gravity surveys, was previously done, along some profiles across the SGB (Cheraghi *et al.*, 2019).

Gravity Data

In 2017, the SGB was an area of study of the Metal Earth project carried out by the MERC with the purpose of refining

the geological knowledge of the Abitibi greenstone belt. To accomplish this task, the Metal Earth studies investigated the crust of the Swayze area along transects perpendicular to the strike of major structures and units, using reflection seismic, magnetotelluric and gravity surveys (Haugaard *et al.*, 2017). Nevertheless, these data are not publicly available for free use. Instead, the gravity data used in this project was downloaded directly from the Geoscience Data Repository for Geophysical Data of the Natural Resources Canada. For the downloaded gravity dataset, the original coordinates in the geographic coordinate system were converted to NAD83 UTM Zone 17. The Bouguer Anomaly dataset (Figure 3) was downloaded from the Geoscience Data Repository as a grid with a 2-km grid-cell size that extends between 47.5° to 48.27° N and -81.9° to -83° W, which corresponds to the area underlain by the Swayze greenstone belt and its surroundings.

Qualitative Analysis

The Bouguer gravity anomalies correspond to lateral variations in density and mass in the upper mantle and the crust that reflect differences in composition and thickness of geological bodies. High-frequency anomalies are caused by near-surface bodies of rocks that have significantly different densities. Longer wavelength anomalies are generally associated with variations in crustal thickness or deeper intra-crustal mass anomalies.

In the area of this study, the values of the Bouguer Anomaly range from -16,9 to -77 mGal (Figure 3). In the area labelled A1 in Figure 3 exists a symmetry with respect to the fold axis of the Brett Lake Syncline (BL). This also occurs in the area A2 with respect to the fold axis of the Woman River Anticline (WR). Despite their symmetry, these areas do not show significant changes in the value of the Bouguer anomaly away from the fold axes. On the other hand, the areas A3 (Kenogamissi granitoid complex), A4 (Biggs Pluton) and A5 (Nat River granitoid complex) are characterized by the lowest values of the anomaly, which indicates that the rocks underlying these areas are less dense than their surroundings. These areas correspond to granitic plutons that are less dense than the volcanic rocks they surround. There are also other small intrusions throughout the SGB but those do not represent significant gravity lows in the values of the Bouguer Anomaly.

Modelling

In order to study and understand the Bouguer anomalies caused by density contrasts between bodies underneath the

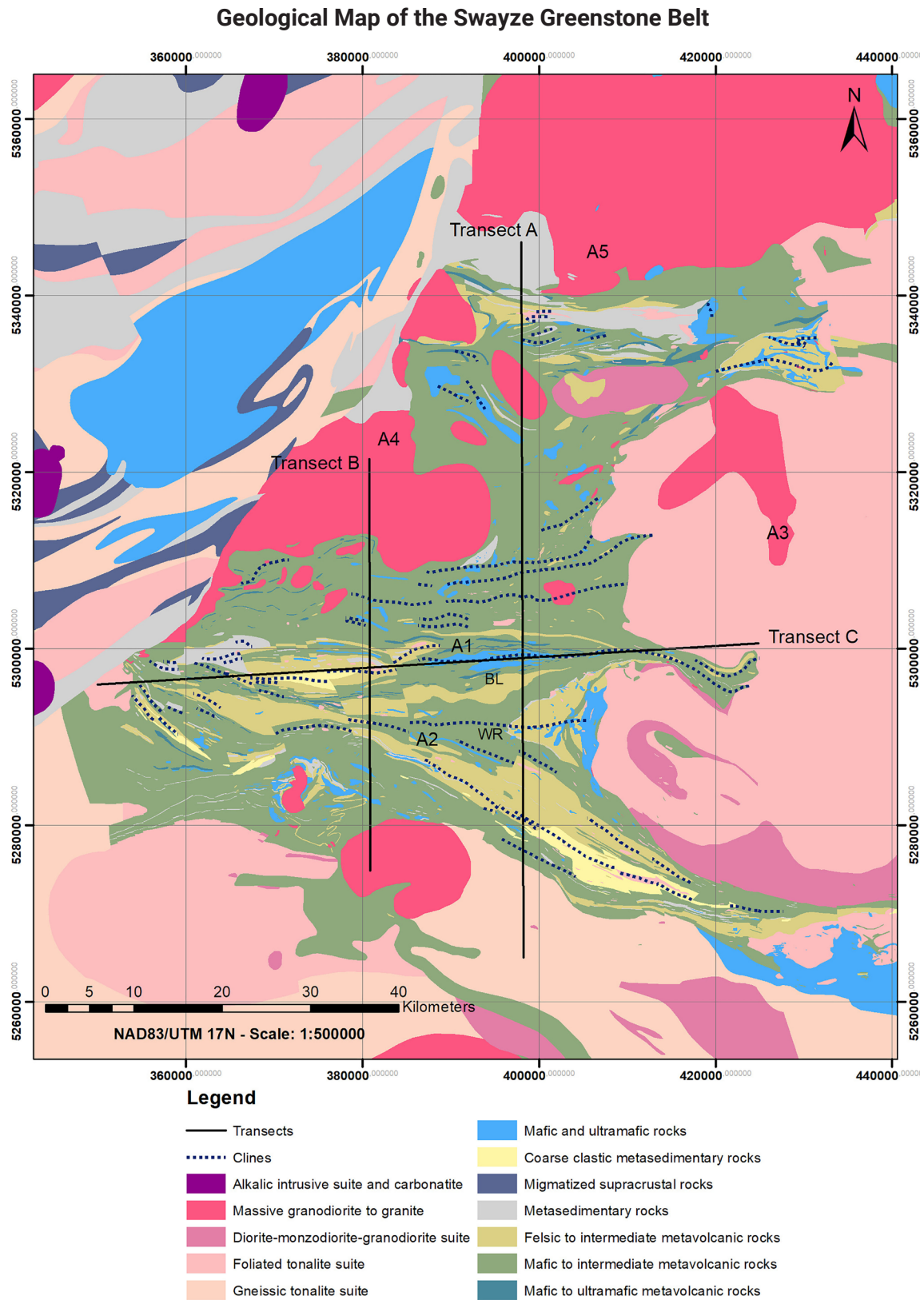


Figure 2. Geological map of the Swayze greenstone belt. Coordinate System NAD-83/ UTM Zone 17 N. The black solid lines indicate the traces of the profiles (transects) along which 2.75D forward modelling was conducted. BL and WR correspond to the Brett Lake and the Woman River folds, which are discussed in the text. In dark blue dashed lines are shown the axes of the different folds in the Swayze area. A1 to A5 indicate the different areas discussed in the Qualitative Analysis section. The digital geological dataset was downloaded in ArcGIS format from the website of the Ministry of Northern Development and Mines of Ontario: (http://www.geologyontario.mndm.gov.on.ca/mndmaccess/mndm_dir.asp?type=pub&id=MRD126-REV1).

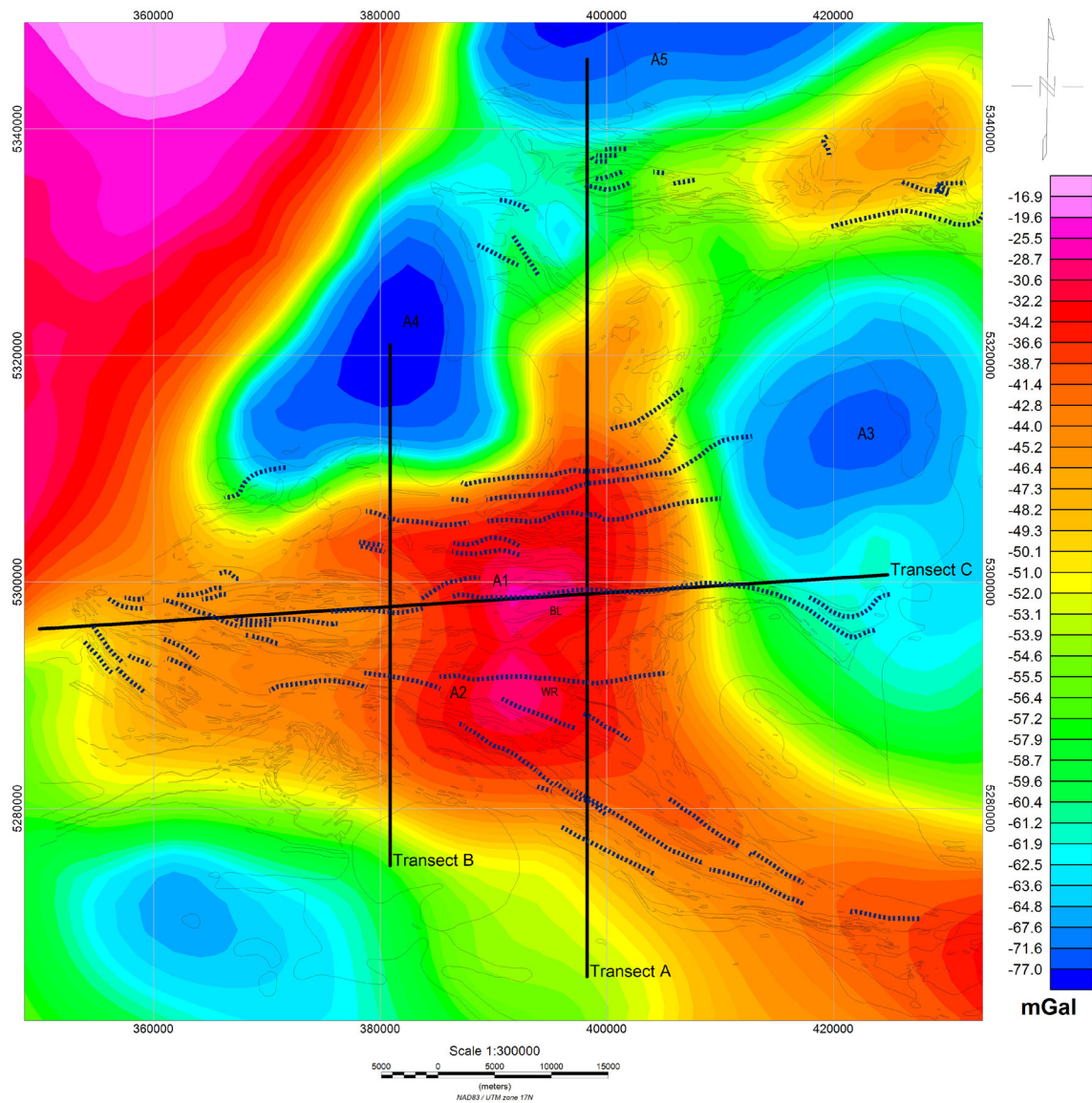


Figure 3. Bouguer anomaly map of the SGB (mGal). Coordinate System NAD-83/ UTM Zone 17 N. The black solid lines indicate the traces of the profiles (transects) along which 2.75D forward modelling was conducted, in order to study the depth and geometry of the geologic bodies and structures of the area. In grey thin lines are represented the geological contacts that occur in the Swayze area (see also the Geological Map in Figure 2). The thick dark blue dashed lines indicate fold axes in the Swayze greenstone belt area. BL and WR correspond to the Brett Lake and the Woman River folds, which are discussed in the text. A1 to A5 indicate the different areas discussed in the Qualitative Analysis section. The Bouguer Anomaly grid file was downloaded from the Geoscience Data Repository of Natural Resources Canada.

surface, a quantitative model can be constructed to fit a certain set of gravity observations, by changing, for instance, the geometry and depth extent of the model bodies. For the modelling of the selected transects (see Figures 2 and 3), the contacts between the main geological units (mafic metavolcanic rocks and granitoid plutons), the main fold location and their type as well as the densities of the types of rocks cropping at the surface were taken into account and were used as constraints. The density values of the geological units in

the area of study were based on a generalized density table of the Abitibi greenstone belt published by Eshghi *et al.* (2019). Horizontal extents of the geological bodies that extend beyond the ends of the profile were also considered, in order to model these rock bodies and resolve the calculated gravity. Furthermore, for the rock bodies intersected by the profiles, variable extents perpendicular to the strike of the transects were considered, which created 2.75D gravity models.

The density contrasts of the modelled geological bodies

Table 1. Density values (g/cm^3) used in the forward models.

Type of Rock	Density
Mafic metavolcanic bodies	2.89 g/cm^3
Granitoid plutons	2.66 g/cm^3
Crustal back-ground	2.72 g/cm^3

were considered relative to an average upper crustal density in the Superior Province of 2.72 g/cm^3 , based on previous studies (e.g. Nătescu *et al.*, 2006; Maleki *et al.*, 2021). Three gravity models were obtained with the Oasis montaj GM-SYS tool along the profiles shown in Figures 2 and 3.

For the three models, the geologic bodies were grouped into two categories with different density values, as well as density contrasts, relative to the upper crustal back-ground: mafic metavolcanic bodies, $\rho=2.89 g/cm^3$ and a density contrast of +0.17 g/cm^3 relative to the crustal background; granitoid plutons, with $\rho=2.88 g/cm^3$ and a density contrast of -0.06 g/cm^3 relative to the crustal background. The density values used in the forward models are also summarized in Table 1.

Model A

This model corresponds to a profile that is perpendicular to the general direction of the main fold axes of the SGB, such as the Brett Lake Syncline and the Woman River Anticline, in a north-south direction in the eastern part of the Swazye greenstone belt and covers a distance of approximately 81 *km*.

In Figure 4, it is observed that the highest peak of the Bouguer anomaly is located mainly on the axis of the Brett Lake Syncline. The lowest values of the Bouguer anomaly along the profile correspond to the Nat River granitoid complex north of the Swayze greenstone belt. The deepest parts of the model of the greenstone belt occurs where the Brett Lake Syncline and Woman River Anticline are located, between kilometers 45 and 55, in two roots with observed depths of 4 and 5 *km*, respectively. On the other hand, in the northern part of the profile, outcropping mafic volcanic rocks appear to extend to a depth of less than 1 *km*.

Model B

This model corresponds to a profile that is perpendicular

to the general direction of the Brett Lake Syncline and Woman River Anticline in a north-south direction in the western part of the Swayze greenstone belt. It covers a distance of approximately 46 *km*. The model (Figure 5) indicates that along this profile the greenstone belt body reaches its deepest part (12 *km* depth) in the northern half of the profile (at kilometer 17), where the highest values of the Bouguer anomaly are observed. The lowest values of the Bouguer Anomaly correspond to the Biggs Pluton at the north end of the profile, which has a modelled depth of 8 *km*.

The Brett Lake Syncline and the Woman River Anticline present modelled depths of 4 to 5 *km* in the interval between kilometers 21 and 31 of the profile.

Model C

This model corresponds to a profile that follows the general direction of the Brett Lake Syncline in a west-east direction of the Swayze area. It covers a distance of approximately 75 *km*. It is observed in the Figure 6 that the highest value of the Bouguer Anomaly occurs at kilometer 41 of the profile, where the model of the greenstone belt body reaches its deepest part of about 7 *km* depth. The thickness of the mafic metavolcanic unit remains constant between the western end of the profile and the kilometer 32 along the profile, with a model depth of approximately 2 *km*.

Discussion

In the area of study, the lowest values of the Bouguer Anomaly correspond to intrusive granitoid bodies that typically have lower densities than the rocks surrounding them. The highest values of the Bouguer Anomaly correlate with metavolcanic rocks, which have undergone deformation processes often related to high strain zones, resulting in various folds with an axial plane in the west-east direction. With regards to the depth of the structures, it is observed that the Brett Lake Synclinal extends in depth between 2 to 7 *km*, whereas the Woman River Anticline extends in depth between 3 to 5 *km*.

The depth and geometry of the geological units of the SGB are comparable with those of other Archean greenstone belts such as the models presented by Peschler *et al.* (2004) of the Abitibi greenstone belt, which typically are part of the dome-and-keel structural patterns of the Archean terrains. Dome-and-keel provinces consist of synclinal keels composed of greenstone rocks that are surrounded by ellipsoidal and

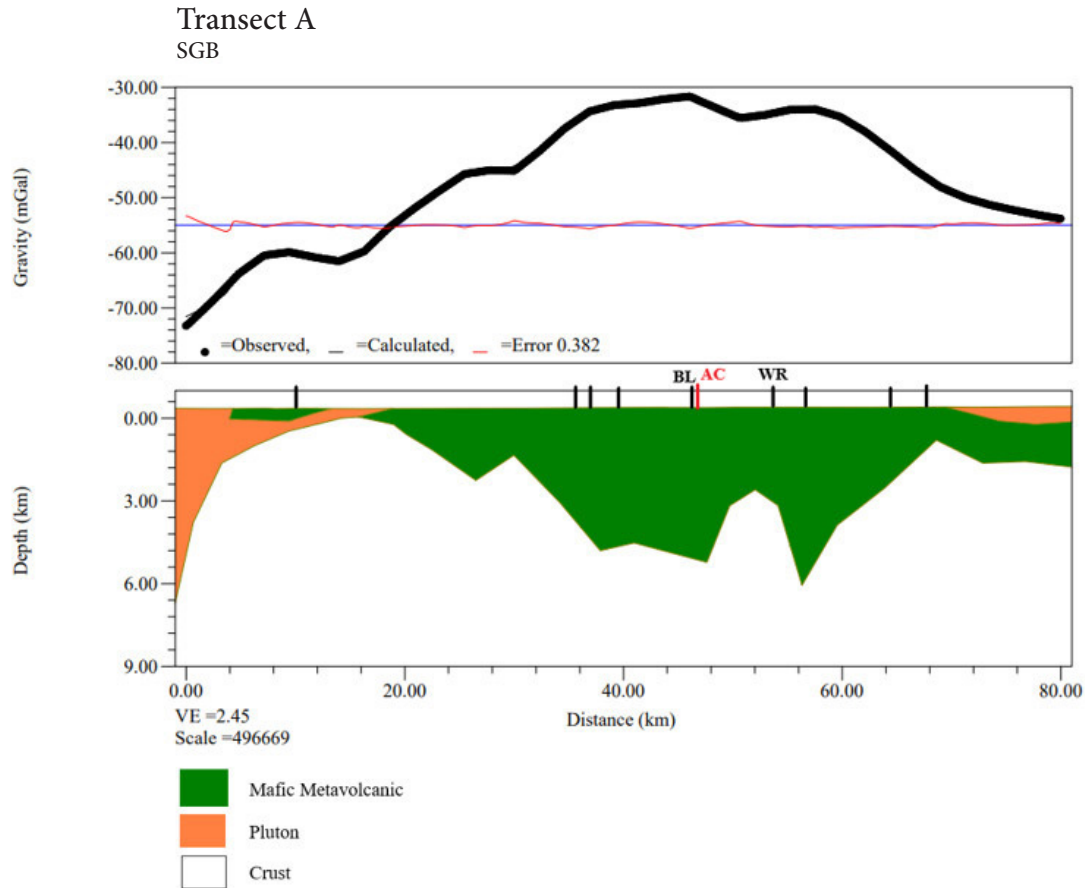


Figure 4. Gravity model along Transect A: Mafic Metavolcanic, $\rho=2.89 \text{ g/cm}^3$; Pluton, $\rho=2.66 \text{ g/cm}^3$; Crust, $\rho=2.72 \text{ g/cm}^3$. The black vertical lines shown at the top of the model panel indicate the locations of the different fold axes crossed by the transect. The red vertical line represents the crossing location between Transect A and Transect C. WR-Woman River Anticline, BL-Brett Lake Syncline, AC-Crossing between Transect A and Transect C. The RMS error was of 0.382. The model was obtained with the GM-SYS Extension of the Geosoft – Oasis montaj software.

ovoid-shaped domes composed of gneiss, granitoid, and migmatite (Kearey *et al.*, 2009). The Archean greenstone belts are a fundamental part of this unique structural style consisting of alternating granitoid-cored domes and volcanic dominated keels, where the synclinal keels are cut by major transcurrent shear zones (Thurston, 2015). The greenstone successions feature mafic to felsic volcanic cycles of mixed tholeiitic and calc-alkalic compositions, commonly with overlying sedimentary rocks, typically in contact with younger intrusive granitic rocks (Goodwin, 1981).

Various previous studies presented gravity models of Archean greenstone belts in the Superior Province with the aim of defining their depth and geometry. Nitescu *et al.* (2006) presented models of Archean greenstone belts in the western part of the Superior Province that indicate synform-shaped, ca. 3-km-thick bodies of metavolcanic rocks,

surrounded by thick intrusive bodies of 9 to 10 km. Thomas *et al.* (1986) indicated that greenstone belts are restricted to the uppermost 10 km of the crust and that many greenstone belts have a basin-shaped form with some having deep keels. Gupta *et al.* (1982) applied different constraints in models of the Uchi subprovince greenstone belts, in which suggest vertical extents between 4 and 9 km for the greenstone bodies. Gorman *et al.* (1978) presented an Archean greenstone belt model that in cross-section resembles the shape of an inverted mushroom. Grant *et al.* (1965) presented a gravity model of the Red Lake greenstone belt, which extends to a depth of 8 km and is basin-shaped, being underlain by granitic batholiths and gneiss. Peschler *et al.* (2004) presented different models of the Abitibi greenstone belt where the plutons have depth extents between 1 to 4 km and tabular shapes, whereas the greenstones bodies form keels with depths extents up to

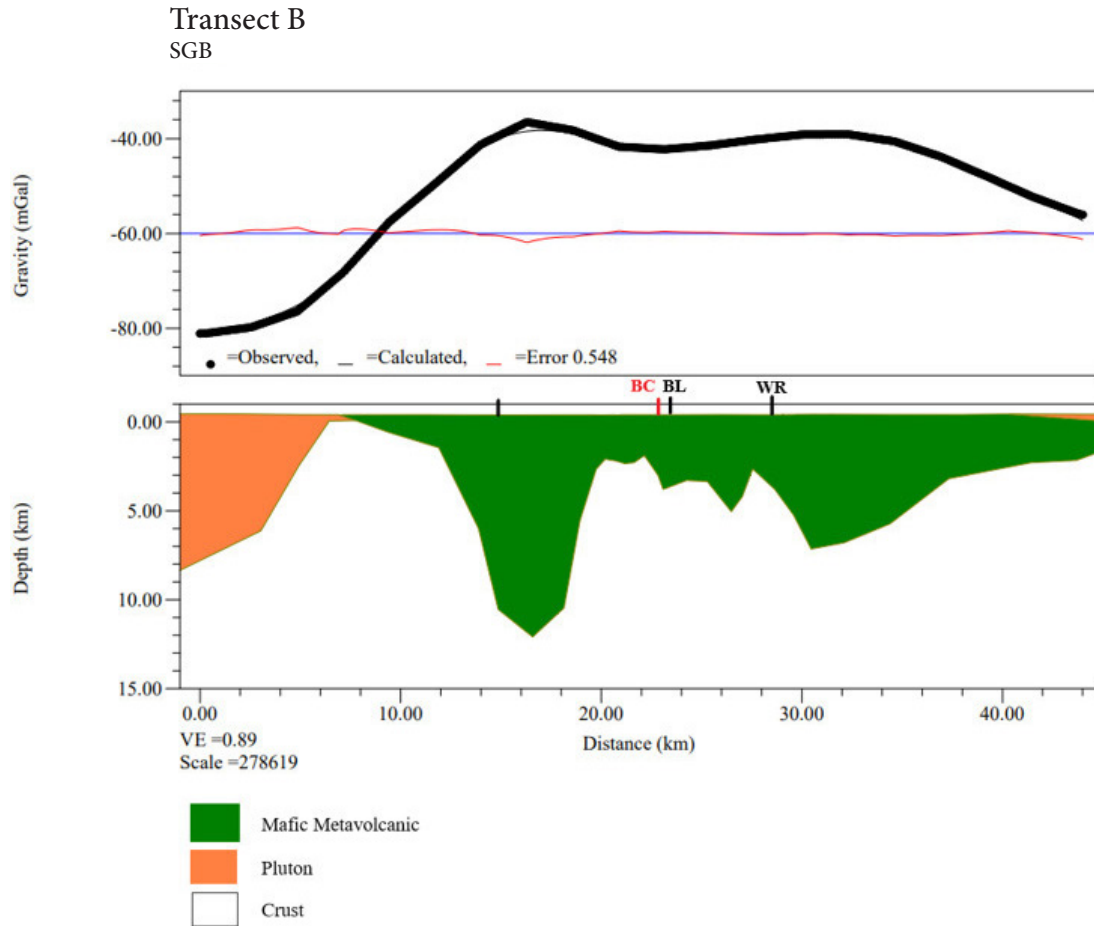


Figure 5. Gravity model along Transect B: Mafic Metavolcanic, $\rho=2.89 \text{ g/cm}^3$; Pluton, $\rho=2.66 \text{ g/cm}^3$; Crust, $\rho=2.72 \text{ g/cm}^3$. The black vertical lines shown at the top of the model panel indicate the locations of the different fold axes crossed by the transect. The red vertical line represents the crossing location between Transect B and Transect C. WR-Woman River Anticline, BL-Brett Lake Syncline, BC-Crossing between Transect A and Transect C. The RMS error was of 0.548. The model was obtained with the GM-SYS Extension of the Geosoft – Oasis montaj software.

8 to 10 km. Maleki *et al.* (2021) presented various detailed models of the Chibougamau area in the Abitibi greenstone belt, based on gravity, magnetic and seismic data, where the mafic metavolcanic rocks have a vertical extent of 3 to 7 km and the plutons have depth extents to 9 km.

In general terms, the vertical extents of the geological units observed in the models of this project fit the range found for the Archean greenstone belts in the Superior Province. In terms of the shape of the SGB gravity models, they indicate synclinal keel shapes with steeply dipping volcanic sequences, surrounded by granitoid domes, typical of the dome-and-keel structural style.

Even though the calculated model error is less than 1% for each of the profiles analyzed in this study, the obtained models are not a complete answer on the geometry details and true depth extents of the geological units of the SGB. In order

to have a better understanding of their geometry and depth, incorporation of magnetic and seismic data could constrain better the geophysical models. Moreover, a denser network of gravity data stations and an improved density database from available drill-core in the area of the SGB would provide better constraints on gravity models. Despite the limited constraints and simplifying assumptions used in this study, its results present an attempt to characterize the geometry and depth of the different geological bodies composing the SGB from public gravity data through forward modelling.

Conclusions

The gravity models obtained in this study lead to a general perspective of the geometry and depth extent of the geolog-

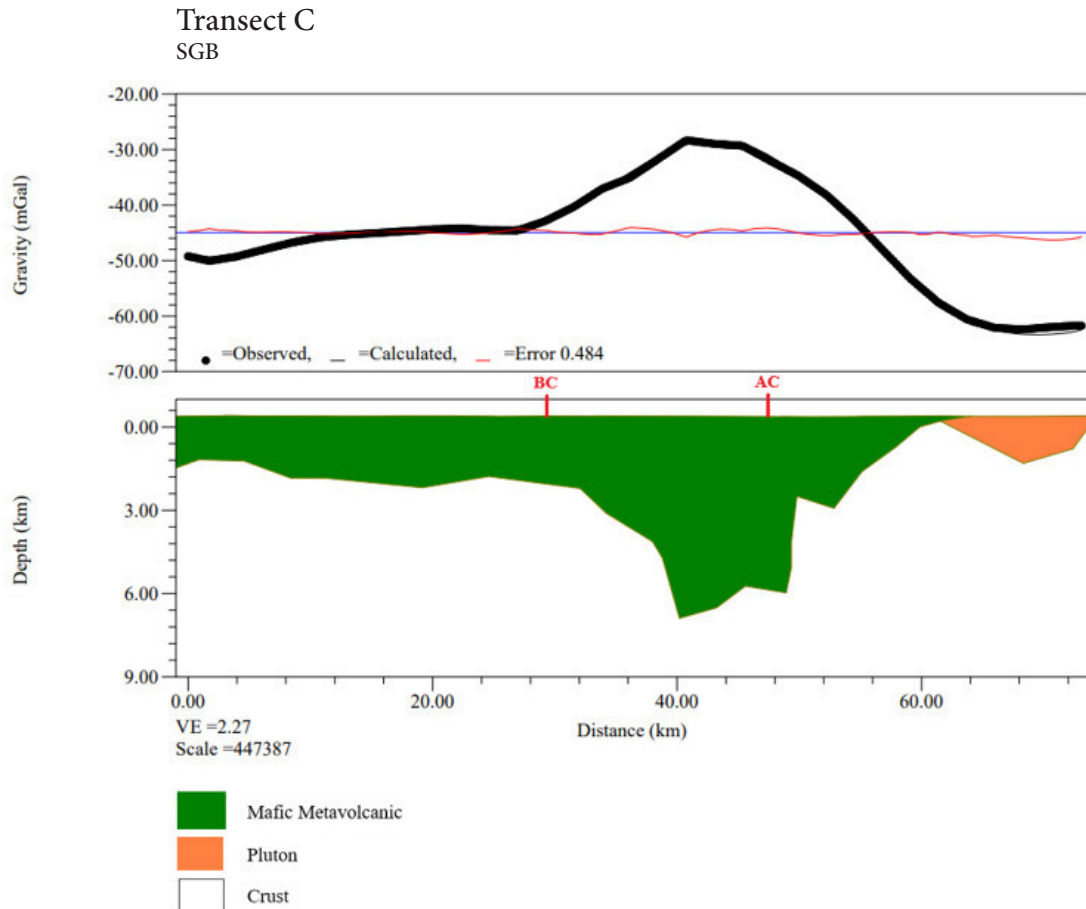


Figure 6. Gravity model along Transect C: Mafic Metavolcanic, $\rho=2.89 \text{ g/cm}^3$; Pluton, $\rho=2.66 \text{ g/cm}^3$; Crust, $\rho=2.72 \text{ g/cm}^3$. The two red vertical lines shown at the top of the model panel and labelled AC and BC represent the crossing location between Transect A and Transect C, and between Transect B and Transect C, respectively. The RMS error was of 0.484. The model was obtained with the GM-SYS Extension of the Geosoft – Oasis montaj software.

ical units that form the SGB. The metavolcanic rocks under the Brett Lake Syncline appear to extend in depth between 2 to 7 km, whereas under the Woman River Anticline appear to extend in depth between 2 to 6 km. The deepest parts of the SGB are located in its central-southern area, extending down to modelled depths of 12 km. The gravity models of surrounding intrusive bodies have depth extents between 1 and 8 km. The geometry of the SGB and the surrounding and intruding tonalite-granodiorite plutons form a typical Archean keel-and-dome pattern.

Competing interests

There are no competing interests. The primary research data that support the findings of this study are located in the Natural Resources Geoscience Data Repository for Geophys-

ical Data page: <http://gdr.agg.nrcan.gc.ca/gdrdap/dap/search-eng.php>. This data is publicly available.

Acknowledgements

The authors would like to thank the anonymous reviewer and the associate editor for their constructive comments and suggestions. This work was supported by Universidad de los Andes (FAPA fund PR.3.2020.7367 granted to B. Nitescu).

References

Cheraghi, S., Naghizadeh, M., Snyder, D., Haugaard, R., & Gemmill, T. (2019). High-resolution seismic imaging of crooked two-dimensional profiles in greenstone belts of the Canadian shield: Results

- from the Swayze area, Ontario, Canada. *Geophysical Prospecting*, 68(1): 62-81. doi:10.1111/1365-2478.12854
- Eshaghi, E., Smith, R. S., & Ayer, J. (2019). Petrophysical characterisation (i.e. density and magnetic susceptibility) of major rock units within the Abitibi Greenstone Belt: Laurentian University Mineral Exploration Research Centre, publication number MERC-ME-2019-144.
- Goodwin, A. M. (1981). Chapter 5 Archaean Plates and Greenstone Belts. *Developments in Precambrian Geology*, pp. 105-135. doi:10.1016/s0166-2635(08)70010-0
- Gorman, B. E., Pearce, T. H., & Birkett, T. C. (1978). On the structure of Archean greenstone belts. *Precambrian Research*, 6(1): 23-41. [https://doi.org/10.1016/0301-9268\(78\)90053-0](https://doi.org/10.1016/0301-9268(78)90053-0)
- Grant, F. S., Gross, W. H., & Chinnery, M. A. (1965). The shape and thickness of an Archaean greenstone belt by gravity methods. *Canadian Journal of Earth Sciences*, 2(5): 418-424. <https://doi.org/10.1139/e65-036>
- Gupta, V.K., Thurston, P.C., & Dusanowskyj, T.H. (1982). Constraints upon models of greenstone belt evolution by gravity modelling, Birch--Uchi greenstone belt, northern Ontario. *Precambrian Research*, 16: 233-255.
- Hastie, E. C., Kontak, D. J., & Lafrance, B. (2020). Gold Remobilization: Insights from Gold Deposits in the Archean Swayze Greenstone Belt, Abitibi Subprovince, Canada. *Economic Geology*, 115(2): 241-277. doi:10.5382/econgeo.4709
- Haugaard, R., Gemmill, T.P., Ayer, J.A., & Thurston, P.C. (2017). Lithological and stratigraphic relationships of the north Swayze and Matheson areas, Abitibi greenstone belt. Ontario Geological Survey, Open File Report 6350, 43-1 to 43-10.
- Heather, K. B., Percival, J. A., Moser, D., & Bleeker, W. (1995). Tectonics and metallogeny of Archean crust in the Abitibi-Kapuskasing-Wawa region. Geological Society of Canada: Open File 3141.
- Heather, K.B. (2001). *The geological evolution of the Archean Swayze greenstone belt, Superior Province, Canada*. [Ph.D. thesis]. Keele University.
- Jackson, S.L., & Fyon, A.J. (1991). The western Abitibi subprovince in Ontario; in *Geology of Ontario*, Ontario Geological Survey, Special Volume 4, pt. 1, pp. 405-482.
- Kearey, P., Klepeis, K. A., & Vine, F. J. (2009). *Global tectonics / the late Philip Kearey, Keith A. Klepeis, Frederick J. Vine*. Oxford: Wiley-Blackwell.
- Maepa, F. M., & Smith, R. S. (2020). Examining the controls on gold deposit distribution in the Swayze greenstone belt, Ontario, Canada, using multi-scale methods of spatial data analysis. *Ore Geology Reviews*, 125, 103671. doi:10.1016/j.oregeorev.2020.103671
- Maleki, A., Smith, R., Eshaghi, E., Mathieu, L., Snyder, D., & Naghizadeh, M. (2021). Potential-field modelling of the prospective Chibougamau Area (northeastern Abitibi Subprovince, Quebec, Canada) using geological, geophysical, and Petrophysical constraints. *Canadian Journal of Earth Sciences*, 58(3): 297-312. <https://doi.org/10.1139/cjes-2019-0221>
- Nitescu, B., Cruden, A. R., & Bailey, R. C. (2006). Crustal structure and implications for the tectonic evolution of the Archean Western Superior craton from forward and inverse gravity modeling, *Tectonics*, 25(1). doi:10.1029/2004TC001717.
- Peschler, A. P., Benn, K., & Roest, W. R. (2004). Insights on Archean continental geodynamics from gravity modelling of granite-greenstone terranes. *Journal of Geodynamics*, 38(2): 185-207. <https://doi.org/10.1016/j.jog.2004.06.005>
- Thomas, M. D., Losier, L., Thurston, P. C., Gupta, V. K., Gibb, R. A., & Grieve, R. A. (1986). Geophysical characteristics and crustal structure of greenstone terranes Canadian Shield. *Workshop on Tectonic Evolution of Greenstone Belts*, pp. 203-206.
- Thurston, P. C. (2015). Igneous Rock Associations 19. Greenstone Belts and Granite-Greenstone Terranes: Constraints on the Nature of the Archean World. *Geoscience Canada*, 42(4): 437-484. doi:10.12789/geocanj.2015.42.081
- van Breemen, O., Heather, K.B. and Ayer, J.A. 2006. U-Pb geochronology of the Neoproterozoic Swayze sector of the southern Abitibi greenstone belt, Geological Survey of Canada, Current research 2006-F1, 32p.

Structural Traits of Cuitzeo Lake, Central Mexico, and Areas of Geothermal Potential

Elizabeth Rivera-Calderón¹  and Román Álvarez² 

Abstract

Cuitzeo Lake, in the central part of the Trans Mexican Volcanic Belt, is in an extensional region associated with the Cuitzeo graben, where magmatic ascent appears to provide the heat sources for the surface, geothermal manifestations. A profuse distribution of andesitic rocks is observed throughout the study area of 50×50 km². Gravity and magnetic field 3D inversions are calculated to obtain density and magnetic susceptibility distributions to 7000 m depth, from which we analyze N-S and E-W cross-sections and obtain density and magnetic susceptibility geosurfaces that help characterize anomaly areas of interest. We use satellite-derived gravity and magnetic data in our evaluation, owing to their high-resolution characteristics and uniform coverage of the study area. Analysis initiates with the San Agustín del Maíz region (SAM), exhibiting surface geothermal manifestations, to characterize its density and susceptibility characteristics, then the analysis is extended to the whole study area. Several outcropping, low magnetic susceptibility regions, like the one associated with SAM, are suggested as potential geothermal targets. Density geosurfaces point to two volumes where magmatic material may intrude, coinciding with active geologic faults. The analysis presented here can be extended to neighboring regions in the Cuitzeo Lake area and may constitute a fast, unexpensive exploration methodology in similar geothermal districts.

Key words: Cuitzeo Lake, Bouguer anomaly, Geothermal exploration, San Agustín del Maíz, 3D inversions, Satellite-derived gravity.

Resumen

El Lago de Cuitzeo se encuentra en la parte central del Cinturón Volcánico Trans Mexicano, en una región de extensión asociada al graben de Cuitzeo, en donde el ascenso magmático parece proporcionar las fuentes de calor que alimentan a las manifestaciones geotérmicas superficiales. Se observa una distribución profusa de andesitas a través del área de estudio de 50 × 50 km². Se calculan inversiones 3D de los campos de gravedad y magnético para obtener distribuciones de densidad y susceptibilidad magnética hasta 7000 m de profundidad, de las cuales obtenemos y analizamos secciones N-S y E-W, obteniendo también geo-superficies que ayudan a caracterizar las áreas de anomalía de interés. Utilizamos datos derivados de observaciones satelitales de gravedad y magnetismo debido a sus características de alta resolución y cobertura uniforme del área de estudio. El análisis se inicia con la región de San Agustín del Maíz (SAM), que exhibe manifestaciones geotérmicas superficiales, para caracterizar sus propiedades de densidad y susceptibilidad, y después el análisis se extiende a toda el área de estudio. Varios sitios en donde afloran regiones de baja susceptibilidad magnética, como en 46 el caso de SAM, se sugieren como blancos potenciales de exploración geotérmica. Dos geo-superficies de densidad apuntan a dos volúmenes en donde material magmático puede estar emplazado, coincidiendo con la presencia de fallas geológicas activas. El análisis presentado aquí puede extenderse a regiones vecinas al Lago de Cuitzeo, y pueden constituir una metodología de exploración rápida y económica en distritos geotérmicos similares.

Palabras clave: Lago de Cuitzeo, Anomalía de Bouguer, Exploración geotérmica, San Agustín del Maíz, Inversiones 3D, Gravedad medida con satélite.

Received: March 12, 2023; Accepted: July 19, 2023; Published on-line: October 1, 2023.

Editorial responsibility: Dr. Marco Antonio Pérez-Flores

* Corresponding author: Román Álvarez, roman.alvarez@iimas.unam.mx

¹ Escuela Nacional de Estudios Superiores-Unidad Morelia, Universidad Nacional Autónoma de México, Antigua Carretera a Pátzcuaro 8701, C.P. 58190, Morelia, Michoacán, Mexico. ecalderonzr@comunidad.unam.mx

² Instituto de Investigaciones en Matemáticas Aplicadas y en Sistemas, Universidad Nacional Autónoma de México, Ciudad Universitaria, México DF, 04510, Mexico.

Elizabeth Rivera-Calderón, Román Álvarez-Bejar

<https://doi.org/10.22201/igeof.2954436xe.2023.62.4.1586>

Introduction

The geologic structure of Cuitzeo Lake is in the central part of Mexico (Figure 1), in the Trans Mexican Volcanic Belt (TMVB, Ferrari *et al.*, 2012) within the volcanic zone known as the Michoacán-Guanajuato Volcanic Field (Ferrari, 2000; Gómez-Vasconcelos *et al.*, 2015, 2020). Recent studies of the Cuitzeo Lake region have focused on the geothermal potential of this area (Gómez-Vasconcelos *et al.*, 2021a; Pola *et al.*, 2016; Trujillo-Hernández, 2017). Several geophysical studies reported anomalous behavior probably associated with magmatic ascent, related to the geothermal sources (Guevara-Alday, 2015). These sources are, in turn, related to the extensional phenomena associated with the Cuitzeo Lake graben (Israde-Alcantara & Garduño-Monroy, 1999; Garduño-Monroy *et al.*, 2009). Olvera-García *et al.*, (2020) established that this deep-seated geothermal system is buried under late Miocene-Holocene lacustrine sediments filling an extensional tectonic depression. Here, we focus on 2D and 3D, regional, gravity and magnetic field interpretations in this area, to highlight the main structural traits of the region to a depth of 7 km. Particular attention is given to areas with geothermal potential.

Regional geology

An extensional tectonic regime, with NNW orientation, originated the basin of Cuitzeo Lake in this volcanic region

(Gómez-Vasconcelos *et al.*, 2021a; Gómez-Tuena *et al.*, 2007). Volcanic activity in the basin has been continuous since the Early Miocene to the Present; there are more than 50 volcanic chimneys, with associated structures such as scoria cones, lava domes, small shield volcanoes, and fissure lava flows (Israde-Alcantara & Garduño-Monroy, 1999; Garduño-Monroy *et al.*, 2009; Pola *et al.*, 2016; Trujillo-Hernández, 2017; Gómez-Vasconcelos *et al.*, 2020, 2021a;). The mountain landscape is conformed by ignimbrites, lava flows, pyroclastic and volcanoclastic deposits (Pola *et al.*, 2016), overlying a granitic basement (Trujillo-Hernández, 2017). Figure 2 shows the topography of the area, with Cuitzeo Lake exhibiting the lowest, regional elevations.

Tectonic activity in the central sector of the TMVB is indicated by widespread seismicity and earthquakes ($M \leq 5$) with focal mechanisms ranging from transcurrent to normal (Quintanar *et al.*, 2004; Quintanar *et al.*, 2018; Suárez *et al.*, 2019).

The geologic map appears in Figure 3. This map represents the main regional geological units, the dominant geological faults are represented by the black lines. The main rock units are basalts, andesites, tuffs and ignimbrites that belong to the Sierra de Mil Cumbres and some from the Caldera de Atécuaro (Garduño-Monroy *et al.*, 2009). The topography of the area is conditioned by the structures of the Morelia-Acambay Fault System (Garduño-Monroy *et al.*, 2009; Gómez-Vasconcelos *et al.*, 2020; Israde-Alcantara & Garduño-Monroy, 1999) and the inferred Tzitzio-Valle de Santiago Fault. The semigraben and the graben of Cuitzeo can be observed in the central zone. The Morelia Acambay Fault System conditions the blocks of the

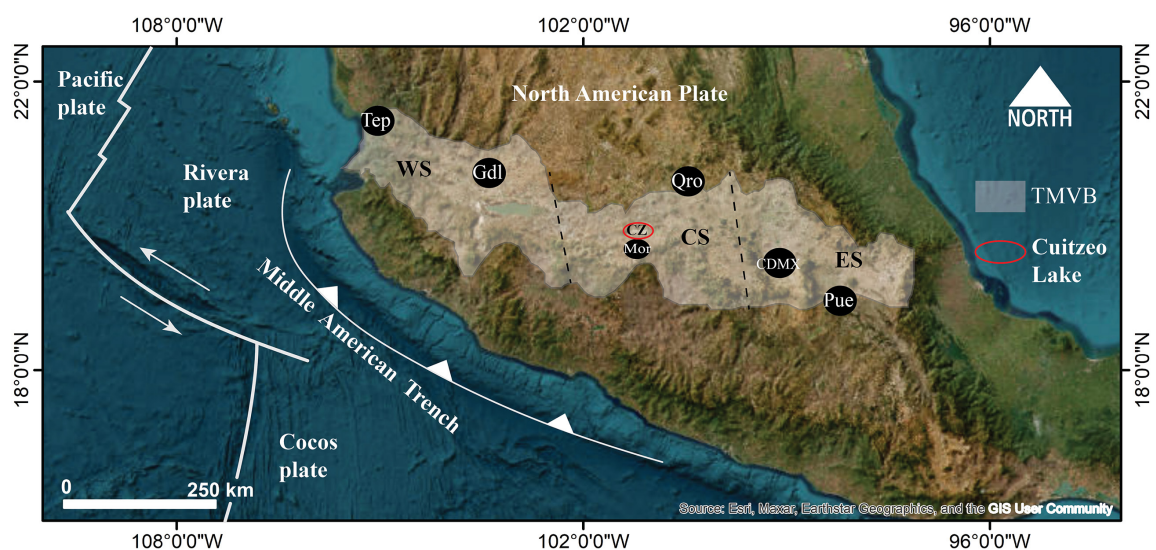


Figure 1. Location of Cuitzeo Lake (red ellipse) in the Central Sector (CS) of the Trans Mexican Volcanic Belt (TMVB, light brown). Parallel, dashed lines limit the sectors of the TMVB. CZ, Cuitzeo Lake. WS, Western Sector. ES, Eastern Sector (based on Correa-Gómez, 2019). Tep, Tepic. Gdl, Guadalajara. Mor, Morelia. Qro, Querétaro. CDMX, Mexico City. Pue, Puebla.

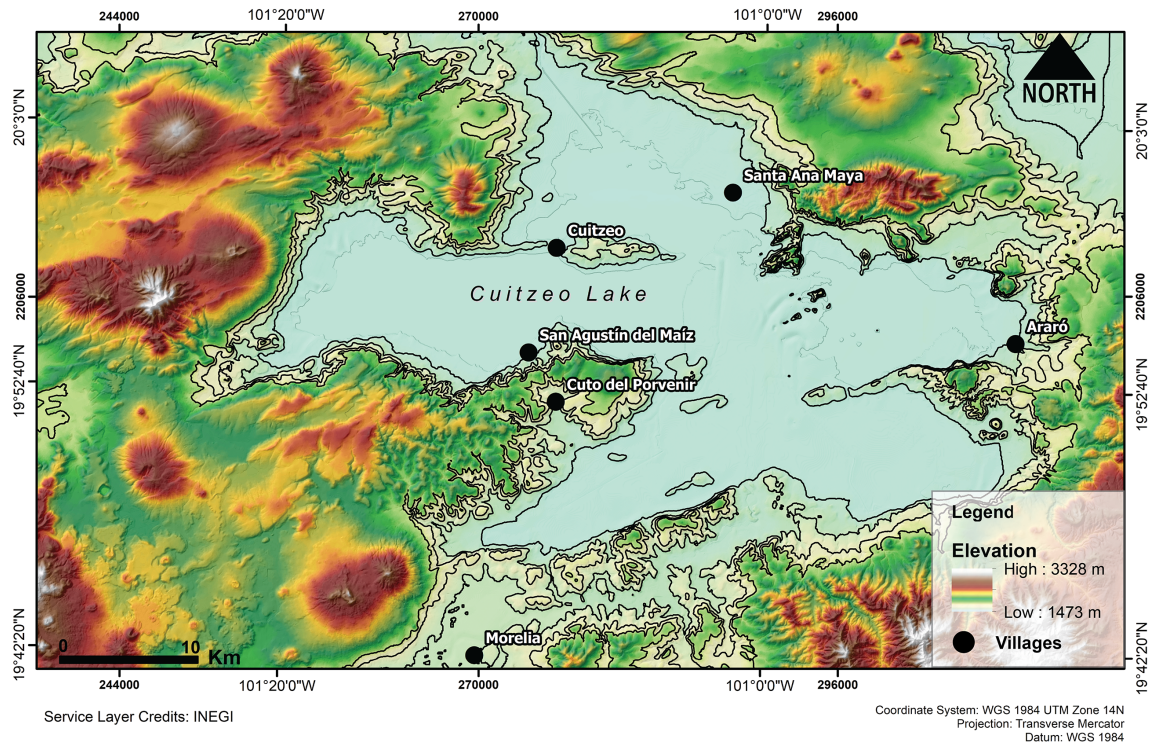


Figure 2. Topography around Cuitzeo Lake. Contours are at 50 m intervals between elevations of 1500 to 2000 m; these contours will be incorporated to the maps for reference. The highest elevation is at 2500 m. The lake is shallow, a few meters deep, and retreats considerably in some areas in the dry season. CU, Cuitzeo. AR, Araró, SAM, San Agustín del Maíz.

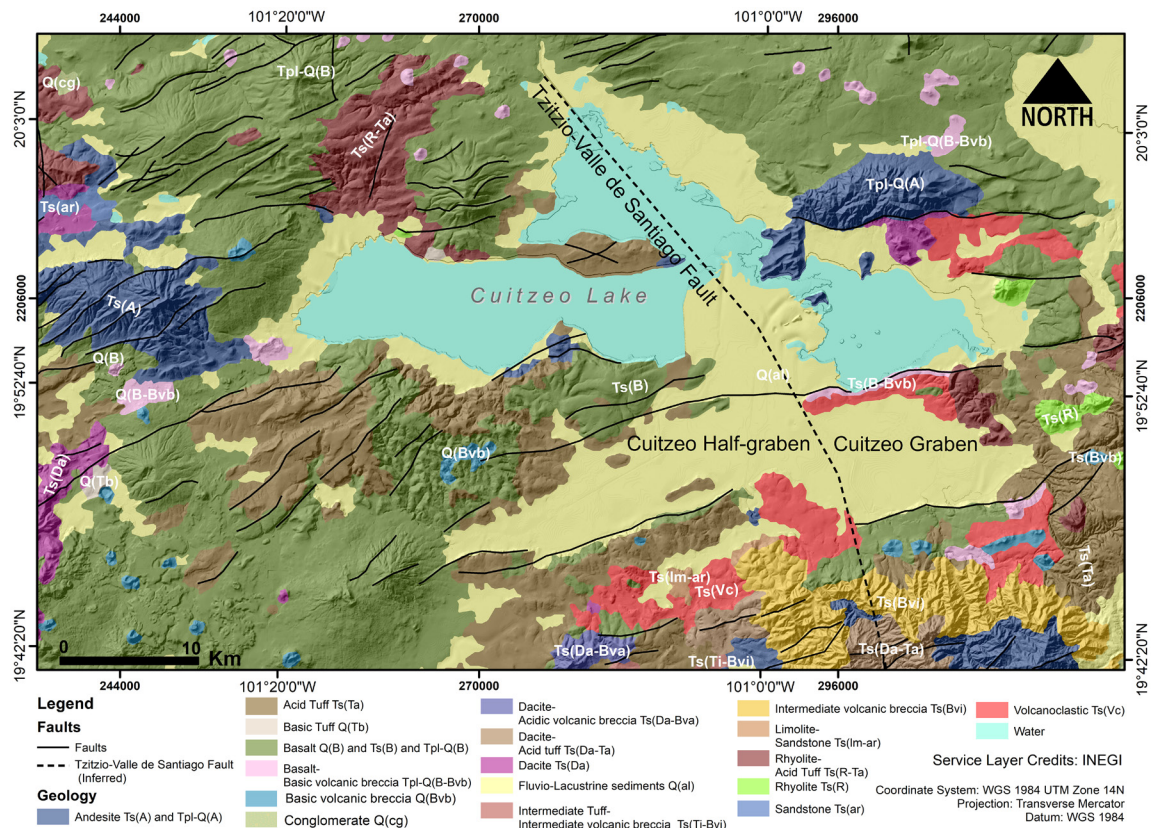


Figure 3. Regional, geologic map of the Morelia-Cuitzeo Lake region showing the Cuitzeo half-graben and graben, separated by the Tiztio-Valle de Santiago Fault.

Cuitzeo graben, mainly conformed by normal and listric faults. In addition, they are the main zones of geothermal fluid ascent as in the case of SAM in the area of Cuitzeo Lake (Garduño-Monroy *et al.*, 2009; Israde-Alcantara & Garduño-Monroy, 1999; Olvera-García *et al.*, 2020).

Data acquisition

Gravity and magnetic data were obtained in the study area; magnetic data correspond to the North America Magnetic Field data set (NAMAG, 2002); they were reduced to the pole according to the standard procedure (Baranod & Naudy, 1964). The Bouguer gravity anomaly (simple) data were obtained from the EIGEN 6C4 satellite-derived data set of the International Centre for Global Earth Models (ICGEM, Barthelmes and Kohler, 2016), with a node separation of .01°. For the topography we used the Digital Elevation Model (DEM) of ASTER (<https://gdex.cr.usgs.gov/gdex/>) with a 30 m resolution. Bouguer anomaly (BA) was obtained by the classical gravity anomaly minus the attraction of the Bouguer plate, calculated by the spherical approximation of the classical gravity anomaly minus $2\pi G\rho H$, where the topographic heights $H(\lambda, \varphi)$ are calculated from the spherical harmonic model of topography (ETOPO1) used up to the same maximum degree as the gravity field model, with $\rho = 2670 \text{ kg/m}^3$, and a resolution of 0.01°.

Figure 4 shows the magnetic map of the study area and Figure 5 shows the map corresponding to the gravity distribution. After the inversion process one obtains a distribution of magnetic susceptibilities in the case of the magnetic data, and a density distribution in the case of gravity data (Ellis *et al.*, 2012; MacLeod and Ellis, 2013). Various examples of 3D inversions are available (e.g., Alvarez & Yutsis, 2015; Alvarez & Yutsis, 2017; Guevara *et al.* 2021; Camacho and Alvarez, 2021; Alvarez and Camacho, 2023).

The 3D inversion

We used the method described by Macleod and Ellis (2013) based on the theoretical considerations of Ellis *et al.* (2012) to perform the 3D inversions presented here. The code runs in the Oasis Montaj program of Geosoft, where a 3D mesh of parallelepipeds is established in the region to be inverted. The program uses a Cartesian Cut Cell algorithm (CCC) to represent geologic volumes whose values are modified to reach the observed gravity/magnetic response. An Iterative Reweighting Inversion algorithm (IRI, Ingram *et al.*, 2003) is used to match the observed results with the calculated ones within established

error limits; in the present cases is 5% of the standard deviation. It is expressed as the measure of errors between paired observations; in this case the gravity or magnetic field observed and the corresponding calculated field:

$$\sum_{i=1}^n |y_i - x_i| / n = \sum_{i=1}^n |e_i| / n$$

with

$$e_i = |y_i - x_i|$$

where y_i is the prediction and x_i is the true value.

The inversion results are provided as densities in g/cm^3 when making a gravity inversion, and magnetic susceptibility (SI units) when performing a magnetic inversion. The depth of the inverted volume is proportional to the size of the volume selected for the calculation. Typically, areas of $50 \times 50 \text{ km}^2$ will attain depths of 5-6 km and greater depths can be obtained at the expense of the resolution. When referring to resolution we must bear in mind that there is the high-resolution of the data used to obtain the Bouguer anomaly in Figure 5a, in the gravity data case, and there is the resolution of the model proper. Models may have different dimensions and different resolutions; in this study we used models of dimensions in the X-Y plane of 1000 m, which we call the model resolution. To optimize computation, a subset of the high-resolution gravity data set is used, selected according to the model resolution, to perform the inversion. Figures 6a and 6b show the inverted volumes of the magnetic and the gravity inversions used in here; the latter shows the gravity station distribution used for that inversion.

Results

1) San Agustín del Maíz 1000m

We analyze first the region of San Agustín del Maíz (SAM), for its geothermal relevance. Olvera-García *et al.*, (2020) described its geothermal manifestations as distributed in an area characterized by fluvio-lacustrine sediments unconformably resting on volcanic rocks. They attribute the rising of geothermal fluids to permeable rock volumes located at the intersection of geologic fault systems where normal faults interact with transfer faults that together create rock zones of high permeability. High permeability usually implies high porosity and, consequently, low density values; density is one of the two variables that we use in our analysis, the other being the magnetic susceptibility. In the maps of Figures 4 and 5 two, perpendicular yellow lines

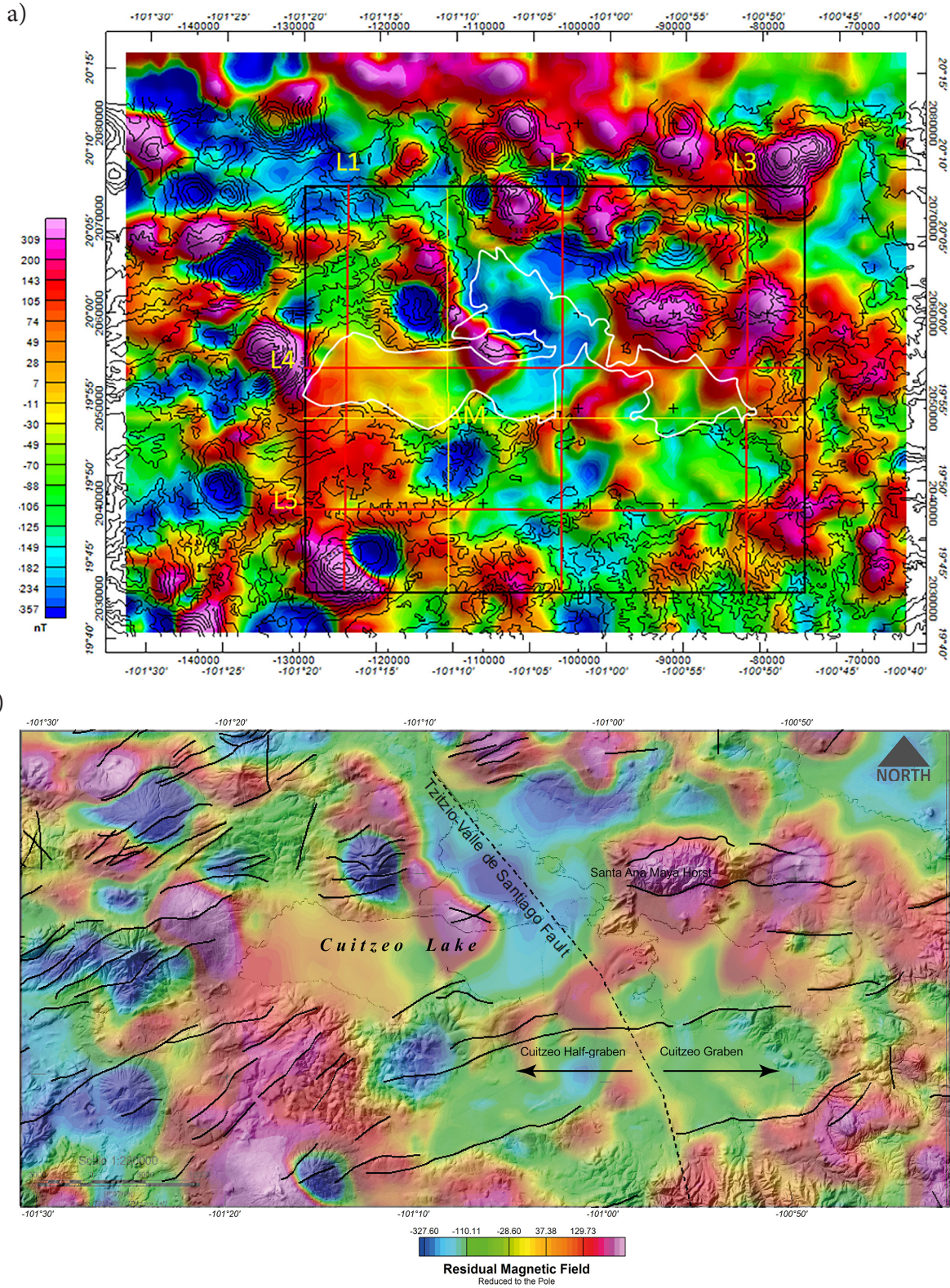


Figure 4. a) Magnetic map reduced to the pole of the Cuitzeo Lake region; elevation contours are shown for correlation, as well as the lake's outline (white). The black rectangle indicates the region in which a 3D inversion of the magnetic field is performed; the red lines (L1-L5) indicate where magnetic susceptibility cross-sections are obtained from such an inversion. SAM, Location of San Agustín del Maíz at the intersection of the two, perpendicular, yellow lines. b) Magnetic map reduced to the pole (Baranod and Naudy, 1964), superposed to the geologic map in Figure 3. Parameter values of the magnetic field: Inclination 47.60°, Declination 7.47°.

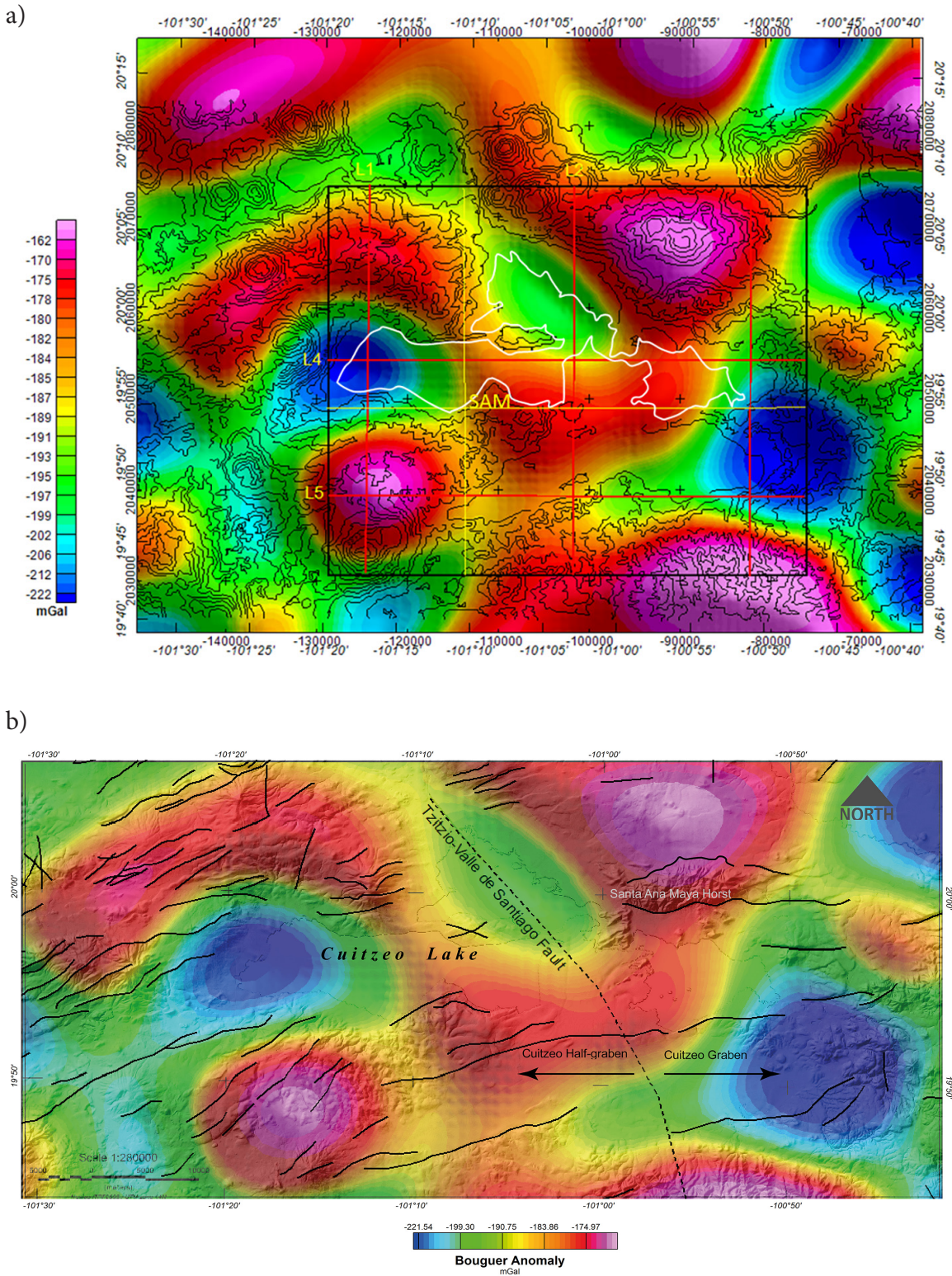


Figure 5. a) Bouguer anomaly (simple) map of the Cuitzeo Lake region; elevation contours are shown for correlation, as well as the lake's outline (white). The black rectangle indicates the region in which a 3D inversion of the gravity field is performed; the red and yellow lines indicate where density cross-sections are obtained from such an inversion; red and yellow lines are identified as in Figure 4. b) Bouguer anomaly map, superposed on the corresponding portion of the faults in the geologic map of Figure 3.

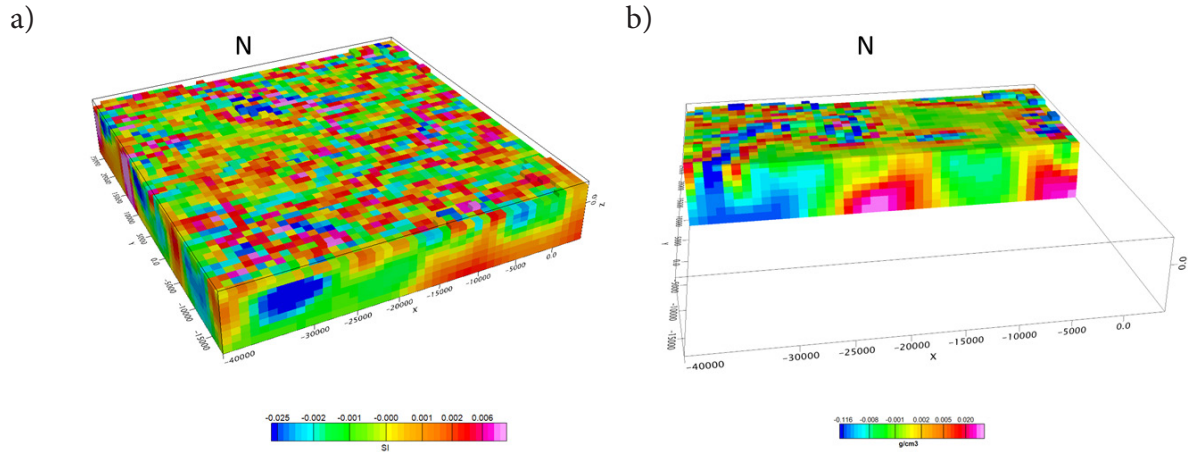


Figure 6. a) Full volume of the inverted model of the magnetic field reduced to the pole (Baranod & Naudy, 1964). b) E-W cross-section of the 3D gravity inversion showing the high-density (reds) and low-density (blues) voxels involved. Similar density cross-sections will be obtained along the yellow and red lines in Figure 5a, for the analysis of the density distribution. The mesh of points above the volume are the gravity stations used in the 3D inversion; the height of the stations is 500 m above the terrain. A similar set was used for inverting the magnetic data. Gravity scale + 2.67 g/cm³, magnetic scale +0.032 SI.

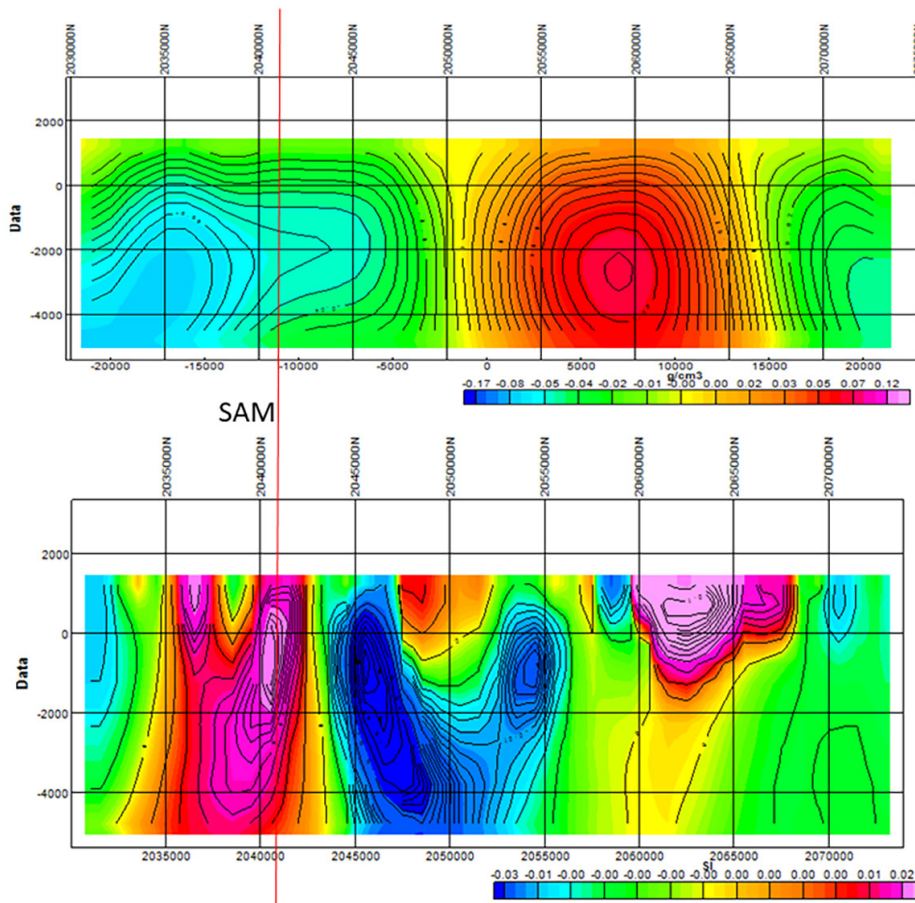


Figure 7. N-S cross-sections obtained from the 3D inversion of the gravity (above) and magnetic data crossing the location of San Agustín del Maíz (thin, red line). See Figures 4 and 5 for the location of the cross-sections. The horizontal scales are matched. Gravity scale + 2.67 g/cm³, magnetic scale +0.032 SI.

show the location of two cross-sections that intersect in the vicinity of SAM; the N-S and E-W cross-sections appear in Figures 7 and 8, respectively. In each instance the density section (in g/cm^3) appears above, and the magnetic susceptibility (in SI units $+0.032$ SI.) appears below.

In Figure 7, the density cross-section shows an important low-density region centered at -3000 m extending to the N, with a minimum at -2000 m under the location of SAM, suggesting that the low-density region feeds the geothermal manifestations in SAM. The presence of thermal springs and siliceous sinter deposits west of SAM (Olvera-García *et al.*, 2020) tend to confirm our observations. We consider the association of low-density regions with high temperatures as favorable to geothermal sources, since it may contain fluids at high temperatures that decrease magnetic susceptibility, and low-density, porous materials allowing fluid circulation. Continuing northwards, there is a considerable block of high-density material. The magnetic susceptibility cross-section shows a channel of low-susceptibility, rising from the bottom of the model (-5000 m) that emerges at

the location of SAM (thin, red line).

The boundary between the regions of high- and low-susceptibility regions is conspicuously associated with the normal fault through SAM, reported by Olvera-García *et al* (2020); the region of minimum susceptibility extends down to -5000 m showing some obliquity and confirming that these are deep-seated faults. Given the associated thermal manifestations in the surface, we conclude that the low-susceptibility of this region arises from materials subject to high temperatures, probably reaching close to the temperature of the Curie isotherm (Ravat, 2000). The simultaneous presence of the low-density material, as shown by the density cross-section, and the outcropping region of low-susceptibility, suggest that the surface geothermal manifestations are fed from a deep source, extending below -5000 m. A bifurcation to the N, of the low-susceptibility conduit is observed starting at -3000 m, which also reaches close to the surface; this region also appears of geothermal potential and should be further analyzed by other means. A good portion of the high-density region is also occupied by high-susceptibility

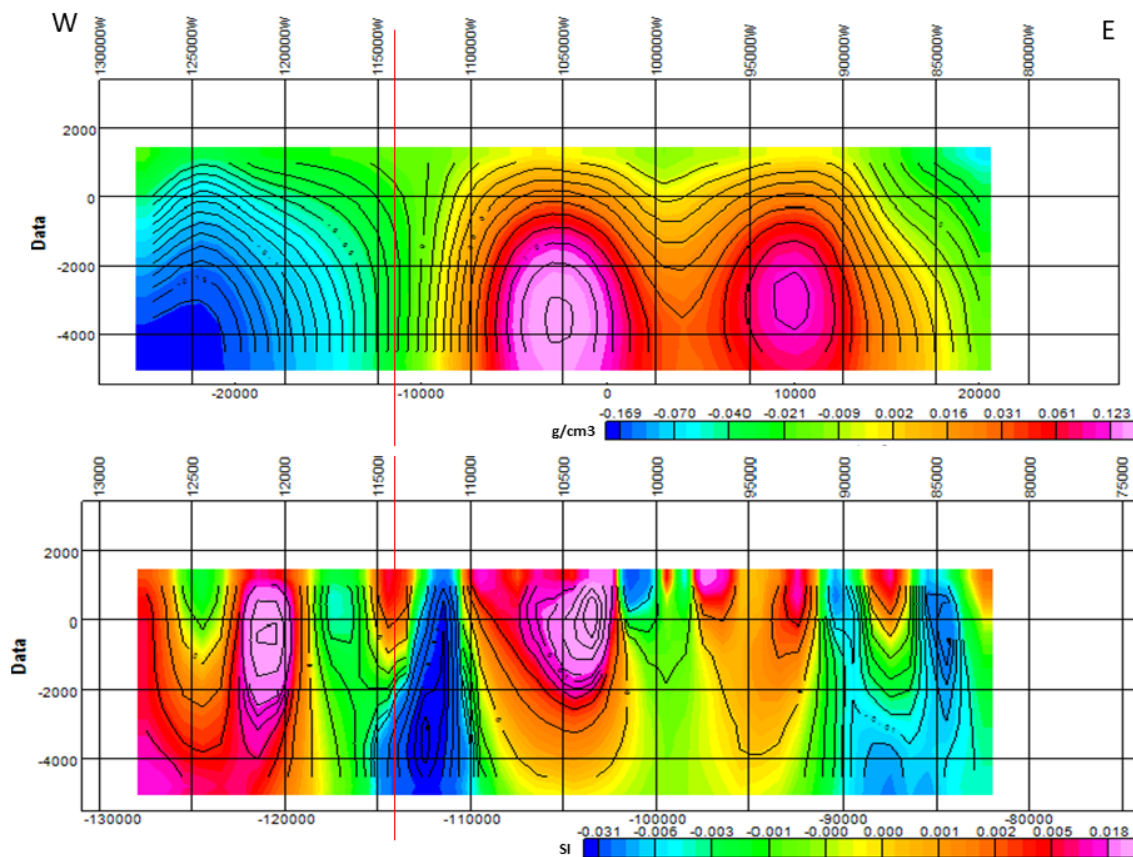


Figure 8. E-W cross-sections obtained from the 3D inversion of the gravity and magnetic data crossing the location of San Agustín del Maíz (thin, red line). See Figures 4 and 5 for the location of the cross-sections. The horizontal scales are matched. Gravity scale $+2.67 \text{ g/cm}^3$, magnetic scale $+0.032$ SI.

geologic formations; the joint effect of high density and high susceptibility suggests the presence of cold, volcanic materials emplaced significant time ago.

The density low observed in the southern portion of Figure 7, appears to extend westward in Figure 8, constituting a major anomaly in that region. The low-susceptibility region associated with the location of SAM (thin, red line) also appears bifurcated in this cross-section, hinting there is a circular distribution of low-susceptibility materials on the surface. The two density maxima correspond to two high-susceptibility regions. At the eastern end of the line, there is a similar distribution of low-density materials, with a shallow, central, high-susceptibility region, which is occupied by a density section, transitional between high- and medium-density.

We conclude that the density and magnetic susceptibility signatures around SAM are consistent with a region of high temperature of, at least 7 km depth and 20 km in length in the N-S direction, and 15 km in the E-W direction. With the help of X-ray analysis (DRX) Trujillo-Hernández, (2017) concludes that the abundant concentration of hydrothermally altered minerals, as well as the geologic evidence showing a high-degree of fracturing, mainly on the basaltic andesite lava flows, suggest that the chemical components travelled large distances, closing that the transport of hydrothermal fluids occurs mainly by infiltration.

With the experience gained analyzing the responses of the SAM region containing geothermal manifestations, we proceed to the analysis of L1-L5 cross-sections.

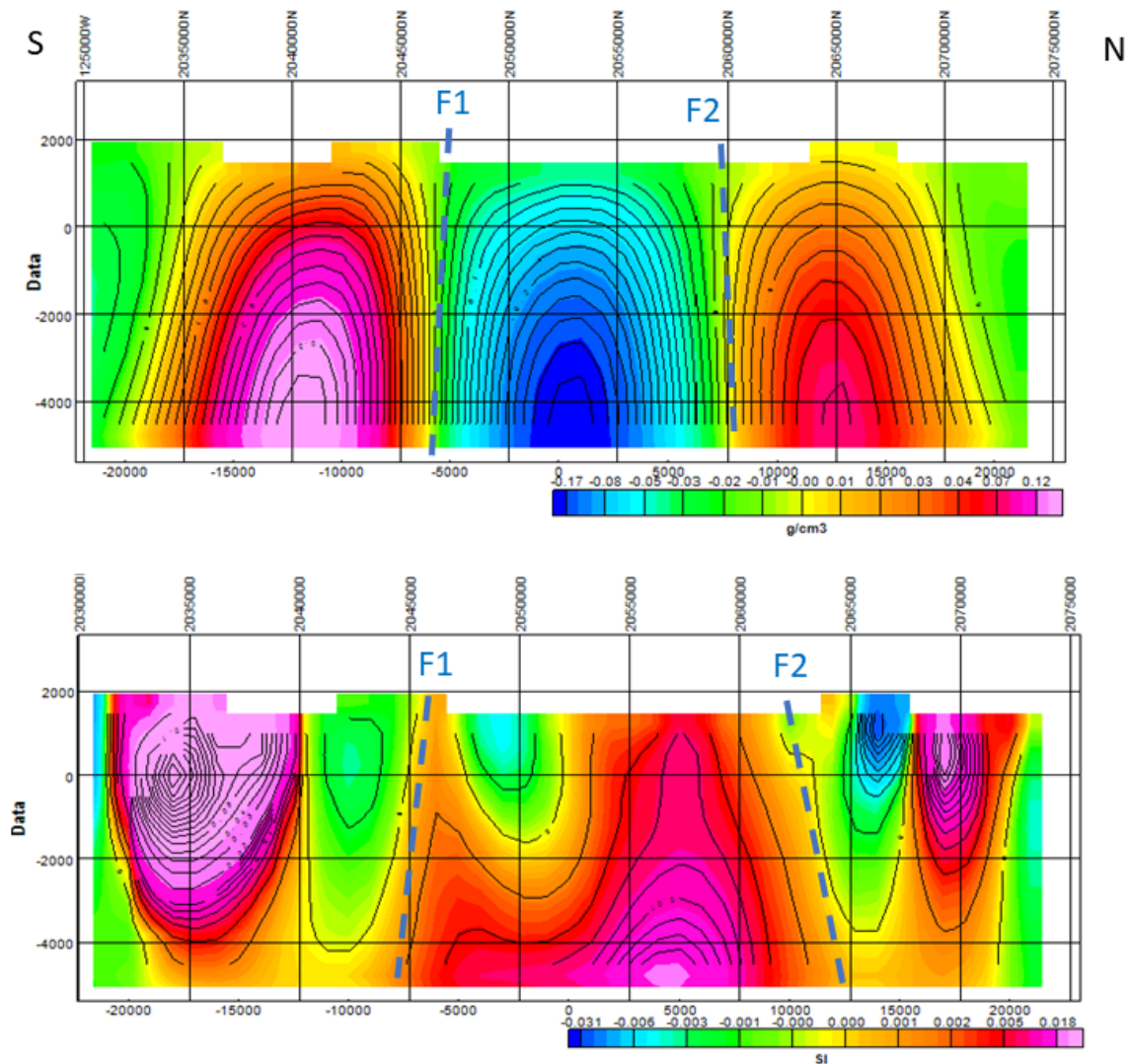


Figure 9. L-1, N-S cross-sections obtained from the 3D inversion of the gravity (above) and magnetic data. See Figures 4 and 5 for the location of the cross-sections. The horizontal scales are matched. F1 and F2 represent boundaries between contrasting properties in the cross-sections. Gravity scale $+2.67 \text{ g/cm}^3$, magnetic scale $+0.032 \text{ SI}$.

2) The N-S Lines

Here we analyze the group of three N-S lines labeled L1-L3 in Figure 4.

L1 is the westernmost line, oriented N-S. The density cross-section exhibits a large negative anomaly well constrained by two high-density regions with vertical boundaries F1, F2; it resembles a graben structure, but lacks an extended graben axis. The lowest density values are close to the 5 km depth, probably linked to the corresponding anomalies in the N-S and E-W cross-sections of SAM (Figures 7 and 8). The central portion of the magnetic susceptibility cross-section shows structural characteristics similar to those of the central anomaly of the density cross-section; that is, it has the same width and depth. The bounding limits F1 and F2 are followed by a low and a high susceptibility region, respectively. From these observations we

conclude that the central region of this cross-section is a major anomaly of geothermal potential.

L-2 presents structural characteristics like those observed along L1. There is a main low-density region, not centered but slightly displaced to the N, also bounded by two high-density regions, whose boundaries also reach to the bottom of the cross-section. Given the density similarities between L1 and L2, and their proximity, one would tend to connect the main low-density anomalies; however, from Figure 5a one can see that they are separated by a region of high gravity values, which prevents such a connection. The corresponding region in the magnetic susceptibility cross-section, exhibits a bifurcation of the low-susceptibility region, similar to the one displayed in Figure 7, that surfaces at the F2 boundary, indicating that it also may represent the source of a potential geothermal area. Of particular interest is noting that this isolated anomaly is crossed

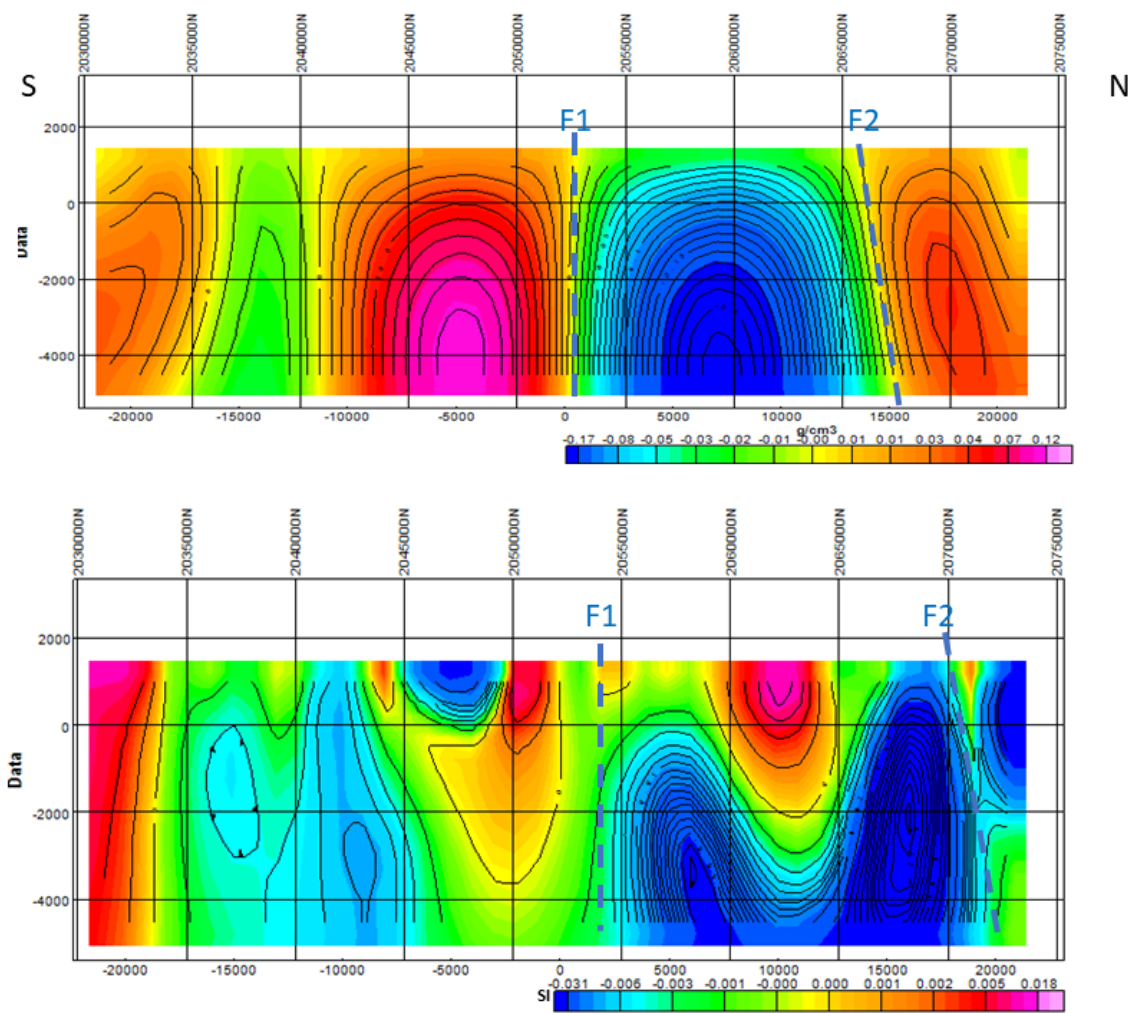


Figure 10. L-2, N-S cross-sections obtained from the 3D inversion of the gravity (above) and magnetic data. See Figures 4 and 5 for the location of the cross-sections. The horizontal scales are matched. F1 and F2 represent boundaries between contrasting properties in the cross-sections. Gravity scale $+2.67 \text{ g/cm}^3$, magnetic scale $+0.032 \text{ SI}$.

by the Tzitzio-Valle de Santiago fault (see Figure 3), which may have facilitated the intrusion of a heat source at depth.

According to Trujillo-Hernández (2017) this fault, that cuts through Cuitzeo Lake, is the most important NNW-SSE construct, defined as an old, buried fold-fault structure, responding to the present stress regime as a right-lateral fault. This system is presently active, cutting from old Early Miocene formations to Recent soils and volcanoclastic formations.

This line samples the Cuitzeo graben (Figure 5b) from S to N. It presents a different behavior from those observed at L1 and L2, since the low-susceptibility region at the center of the section corresponds with a high-density region in the density section, flanked by low-density areas which, in turn, correspond to two high-susceptibility regions.

3) The E-W cross-sections

Lines 4 and 5 in Figure 4 are the two E-W cross-sections that appear in Figures 12 and 13, respectively.

L4 crosses the study area from W to E (Figure 4). Regions of low and high density alternate in the cross section, corresponding to the low and high values of the BA; the density cross-section shows that transitions from low- to high-density regions reach vertically the full depth of the inversion (from +2000 m to -5000 m), suggesting a tectonic control of the distribution of geologic materials. The magnetic susceptibility cross-section shows that the portion corresponding to the high-density section has low-susceptibility regions similar to those observed in SAM (Figure 7), also divided by a small, high-susceptibility region,

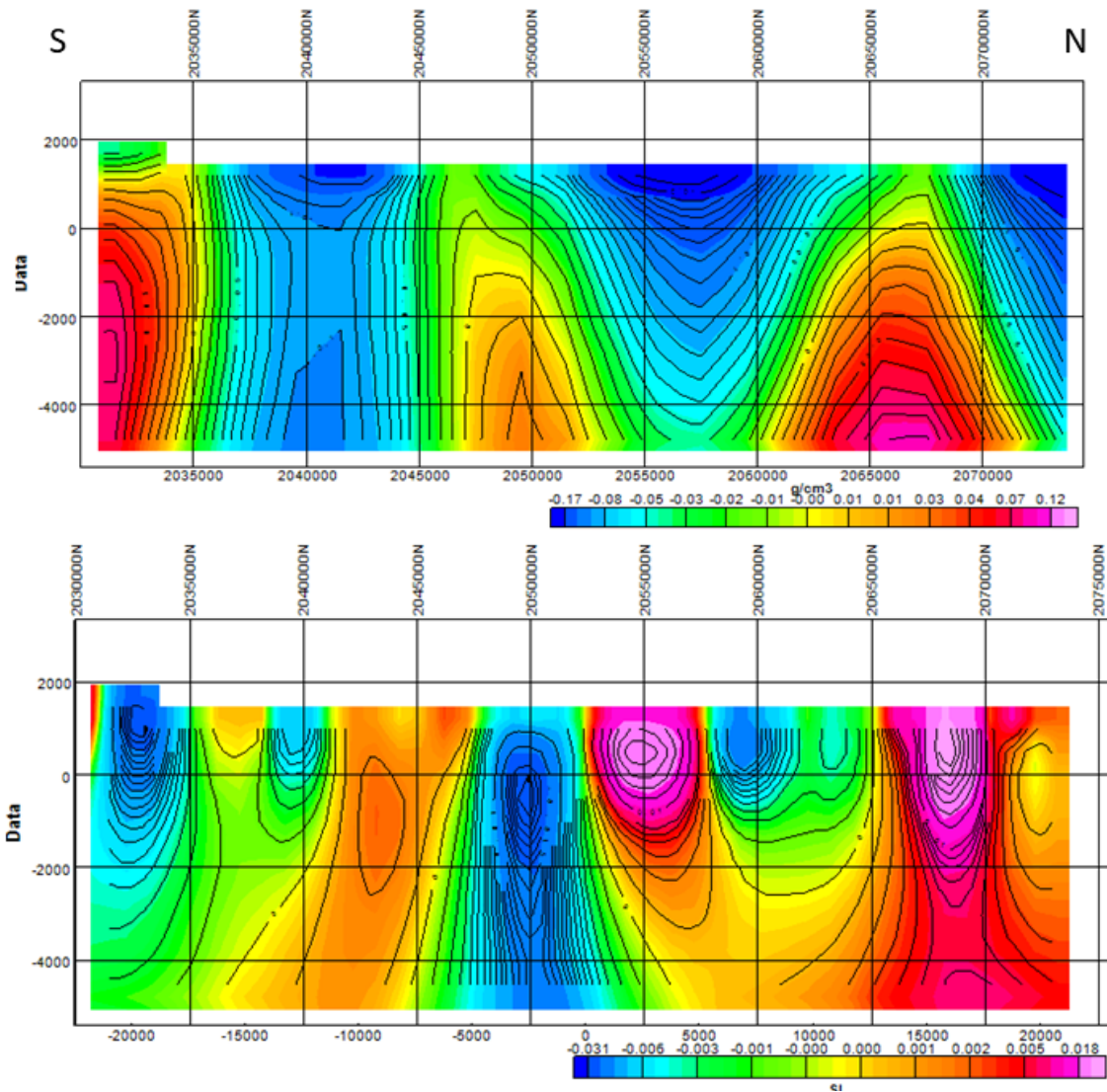


Figure 11. L3 N-S cross-sections obtained from the 3D inversion of the gravity (above) and magnetic data. See Figures 4 and 5 for the location of the cross-sections. The horizontal scales are matched. Gravity scale $+2.67 \text{ g/cm}^3$, magnetic scale $+0.032 \text{ SI}$.

suggesting that this anomaly distribution occupies a considerable area of this region. Close to the end of the line (88000E or $100^{\circ}-53'$) in the N side, a negative low-susceptibility region with deep roots reaches the surface; it corresponds to a medium-density region, which could also be considered a potential exploration target for geothermal objectives, since it appears close to the south fault of the Santa Ana Maya horst (Figure 5).

L5 samples the S portion of the study area from W to E. The pattern observed in L4 regarding the vertical boundaries between high- and low-density regions is observed in two thirds of the length of L5, noticing a considerable departure from this behavior in the N portion of this section, where low density distributions predominate. There, the minimum of the low-density portion is located at -4000m depth; this anomaly outcrops almost directly above this minimum. At the E end of L5 there is another

outcropping region of low density, except it has density values like those observed at the anomaly located at -4000m, making it another potential target for geothermal evaluation.

The magnetic susceptibility cross-section shows a low-susceptibility region well constrained by high-susceptibility regions, extending from the surface to -5000m depth, corresponding with the high-density region. At the E end of the line, there is a good match of shallow, low-susceptibility regions with the low-density regions reported above as potential geothermal targets, reinforcing such a statement.

4) Geosurfaces

A geosurface is obtained from an inverted volume, as the region in which the volume has a constant value, in g/cm^3 if the

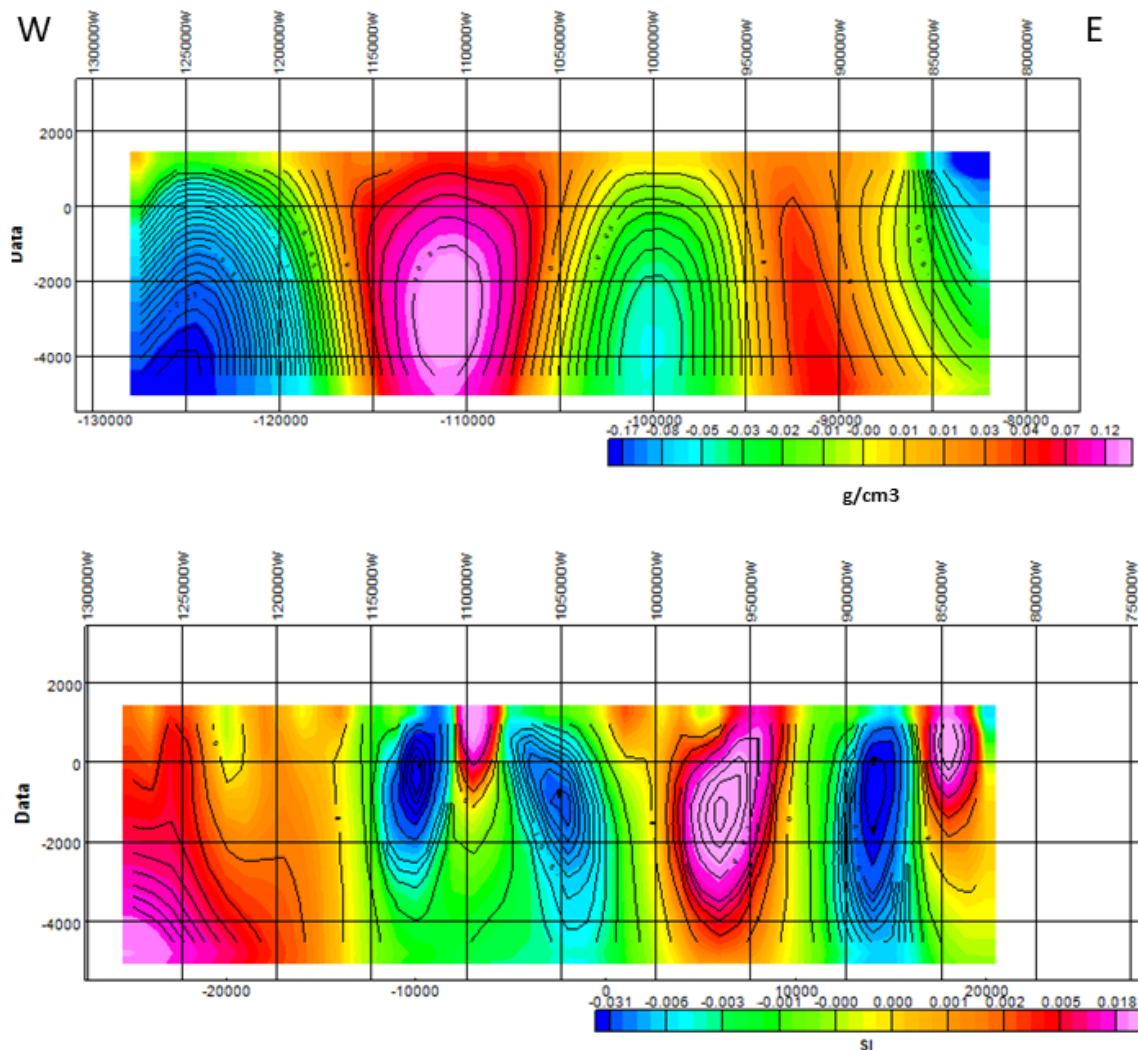


Figure 12. L4 in Figure 4, showing the cross-sections of density and magnetic susceptibility along the E-W direction; the horizontal scales are the same. Gravity scale $+ 2.67 \text{ g}/\text{cm}^3$, magnetic scale $+0.032 \text{ SI}$.

inverted volume is a density distribution, and in SI units if it is a distribution of magnetic susceptibilities. Geosurfaces complement observations made with the cross-sections.

A set of calculated density geosurfaces is in Figure 14; they range from 2.76 to 2.46 g/cm³; in the calculation, the whole inverted volume is scanned to determine where those density values are located and, then plotted. The blue surfaces are close to the vertical and, in the present case, extend from the surface to the bottom of the inverted volume, or about 7 km in depth. We searched for lower densities, down to 2.46 g/cm³, finding only two locations in which they are present; they are labeled as A1 and A2 in Figure 14. A1 is located close to the geothermal manifestations in SAM, and we submit that this is most likely the heat source feeding these geothermal manifestations. In A2 the green surface is cut to allow looking at the orange surface; below it, we could not locate a magenta surface. A2 is traversed

by the Tzitzio-Valle de Santiago fault (Figure 5) and we propose that it should be considered a geothermal exploration target, for its similarity with A1. The geothermal fluids can pass through the impervious cover owing to the persistent tectonic activity maintaining the permeability.

In Figure 14 there are four geosurfaces of different colors, corresponding to four density values. The geosurfaces in blue call the attention, since they start at the surface and end at the bottom (7 km) of the inverted volume, following vertical, or close to vertical inclinations; furthermore, they are thin, and cross the study area in various directions, restraining the regions of high gravity values, as seen in Figure 15, where we have superposed the geosurfaces to the BA map. We interpret them as vertical, boundary, or transitional regions, between high- and low-density regions, yielding the observed responses. Portions of these boundary surfaces are also present in the cross-sections presented

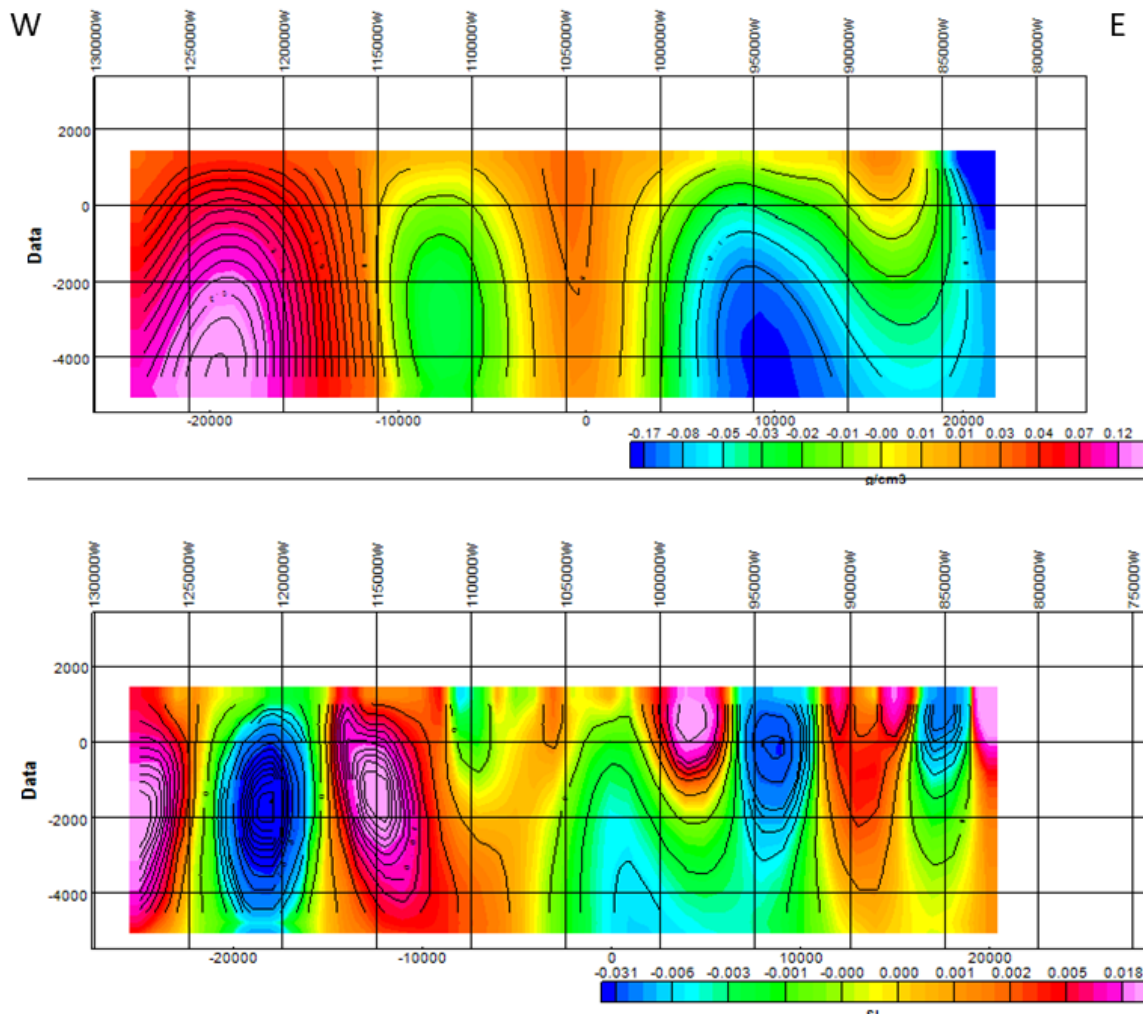


Figure 13. L5 in Figure 4 showing the cross-sections of density (above) and magnetic susceptibility, along the E-W direction; the horizontal scales are equal. Gravity scale +2.67 g/cm³, magnetic scale +0.032 SI.

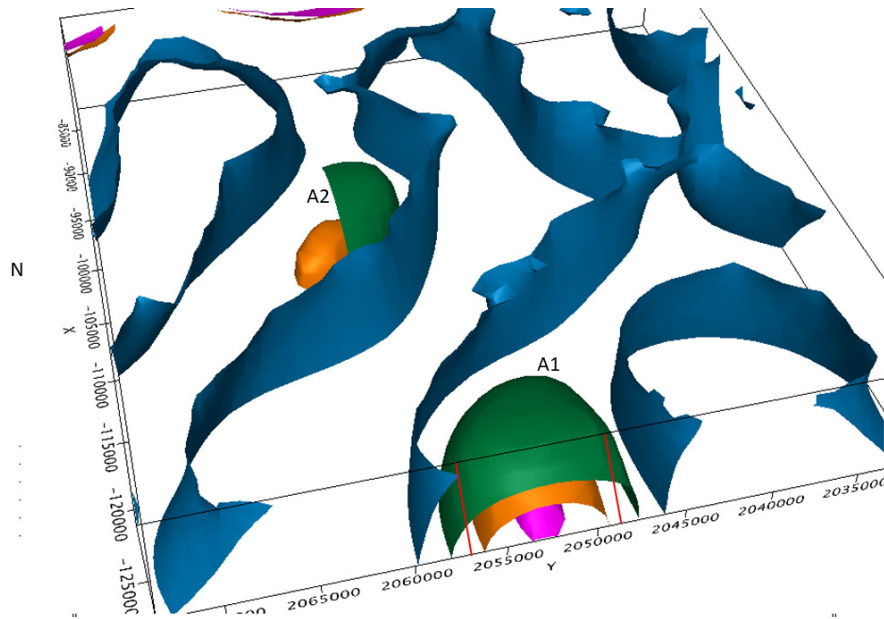


Figure 14. 3D display of geosurfaces for various densities (g/cm^3): blue (2.76), green (2.66), orange (2.56), magenta (2.46). North is to the left; this view allows to appreciate how low-density varies with depth in anomaly A1; the green geosurface, in anomaly A2, is clipped to allow viewing the orange surface, no magenta surface is present. The brown, dashed line crossing the figure from N to S is the trace of the Titzio-Valle de Santiago fault. The red line is the outline of Cuitzeo Lake.

above; in some places they may be identified with faults bounding the low-density regions.

If we consider the superposition of the inverted results over the Bouguer anomaly map, in Figure 15, we note i) that the surface geothermal manifestations of SAM are located over one of these blue geosurfaces, and ii) that they are quite close to the anomalous density region A1, shown in section in Figure 14. Since there are only two anomalies with low-density characteristics in the inverted 3D region, A1 and A2, we infer that they are potential heat sources for geothermal fluids. The proximity of anomaly A1 to SAM, also illustrated in the density cross-section of Figure 6, tends to validate our inference. Although there appear to be no surface, geothermal manifestations in the region of anomaly A2, it should be considered a potential exploration target; the center of the anomaly is located 11 km E of Cuitzeo del Porvenir town, over the Tzitzio-Valle de Santiago fault (see Figure 3).

Figure 16 shows the vertical superposition of density geosurfaces, with some transparency, and susceptibility prisms of values between 0.042 and 0.012 SI. We observe two branches (NW and SE) and a central channel between them, oriented SW-NE; the latter shows a minor presence of prisms with such values. At present we cannot offer a hypothesis about the reason for this peculiar susceptibility distribution. The NW branch exhibits

concentrations of these prisms in the rim of A1 (at SAM) and in the location of A2 (see Figure 15), allowing the association of these susceptibility concentrations with such anomalous regions. The largest concentration of prisms in the SE branch may be associated with the eastern portion of L4 (Figure 12).

5) 2D model

To complement these results and discussion, we calculated several 2D models to ascertain the regional structural characteristics of the area; an example appears in Figure 17 displaying the resulting model along L1. It shows that andesitic formations dominate the region and comprise the high-density regions, whilst the central portion contains conglomerates and sediments of approximately 500 m depth, overlaying a volcanic formation. The deepest layer is the granitic basement. Andesites appear to be the geologic formations sealing the geothermal fluids heated by intrusions. Tectonic movements and geologic faults must create the paths through which these fluids reach the surface at several locations. In particular for this model, the SW-NE fault system identified in Figure 3 intersecting Cuitzeo Lake, with one of its components going through SAM region, appears to be the one controlling fluid migration.

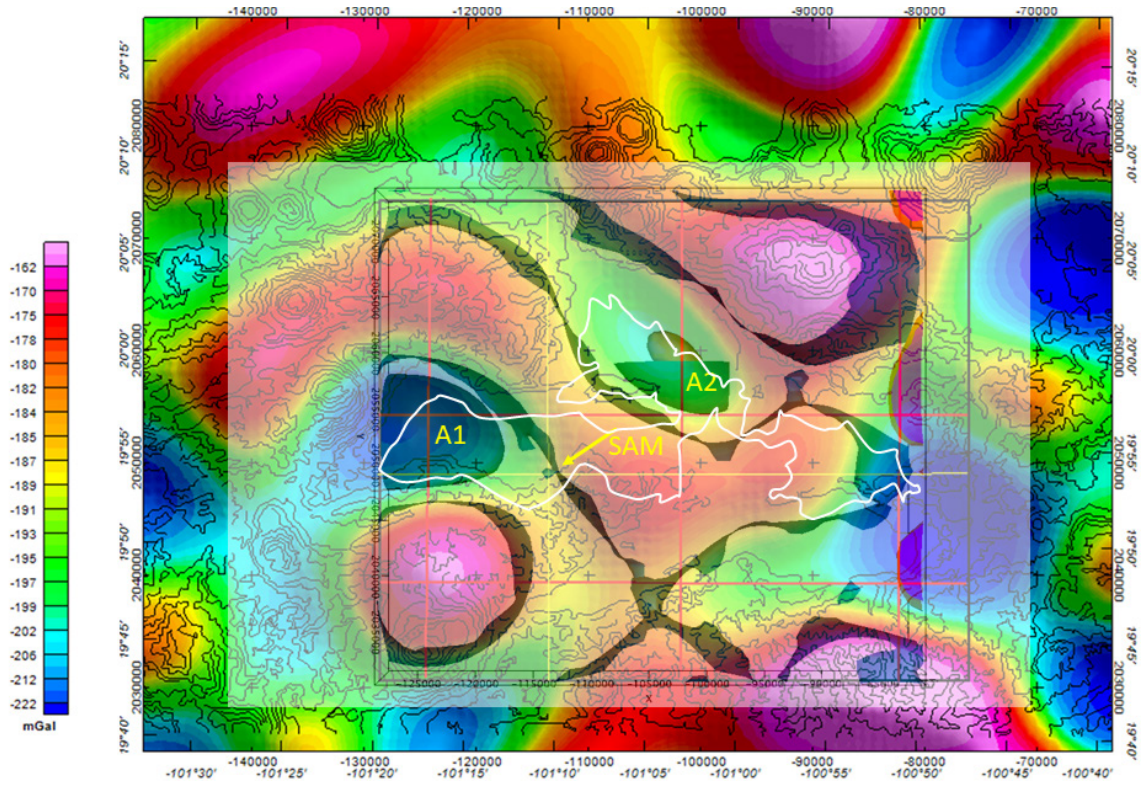


Figure 15. Vertical view of the geosurfaces obtained from the 3D gravity inversion, superposed (gray rectangle) on the BA map. A1 and A2 are the anomalies indicated in Figure 14. Red and yellow lines are labeled in Figure 4. The lake's outline in white.

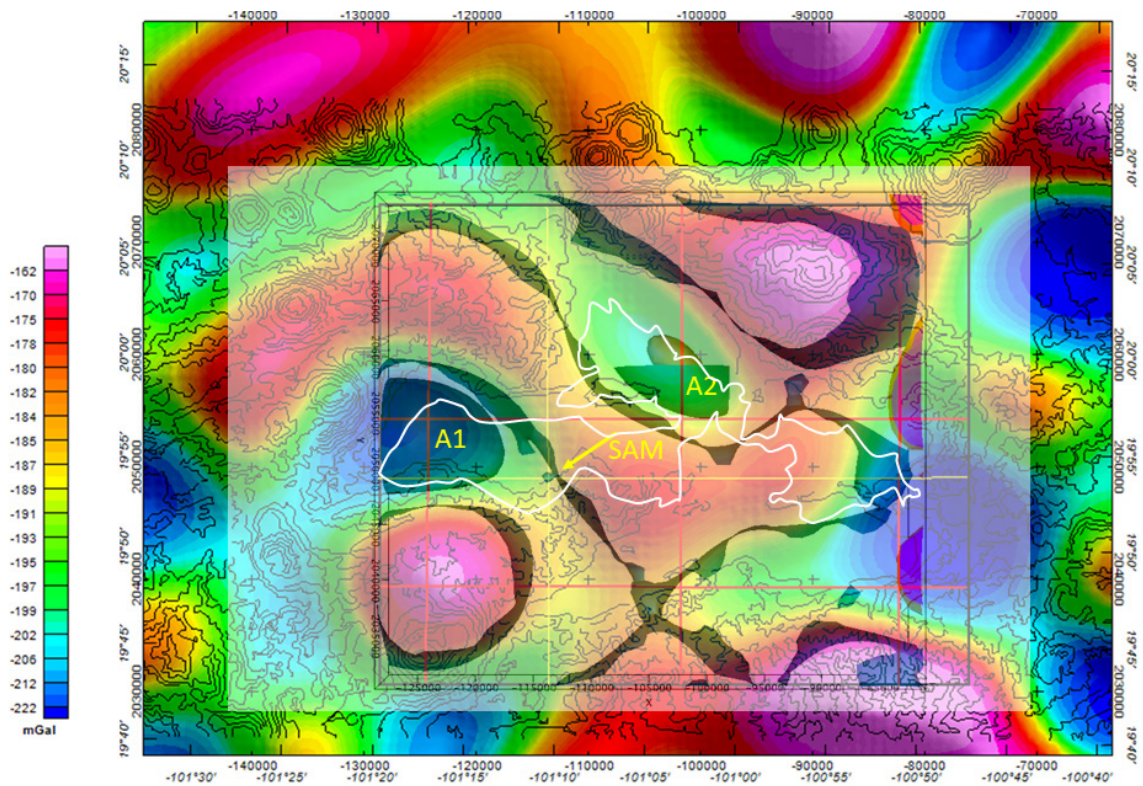


Figure 16. On the BA map we superposed the density geosurfaces and selected magnetic susceptibility prisms in the inverted region (gray rectangles). Magnetic susceptibility between 0.042 and 0.012 SI; the latter are the darker prisms.

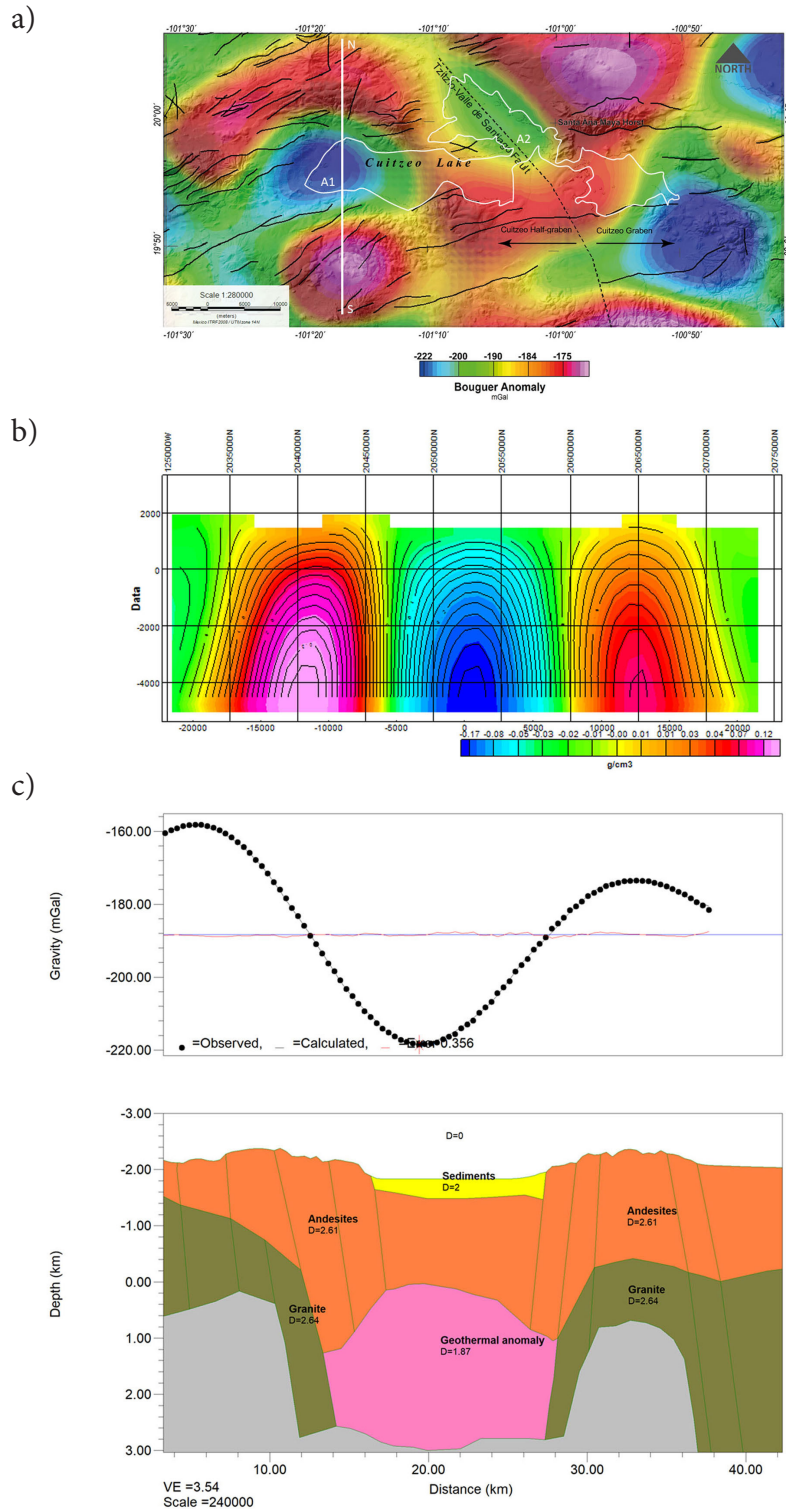


Figure 17. Two-dimensional gravity model along L1. a) N-S line L1 in which the model is calculated; volcanic products dominate the background. The Bouguer anomaly is superposed to a topography map (Figure 5) where several locations are identified, b) cross-section derived from the inverted density volume with a resolution of 1000m, and c) 2D model 5 km in depth identifying geologic formations along the cross-section; distributions of Miocene to Quaternary andesitic lavas and dacitic ignimbrites described in Figure 3. A region, designated geothermal anomaly, is emplaced below sea level (0m elevation) coinciding with A1 in Figure 14; an intrusive body may be responsible for the graben-like structure in the surface, and for the location of a low-density, high-temperature region. We define the geothermal anomaly as the joint occurrence of heated regions, fluid sources, and confining geologic structures.

Conceptual model

A conceptual model is shown in Figure 18, of an intrusive body causing the materials and fault distribution in the model of Figure 17, particularly the downward displacement of the region corresponding to Cuitzeo Lake. This intrusive is also the heat source for the geothermal manifestations. Motion along geologic faults would assist the flow of geothermal fluids reaching the surface.

Conclusions

The 3D inversion of gravity and magnetic data provided volume distributions of density and magnetic susceptibility that reproduced the observed fields within 5 percent of the respective standard deviations. From these results, we extracted cross-sections and geosurfaces that allowed the location of regions of potential geothermal interest. Analysis of two perpendicular cross-sections at a location with surficial geothermal manifestations (SAM) provided criteria that were used to analyze the

whole inverted volume. We established that vertical boundaries between neighboring density and magnetic susceptibility regions, often extended throughout the entire thickness of the cross-sections (7 km), suggesting that such boundaries may be associated with deep geologic faults. We propose that the SW-NE trending fault system in Figure 3, is responsible for geothermal fluid migration in the SAM region. With these results, however, we cannot establish a uniform criterium, such as the association of low-density regions with regions of low susceptibility, to establish the existence of geothermal sources. We found zones in which, in addition to the above combination, regions of high density and low magnetic susceptibility, or high density and high susceptibility, may also represent potential geothermal targets in the surveyed region. More research is needed in this direction to characterize regions of geothermal potential. Concurrence of other geologic and geophysical methods will help refine the location of geothermal targets.

We conclude that the detection of geothermal exploration targets, using gravity and magnetic fields, is viable when adequate data sets are used; however, we recognize that, given the nature of the potential fields, results should be taken only as indications

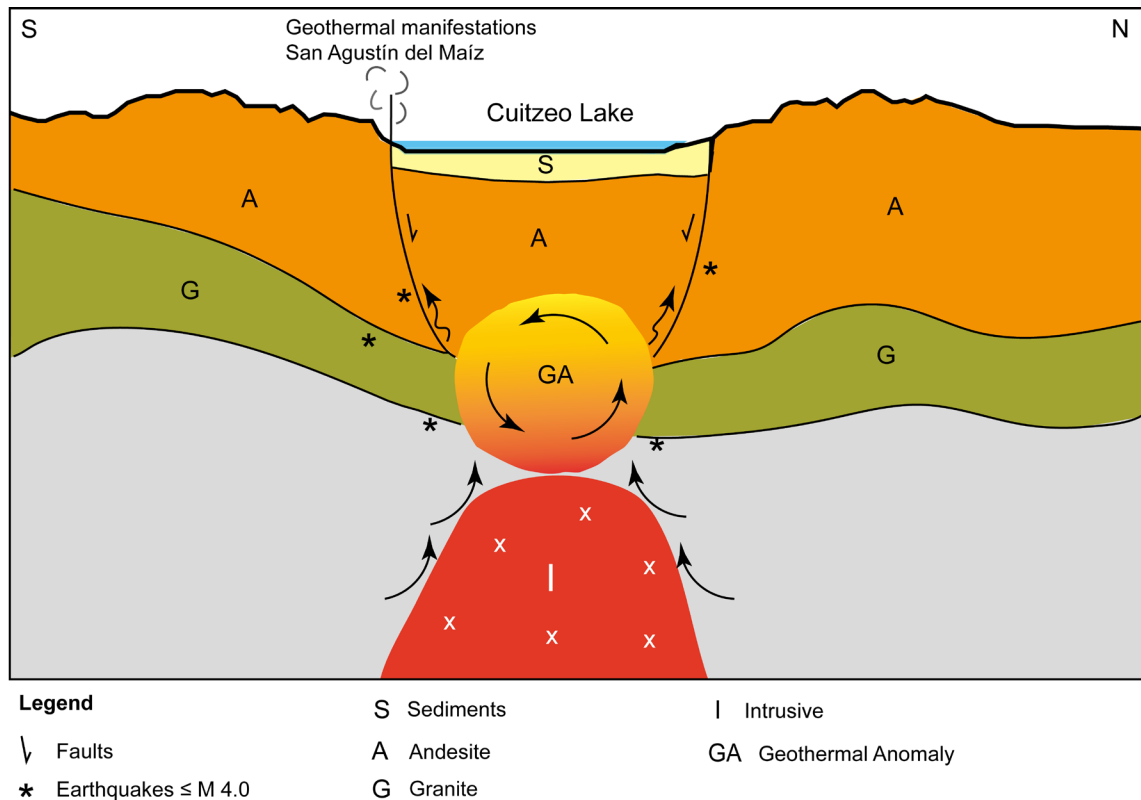


Figure 18. Conceptual model of the geothermal system feeding San Agustín del Maíz, in Cuitzeo Lake. The intrusive body heats the geothermal anomaly; its emplacement induces motion along the fault system, which in turn generates small magnitude earthquakes. Units described as sediments, andesite, and granite are only indicative of the type of rocks located in those regions. The gray region represents basement rocks containing an igneous intrusion I.

of the existence of such regions. Additional exploration methods should complement the results presented in this contribution. The advantage of using Potential Methods in exploration geophysics is that data is often available free, and large areas can be explored with limited resources before more costly methods can be applied. Data resolution should also be of primary concern when using this methodology; higher-resolution data sets will allow for a finer location of potential targets.

Declaration of Competing Interest

The authors declare that they have no known competing financial interests or personal relationships that could have influenced the work reported in this paper.

Authors statement

Both authors participated in conception and structure of the paper's lineaments. ER contributed mainly to the geological facets and RA in the geophysical analysis and interpretation of the data. Among them wrote and approved the final version.

Acknowledgments

During development of this work, ER received support from Consejo Nacional de Ciencia y Tecnología (CONACYT), Mexico. We thank Posgrado en Ciencias de la Tierra, UNAM, for access to computational resources. This study has been supported by IIMAS, UNAM; we acknowledge material support from the three institutions. This research did not receive any specific grant from funding agencies in the public or private domain.

References

- Alvarez, R. & Camacho, M. (2023). Plumbing System of Hunga Tonga Hunga Ha'apai Volcano. *Journal of Earth Science*, 34(3): 706–716. <https://doi.org/10.1007/s12583-022-1792-0>
- Alvarez, R. & Yutsis, V. (2015) Southward Migration of Magmatic Activity in the Colima Volcanic Complex, Mexico: An Ongoing Process. *International Journal of Geosciences*, 6, 1077-1099. <http://dx.doi.org/10.4236/ijg.2015.69085>
- Alvarez, R & Yutsis, V. (2017) Potential fields modeling of the Serdán Oriental basin, Eastern Mexico. *Jour. South American Earth Sci.* 80 (2017) 375-388. <https://doi.org/10.1016/j.jsames.2017.10.003>
- Baranod, V. & Naudy, H. (1964). Numerical calculation of the formula of reduction to the magnetic pole. *Geophysics*, 29, 67-79.
- Barthelmes, F. & Kohler, W. (2016). International Centre for Global Earth Models (ICGEM), in: Drewes, H., Kuglitsch, F., Adam, J. *et al.*, The Geodesists Handbook, 2016. *J. Geod.* 90 (10), 907–1205. <https://doi.org/10.1007/s00190-016-0948-z>.
- Camacho, M. & Alvarez, R (2021) Geophysical modeling with satellite gravity data: EIGEN6C4 vs GGMplus. *Engineering*, 13, 690-706. <https://doi.org/10.4236/eng.2021.1312050>
- Correa-Gómez, J. G. (2019). Petrophysical characterization of a lithofacies of the Cuitzeo, Michoacan ignimbrite sequence (in Spanish). Universidad Nacional Autónoma de México. Morelia City.
- Ellis, R.G., de Wet, B. & Macleod, I.N. (2012) Inversion of Magnetic Data for Remnant and Induced Sources. Australian Society of Exploration Geophysicists, Extended Abstracts 2012, 1-4, Melbourne.
- Ferrari, L. (2000). Advances in the knowledge of the Transmexican Volcanic Belt during the last decade (In Spanish). *Boletín de La Sociedad Geológica Mexicana*, 53(1), 84–92. <https://doi.org/10.18268/BSGM2000v53n1a5>
- Ferrari, L., Orozco-Esquivel, T., Manea, V., & Manea, M. (2012). The dynamic history of the Trans-Mexican Volcanic Belt and the Mexico subduction zone. *Tectonophysics*, 522–523, 122–149. <https://doi.org/10.1016/j.tecto.2011.09.018>
- Garduño-Monroy, V. H., Pérez-Lopez, R., Israde-Alcantara, I., Rodríguez-Pascua, M. A., Szyndkaruk, E., Hernández-Madrigal, V. M., García-Zepeda, M. L., Corona-Chávez, P., Ostroumov, M., Medina-Vega, V. H., García-Estrada, G., Carranza, O., Lopez-Granados, E., & Mora Chaparro, J. C. (2009). Paleoseismology of the southwestern Morelia-Acambay fault system, central Mexico. *Geofísica Internacional*, 48(3), 319–335. <https://doi.org/10.22201/igef.00167169p.2009.48.3.29>
- Gómez-Tuena, A., Orozco-Esquivel, M. T., & Ferrari, L. (2007). Igneous petrogenesis of the Trans-Mexican Volcanic Belt. *Special Paper of the Geological Society of America*, 422(303), 129–181. [https://doi.org/10.1130/2007.2422\(05\)](https://doi.org/10.1130/2007.2422(05))
- Gómez-Vasconcelos, M. G., Garduño-Monroy, V. H., Macías, J. L., Layer, P. W., & Benowitz, J. A. (2015). The Sierra de Mil Cumbres, Michoacán, México: Transitional volcanism between the Sierra Madre Occidental and the Trans-Mexican Volcanic Belt. *Journal of Volcanology and Geothermal Research*, 301(June 2016), 128–147. <https://doi.org/10.1016/j.jvolgeores.2015.05.005>
- Gómez-Vasconcelos, M. G., Macías, J.L., Avellán, D. R., Sosa-Ceballos, G., Garduño-Monroy, V. H., Cisneros-Máximo, G., Layer, P. W., Benowitz, J., López-Loera, H., López, F. M., & Perton, M. (2020). The control of preexisting faults on the distribution, morphology, and volume of monogenetic volcanism in the Michoacán-Guanajuato Volcanic Field. *Bulletin of the Geological Society of America*, 132(11–12), 2455–2474. <https://doi.org/10.1130/B35397.1>
- Gómez-Vasconcelos, M. G., Avellán, D. R., Soria-Caballero, D., Macías, J. L., Velázquez-Bucio, M. M., Jiménez-Haro, A., Israde-Alcántara, I., Garduño-Monroy, V. H., Ávila-Olivera, J. A., Figueroa-Soto, Á. G., Cisneros-Máximo, G., & Cardona-Melchor, S. (2021a). Geomorphic characterization of faults as earthquake sources in the

- Cuitzeo Lake basin, central México. *Journal of South American Earth Sciences*, 109(February), 103196. <https://doi.org/10.1016/j.jsames.2021.103196>
- Gómez-Vasconcelos, M. G., Avellán, D. R., Soria-Caballero, D., Macías, J. L., Velázquez-Bucio, M. M., Jiménez-Haro, A., Israde-Alcántara, I., Garduño-Monroy, V. H., Ávila-Olivera, J. A., Figueroa-Soto, Á. G., Cisneros-Máximo, G., & Cardona-Melchor, S. (2021b). Geomorphic characterization of faults as earthquake sources in the Cuitzeo Lake basin, central México. *Journal of South American Earth Sciences*, 109(January), 103196. <https://doi.org/10.1016/j.jsames.2021.103196>
- Guevara, R., Yutsis, V., Varley, N., Almaguer, J., Calderón-Moctezuma, A., & Guevara- Mansilla, O. (2021). *Geophysical determination of the Jalisco and Michoacán blocks boundary along the Colima graben. Journal of South American Earth Sciences*. **109**, 382–103208. <https://doi.org/10.1016/j.jsames.2021.103208>
- Guevara-Alday, J. A. (2015). Geological and geophysical studies for the elaboration of a conceptual model of the geothermal reservoir of San Agustín del Maíz, Michoacán, México (in Spanish). Universidad Michoacana de San Nicolás de Hidalgo. Morelia, Mich. http://bibliotecavirtual.dgb.umich.mx:8083/xmlui/handle/DGB_UMICH/5276
- INEGI (1993). Vectorial Data Model (in Spanish). Instituto Nacional de Estadística, Geografía e Informática. Ags., México. <https://sinegi.page.link/DLNP>
- Ingram, D.M., Causon, D.M. & Mingham, C.G. (2003) Developments in Cartesian cut cell methods. *Math Comp Simulation*, 61 (3–6): 561–572.
- Israde-Alcantara, I., & Garduño-Monroy, V. H. (1999). Lacustrine record in a volcanic intra-arc setting: the evolution of the Late Neogene Cuitzeo basin system (central-western Mexico, Michoacán). *Palaeogeography, Palaeoclimatology, Palaeoecology*, 151(1–3), 209–227. [https://doi.org/10.1016/S0031-0182\(99\)00024-3](https://doi.org/10.1016/S0031-0182(99)00024-3)
- Macleod, I.N. & Ellis, R.G. (2013) Magnetic Vector Inversion, a Simple Approach to the Challenge of Varying Direction of Rock Magnetization. Australian Society of Exploration Geophysicists, Extended Abstracts 2013, 1-4, Melbourne.
- NAMAG, (2002). North American Magnetic Anomaly Group. Magnetic Anomaly Map of North America. In: US Department of the Interior and US Geological Survey. Scale 1:10000000.
- Olvera-García, E., Garduño-Monroy, V. H., Liotta, D., Brogi, A., Bermejo-Santoyo, G., & Guevara-Alday, J. A. (2020). Neogene-Quaternary normal and transfer faults controlling deep-seated geothermal systems: The case of San Agustín del Maíz (central Trans-Mexican Volcanic Belt, Mexico). *Geothermics*, 86 (January), 101791. <https://doi.org/10.1016/j.geothermics.2019.101791>
- Pola, A., Martínez-Martínez, J., Macías, J. L., Fusi, N., Crosta, G., Garduño-Monroy, V. H., & Núñez-Hurtado, J. A. (2016). Geomechanical characterization of the Miocene Cuitzeo ignimbrites, Michoacán, Central Mexico. *Engineering Geology*, 214, 79–93. <https://doi.org/10.1016/j.enggeo.2016.10.003>
- Quintanar, L., Cárdenas-Ramírez, A., Bello-Segura, D.I., Espíndola, V.H., Pérez-Santana, J.A., Cárdenas-Monroy, C., Carmona-Gallegos, A.L. & Rodríguez-Rasilla, I. (2018). A seismic network for the Valley of Mexico: present status and perspectives. *Seismol. Res. Lett.* **89** (2A), 356–362.
- Quintanar, L., Rodríguez-González, M., & Campos-Enríquez, O. (2004). A shallow crustal earthquake doublet from the Trans-Mexican Volcanic Belt (Central Mexico). *Bulletin of the Seismological Society of America* **94**, 845–855.
- Ravat, D. (2000). Curie Temperature (Curie Isotherm). In Hancock, P.L.; Skinner, B.J. (eds.). *Oxford Companion to the Earth*. Oxford: Oxford University Press. pp. 202–203.
- Suárez, G., Caballero-Jiménez, G.V. & Novelo-Casanova, D.A., (2019). Active crustal deformation in the Trans Mexican Volcanic Belt as evidenced by historical earthquakes during the last 450 years. *Tectonics* **38**, 1–19.
- Trujillo-Hernández, N. (2017). Geological, geochemical and mineralogic study of the volcanic sequences of the southwest portion of Cuitzeo Lake, Michoacan, linked to the geothermal zone of San Agustín del Maíz (in Spanish). Universidad Michoacana de San Nicolás de Hidalgo. https://doi.org/http://bibliotecavirtual.dgb.umich.mx:8083/xmlui/handle/DGB_UMICH/4391